https://doi.org/10.1070/RCR5006

Bioanalytical applications of Mössbauer spectroscopy

Alexander A. Kamnev,* Anna V. Tugarova

Institute of Biochemistry and Physiology of Plants and Microorganisms, Russian Academy of Sciences, prosp. Entuziastov 13, 410049 Saratov, Russian Federation

Data on the applications of Mössbauer spectroscopy in the transmission (mainly on ^{57}Fe nuclei) and emission (on ^{57}Co nuclei) variants for analytical studies at the molecular level of metal-containing components in a wide range of biological objects (from biocomplexes and biomacromolecules to supramolecular structures, cells, tissues and organisms) and of objects that are participants or products of biological processes, published in the last 15 years are discussed and systematized. The prospects of the technique in its biological applications, including the developing fields (emission variant, use of synchrotron radiation), are formulated.
The bibliography includes 248 references.

Contents

1. Introduction 1415
1.1. Historical data and discovery of the Mössbauer effect 1415
1.2. Methodological fundamentals of Mössbauer spectroscopy 1416
1.2.1. Transmission (^{57}Fe) Mössbauer spectroscopy 1416
1.2.2. Emission (^{57}Co) Mössbauer spectroscopy 1418
1.2.3. Use of synchrotron radiation 1419
2. Low molecular weight biologically active compounds and biomacromolecules 1419
2.1. Low molecular weight biologically active substances and biocomplexes, biomaterials and biocomposites 1419
2.2. Metalloproteins and metalloenzymes 1427
3. Supramolecular structures, biological tissues and organisms 1433
3.1. Supramolecular structures and biological tissues of higher organisms 1433
3.2. Microorganisms 1437
3.3. Plants 1445
4. Note added in proof 1447
5. Conclusion 1447
6. List of abbreviations and designations 1448

A.A.Kamnev. PhD, DSc, Professor, Leading Scientist at the Laboratory of Biochemistry, IBPPM RAS.
e-mail: aakamnev@ibppm.ru; a.a.kamnev@mail.ru
Current research interests: development and applications of bioanalytical approaches [using vibrational (FTIR, Raman) and Mössbauer (nuclear gamma-resonance) spectroscopic techniques] to study the processes occurring in microbial systems with the participation of bio(macro)molecules and biocomplexes under the action of external factors.
A.V.Tugarova. PhD, Senior Scientist at the Laboratory of Biochemistry, IBPPM RAS.
e-mail: tugarova_anna@mail.ru
Current research interests: investigation of the metabolism of phytostimulating bacteria, using, in particular, vibrational (FTIR, Raman) and Mössbauer (nuclear gamma-resonance) spectroscopic techniques to solve various problems of microbial ecology and microbial biotechnology.

Translation: Yu.P.Sinkov

1. Introduction

1.1. Historical data and discovery of the Mössbauer effect

The breathtaking and, in many stages of its development, unusual history of Mössbauer spectroscopy (MbS) or, in essence, nuclear gamma-resonance spectroscopy, began in 1957. Specifically at that time the 28-year-old postgraduate Rudolf Ludwig Mössbauer, who had defended his diploma at the Laboratory of Applied Physics of the Technical University of Munich only two years before, discovered on his own a new physical effect. He confirmed experimentally the possibility of resonance fluorescence during nuclear transition between the excited and ground states of the ^{191}Ir nucleus; *i.e.*, emission and absorption of γ-quanta without energy loss for recoil (in solids) was observed,[1] which was later referred to as the Mössbauer effect (ME).[2,3] It is noteworthy that back in 1951 the British physicist Philip B.Moon described the effect of resonance scattering of γ-radiation produced by the radioactive decay $^{198}\text{Hg} \rightarrow {}^{198}\text{Au}$ with an energy of 411 keV.[4] Moon performed experiments with a ^{198}Hg sample placed on a ultracentrifuge rotor (at relative linear velocities between the source and scatterer of the order of 700 m s^{-1}, which compensated to some extent the recoil energy loss of γ-quanta due to the Doppler shift of the spectral line) and a liquid mercury scatterer (with a ^{198}Hg isotope percentage of 10%). However, the resonance was very weak in that case, and its experimental observation did not become a sensation because a recoil during γ-quanta emission was observed as expected. During the next few years several dozens of similar experiments with observation of resonant nuclear fluorescence were performed.[3] Concerning the discovery made by R.L.Mössbauer, only three years after publishing his first studies with description of the discovered phenomenon[5,6] and defending a dissertation, he was awarded a Nobel prize in physics (in 1961). The effect discovered by him formed the basis of a new unique spectroscopic technique: MbS, which started being developed almost instantaneously, in the 1960s, especially after observing the ME for the stable isotope ^{57}Fe.

To date, the ME has been observed for 45 elements (for which more than 85 Mössbauer isotopes were found). However, due to various objective reasons (primarily,

Received 28 August 2020

© 2021 Uspekhi Khimii, ZIOC RAS, Russian Academy of Sciences and IOP Publishing Limited

methodological difficulties of implementation), most of them are unsuitable for use, and only few are applied in practice. Among the latter, the most convenient and widely used is stable isotope ^{57}Fe,[7] whose percentage in natural iron is rather high (2.19%). At the same time, iron is one of the most widespread transition metals in nature, in particular, in living organisms.

The basic principles of the ME and MbS, including the physico-mathematical and technical fundamentals, were described in detail in many monographs and reviews (see, *e.g.* Refs 2, 7 – 12 and references therein), in view of which we will briefly consider only the basic methodological aspects in the beginning of this review. The attention is focused on the transmission variant of MbS on ^{57}Fe nuclei, which is of great importance practically for all fields of analytical materials science, including bioanalytical experimental investigations by this technique — the subject of this review. Bioanalytical studies carried out in the last 15 years using the emission variant of MbS (on radioactive ^{57}Co nuclei) and some other MbS biological applications under development are also considered. We did not aim at compiling all the published studies in this subject area, great in number and differing significantly in performance level, because the MbS application in biology-related fields has not yet become conventional, in contrast to many other fields of materials science. We only presented the most characteristic (in our opinion) examples illustrating the variety of bioanalytical potentials and informativeness of this unique spectroscopic technique.

1.2. Methodological fundamentals of Mössbauer spectroscopy

1.2.1. Transmission (^{57}Fe) Mössbauer spectroscopy

The schemes of the nuclear transformation lying in the basis of the transmission (^{57}Fe) MbS variant, possible hyperfine interactions in a ^{57}Fe-containing sample under study (absorber) with nuclear level splitting, the corresponding general view of recorded Mössbauer spectra and a block diagram of a Mössbauer spectrometer are presented in Fig. 1. In transmission measurements the γ-radiation source is radioactive isotope ^{57}Co (present in a rhodium or chromium matrix in trace amounts with an activity of the order of several tens of millicuries; 1 mCi = 37 MBq) with a half-life of 270.9 days. The decay begins with electron *K*-capture by ^{57}Co nucleus (element No. 27), which is transformed into a nucleus of ^{57}Fe isotope (element No. 26) in a metastable excited state with an energy of 136.5 keV (nuclear spin $I = 5/2$). This transformation is followed by a cascade of γ-radiative transitions to the last sublevel with an energy of 14.4 keV and lifetime ~100 ns. The γ-quantum (14.4 keV) emitted as a result of these transitions is used for resonance absorption in a ^{57}Fe-containing sample (absorber). Since the emission line of the source and the absorption line must be significantly overlapped to implement a resonance, which is observed in a very narrow energy range (the natural width of this emission line is as small as 4.55×10^{-9} eV),[7] the γ-quantum energy is modulated using the Doppler effect. To this end, the source moves relative to the absorber (or *vice versa*, which is equivalent) along the γ-radiation propagation (source – absorber) axis, most often with a constant acceleration, changing only in sign (oscillations along the axis), with velocities generally not larger than ± 12 mm s^{-1}. This velocity range is sufficient to increase or reduce (as a result of the Doppler effect) the energy of the γ-quanta emitted by the source so as to make resonance possible in any states of ^{57}Fe in the absorber (±1 mm s^{-1} corresponds to a variation in energy of ± 48.1 neV). Under these conditions, a spectrum is recorded using the spectrometer measurement system (see Fig. 1).

It should be noted that the main difference between the energy of γ-quanta emitted by the source (when the 'daughter' isotope ^{57}Fe, formed in the source, passes from the lower excited level to the ground level without energy loss for recoil) and the energy absorbed in the sample by the ^{57}Fe isotope is related to the different electronic structure of the latter and the existence of another chemical environment (molecular, atomic or ionic coordination sphere or crystal lattice). As a result, a spectrum recorded for a thin absorber (and source) contains a set of Lorenzian lines[2, 7] (see †) with the corresponding Mössbauer parameters. The latter include the isomer shift of a line and the presence (in certain cases) of quadrupole and (or) magnetic splitting, which corresponds to the chemical state of the ^{57}Fe in the sample studied. One can state with some simplification that the isomer shift (δ) is proportional to the electron density on the nucleus of the ^{57}Fe absorber, while the quadrupole splitting is proportional to the electric field gradient on the nucleus (having a quadrupole moment with a spin $I > 1/2$), which characterizes the degree of electric field asymmetry.

Thus, the isomer shift is mainly sensitive to the oxidation state, spin state and degree of covalence (ionicity) of the chemical bonding of ^{57}Fe atoms; to a smaller extent it is sensitive to the composition and structure of the ^{57}Fe coordination microenvironment. In turn, the quadrupole splitting characterizes the degree of asymmetry of the electron configuration of the ^{57}Fe atom (ion), including the contributions from s-, p- and d-electrons, as well as the degree of distortion of the spherical symmetry of its coordination microenvironment (arrangement of donor atoms in the composition of ligands). The magnetic splitting is characterized by the induction of the effective magnetic field (B_{eff}) on the ^{57}Fe nucleus in the absorber composition (the B_{eff} value is determined by calculating the spacing between the magnetic sextet external lines with the following recalculation coefficient: a spacing of 0.323 mm s^{-1} corresponds to 1 T)[7] (see Fig. 1). If the linewidth (Γ, measured as the FWHM value) in a transmission Mössbauer spectrum substantially exceeds the natural linewidth, which is ~0.19 mm s^{-1} for ^{57}Fe (*e.g.*, $\Gamma > 0.5$ mm s^{-1}), this fact may indicate the presence of equivalent sites with slightly different parameters for ^{57}Fe in the given chemical state in the sample (in particular, the presence of structural and (or) compositional inhomogeneities).

Note that the ME can be manifested with a noticeable probability only in solids;[3] therefore, liquid samples or solutions must be frozen (the use of low temperatures may also facilitate observation of magnetic splitting in spectra, which yields additional information about the composition and structure of the chemical states of the Mössbauer nuclide and its magnetic state).[2, 7 – 10] For biological objects it is also important that their fast freezing (which impedes water crystallization and preserves the solution in a 'glassy' state) almost completely stops all (bio)chemical transformations, and a sample can be stored for a fairly long time

† Possible reasons for deviation of line shapes from Lorentzian, for example, effects of relaxation, anisotropy of lattice vibrations (Goldanskii – Karyagin effect) and sample texture, were described in the special literature.

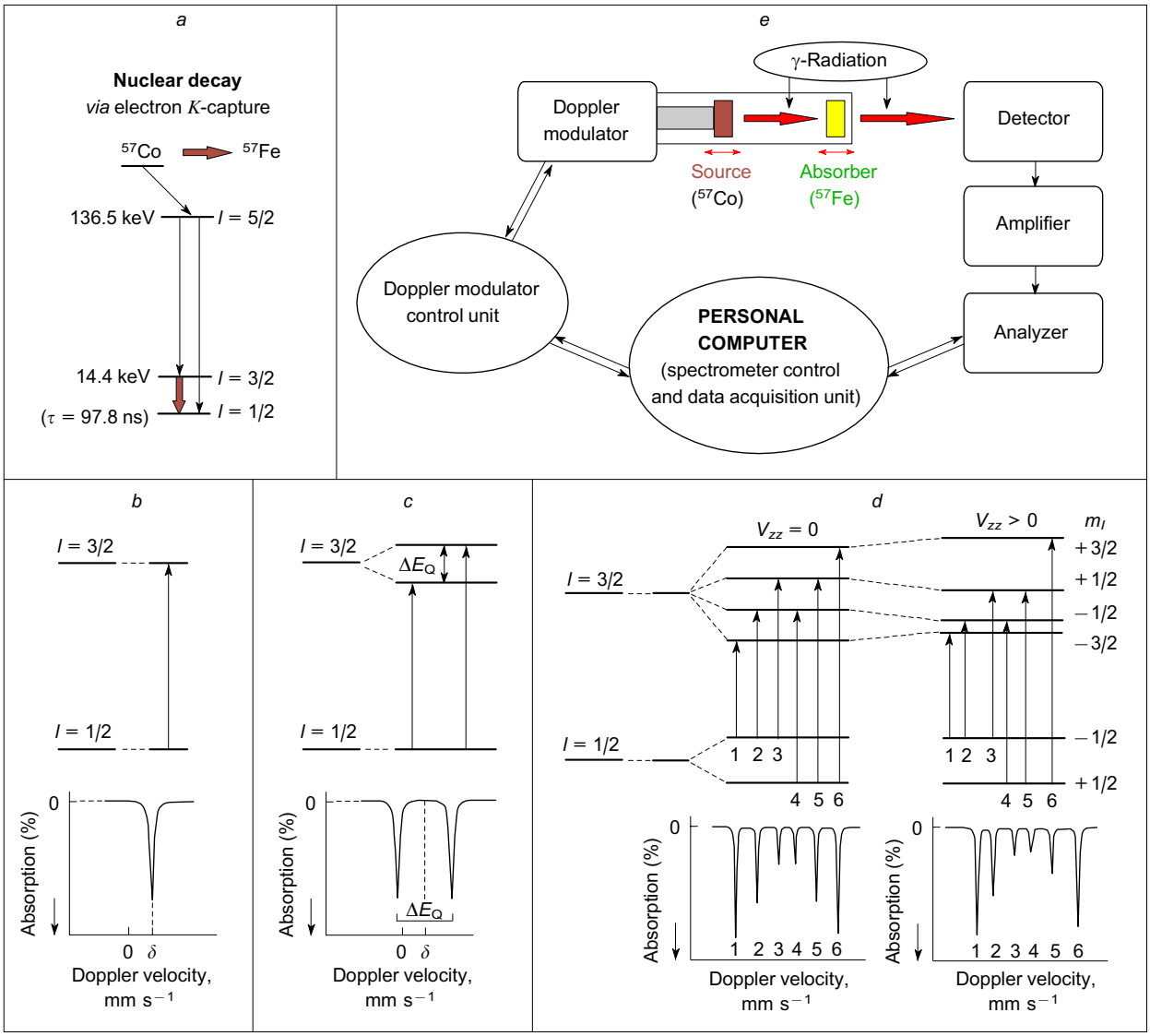


Figure 1. (*a*) Schematic of the $^{57}Co \rightarrow {}^{57}Fe$ radioactive decay, general view of experimental transmission Mössbauer spectra of a ^{57}Fe-containing sample (*b*) in the absence of quadrupole interactions (with zero electric field gradient on the ^{57}Fe nucleus) and (*c*) in the presence of quadrupole interactions, (*d*) in the presence of magnetic interactions with the formation of an effective magnetic field on ^{57}Fe nuclei in the absence ($V_{zz} = 0$) and in the presence of first-order quadrupole interactions ($V_{zz} > 0$, with nonzero electric field gradient on the ^{57}Fe nucleus), and (*e*) a schematic of a Mössbauer spectrometer; τ is the lifetime of the excited nuclear sublevel (with an energy of 14.4 keV); I is a nuclear spin; δ is an isomer shift (measured relative to a standard ^{57}Fe-containing absorber, generally, relative to α-Fe at room temperature, as implied in our review, unless otherwise indicated); ΔE_Q is a quadrupole splitting; V_{zz} is the z component of the electric field gradient on the ^{57}Fe nucleus; and m_I are the magnetic quantum numbers of nuclear energy sublevels. The Figure was prepared by the authors using the information reported in Refs 9 – 11.

without any significant changes. The measured spectrum of this object corresponds to the state of the system under study at the instant of freezing. Thus, if measurements must be performed at low temperatures (by freezing a sample and using a cryostat of special design), in emission measurements (see below) specifically the absorber is most often brought into motion by a Doppler modulator; in this case, a ^{57}Co-containing sample is placed in a cryostat. In transmission measurements, *vice versa*, the source is brought into motion, while a ^{57}Fe-containing sample is placed in a cryostat (see Fig. 1).

It is noteworthy that in the presence of different chemical forms (compounds) of ^{57}Fe in a sample studied, which are characterized by different Mössbauer parameters, the spectrum exhibits a superposition of all the corresponding lines. Their relative areas are calculated by decomposing the spectrum in components; this process has been significantly simplified and improved in all respects due to the use of special computer programs. Nevertheless, in the case of complex spectra, of great importance are researcher's experience and knowledge, which allow for suggesting a possible model of the system studied and obtaining as a result a set of parameters for each chemical form, having a physical meaning and characterizing most adequately a given chemical system. For analytical purposes — determination of the relative content of chemical forms in the sample — it is important that the relative line intensity for each form for a sufficiently thin sample is proportional to the number of ^{57}Fe nuclei and the ME probability for this form [the so-called Lamb – Mössbauer factor (f)]. A reasonable assump-

tion is made in this case: under identical conditions, this probability is almost the same for different forms in a sufficiently homogeneous sample (however, this rule is not always fulfilled; for example, the f value for surface Mössbauer atoms in nanoparticles may differ from the bulk f value[10]). Thus, the relative area of the spectral component for each chemical form of the Mössbauer isotope is directly proportional (with an accuracy up to a change in factor f) to the relative isotope content in the composition of this form in the sample. This fact is the basis of almost all analytical applications of the MbS technique (along with structural studies) in diverse physical, (bio)-chemical biomedical, geochemical and cosmochemical fields, as well as in materials science.[2,7–14]

Along with the numerous regularly published monographs and separate review chapters devoted to MbS (Refs 2, 7, 14 and references therein), there are several reviews devoted to the methodology and general practice of analytical applications of this technique.[8,12,15–18] Some aspects of analytical chemistry with the aid of MbS were considered in a number of studies,[19–24] including the surface analysis of solid samples,[22,23] as well as the problems related to the analysis of complex Mössbauer spectra applying the multivariate curve resolution methodology.[25] There are also a number of reviews devoted to some particular questions concerning the MbS of individual biological objects: the classical monograph by I.P.Suzdalev on proteins and model compounds;[26] a minireview on the rapid freezing technique for tracing intermediate stages and changes in ^{57}Fe-containing enzyme sites during biochemical reactions (which is in a certain sense an analogue of the stopped-flow method in spectrophotometry);[27] a minireview on MbS as a technique for studying solids, with examples of its biological applications;[28] a detailed review on the use of MbS to study the nuclei of special iron storage proteins (ferritins);[29] some more general reviews devoted to ferritins, with description of MbS applications;[30,31] generalizing works on the MbS study of other Fe-containing proteins;[10,11,32,33] and a review chapter devoted to MbS and its applications in analytical geomicrobiology.[34] Some examples of biological MbS applications were presented in review chapters.[35,36] The former[35] is devoted to a great extent to biomedical applications of ^{57}Fe-MbS, while the latter[36] presents the emission variant (on ^{57}Co nuclei). Since many aspects of the biomedical MbS applications aimed at revealing fine structural differences between ^{57}Fe-containing components in various tissues and organs in the normal state and at different pathologies have been considered in detail in specialized reviews,[9,32,35,37–41] they are omitted in our review.

1.2.2. Emission (^{57}Co) Mössbauer spectroscopy

In the emission MbS (EMbS) variant the γ-radiation source (*e.g.*, a ^{57}Co-containing sample) is the object of study; in this case, a ^{57}Fe-containing material with a single Mössbauer line (generally $K_4{}^{57}Fe(CN)_6 \cdot 3\,H_2O$) is used as a standard absorber.[10] In the EMbS variant a γ-quantum carrying information about the state of the initial (parent) ^{57}Co nuclide is emitted after the $^{57}Co \rightarrow {}^{57}Fe$ transformation [*i.e.*, by the daughter nucleus ^{57}Fe (see Fig. 1 *a*)]; therefore, the recorded emission Mössbauer spectrum characterizes the atomic (ionic) state of daughter ^{57}Fe, which is in the coordination microenvironment of initial ^{57}Co. The latter can be explained as follows: for the short lifetime of the Mössbauer sublevel (~100 ns), when the energy released as a result of the nuclear transformation is insufficient for displacing atoms, the atomic positions do not undergo any significant changes. Nevertheless, the ^{57}Co-EMbS technique, whose sensitivity is much higher than that of ^{57}Fe-MbS,[10] possesses a number of specific features and complexities, which will be considered below.

The history of the development of EMbS using radioactive isotope ^{57}Co in the composition of samples studied was briefly outlined in the review chapter of monograph.[36] Primarily, it should be noted that, at a theoretical specific ^{57}Co activity equal to 8.43 Ci mg^{-1} (17.8 MBq nmol^{-1}),[42] the presence of ^{57}Co in a sample in an amount about 0.1 μg (which corresponds to an activity of ~1 mCi) may be sufficient for recording a high-quality emission Mössbauer spectrum. Thus, the EMbS sensitivity is at least ~3 orders of magnitude higher than that of ^{57}Fe-MbS.[10,36] Obviously, the necessity of using a radioactive isotope in the sample composition and, correspondingly, carrying out measurements in a specialized radiochemical laboratory limits significantly the application area of the technique. In this context, the annual number of studies carried out using ^{57}Co-EMbS, after reaching a maximum in the 1970s (~100 papers a year), had gradually decreased by the beginning of the 21st century[36] and currently does not exceed several tens a year. The range of EMbS application in biology is even narrower, and, in our opinion, the necessity of dealing with radioactivity is not the only hindrance.

First, at the rise of MbS development (in the 1960s), the applicability of the emission variant was doubted for the following reason. The Auger cascade developing due to the electron capture by ^{57}Co nucleus,[36,43] with Auger ionization of the ^{57}Fe daughter ion, was believed to cause a break of chemical bonds around it. In particular (as was evidenced by Professor A.Nath, a well-known expert in EMbS[44,45]), the Nobel Prize winner in chemistry in 1960, physical chemist and specialist in radiochemistry, W.F.Libby said the following on this subject: 'What can you learn about a crystal vase using a sledge hammer?' Fortunately, this scepticism did not come true, because it was found that the rather high energy released on the daughter atom after the nuclear decay (~6 keV on the nucleus of the nucleogenic ^{57}Fe) may dissipate in solids in many cases.[36,43,45] Nevertheless, the Auger cascade process developing during $10^{-15}-10^{-14}$ s after the electron capture by a ^{57}Co nucleus is accompanied by ejection of electrons with initial ionization of the nucleogenic ^{57}Fe. By the instant of emission of a 14.4-keV γ-quantum (~10^{-7} s after the electron capture; see Fig. 1 *a*), most of these electrons have enough time to 'return' and form conventional charge states of the daughter ^{57}Fe ion, corresponding to the state of the initial ^{57}Co ion. However, one of the main consequences (post-effects) of possible capture of some of these electrons in the solid phase matrix surrounding the ^{57}Fe ion for a time longer than the Mössbauer sublevel lifetime (~10^{-7} s) is the occurrence of the so-called aliovalent ions (for example, $^{57}Fe^{3+}$, along with the daughter ions $^{57}Fe^{2+}$, corresponding to the initial $^{57}Co^{2+}$). These post-effects, as well as the line broadening (because of the occurrence of local inhomogeneities[43]) complicate emission spectra, in which additional lines arise. At the same time, this circumstance is successfully used when studying the electron-donor (electron-acceptor) properties of materials.[43] In addition, it was proposed to use ^{57}Co-EMbS for detecting potential chemical carcinogens with high electron affinity[46] and studying the post-effects and

stability of chelating agents for radiopharmaceutical preparations at nuclear decay of nuclides.[47]

The second reason for slowing down the development of biological EMbS applications is, in our opinion, the unsuccessful result obtained when studying a more complex object in early emission experiments. Cobalt is known to be a trace element with diverse biochemical and physiological functions in living organisms. Along with the initial experiments on a ^{57}Co-containing label deposited on different parts of a mammal inner ear for studying their vibrations (because the resonance Mössbauer system is sensitive to vibrations with an amplitude of the order of 1 Å), a series of emission experiments was performed with biologically significant complexes — cobalamins (vitamin B_{12} and its analogues), porphyrins, phthalocyanines, hemoglobins and other heme complexes — as well as $^{57}Co^{2+}$ complexes with nucleotides.[36] The first attempt to use enzymes was made when studying the ethanolamine ammonia lyase system with [^{57}Co]-vitamin B_{12} (coenzyme), in which (with confirmed absence of radiation damage of the enzyme system) almost identical Mössbauer parameters were obtained for both the initial coenzyme and the entire system, up to the end of the enzymatic reaction.[48] Based on this result, the conclusion drawn in Ref. 48 was as follows: 'it is unlikely that ^{57}Co emission Mössbauer spectroscopy will contribute greatly to the understanding of vitamin B_{12}-dependent enzymes'. Despite the fact that this conclusion was related to only the aforementioned enzyme system (and based on the reasons that are still unclear, because different results were obtained in other investigations of ^{57}Co-labelled organocobalamins[49]), subsequent emission Mössbauer studies on ^{57}Co-containing enzyme systems were carried out much later (see below).[10, 36]

1.2.3. Use of synchrotron radiation

The use of synchrotron radiation for recording Mössbauer spectra is based on the replacement of a radiation source by tuned monochromatic radiation of a synchrotron; in this case the technique of nuclear resonant forward scattering (NRFS) removes some limitations inherent in the conventional variant of transmission MbS. It was shown in particular[50, 51] that, in view of the small cross-sectional area of the beam, its high intensity and low divergence, as well as the possibility of using samples of much smaller volume, the measurement results are more accurate and unambiguous than the conventional data. This is especially important for studying bioinorganic compounds and metalloproteins, which are generally obtained in small amounts or in diluted solutions. The development of another technique — nuclear resonant inelastic scattering of synchrotron radiation (also referred to as nuclear resonant vibrational spectroscopy) — can be considered as an expansion of the conventional MbS variant (with an energy range of 1 – 100 neV) to the energy range corresponding to molecular vibrations (0.001 – 0.1 eV), which can be compared with resonant Raman scattering.[50]

The synchrotron radiation energy can be tuned in a wide range; this circumstance makes it possible to investigate isotopes having no convenient Mössbauer sources, for example, ^{61}Ni and ^{67}Zn: the lifetimes of the corresponding sources (^{61}Co and ^{67}Ga, respectively) are 99 min and 78 h, values that are too small for most experiments.

The methodological aspects of MbS based on synchrotron radiation (SR-MbS), along with discussion of the results of previous studies of model heme complexes and myoglobin, were reported.[50, 51] The application of nuclear resonant inelastic scattering of synchrotron radiation in bioinorganic chemistry was considered in a review chapter.[52]

The SR-MbS technique in the ^{61}Ni-NRFS variant was applied for the first time to study the Ni-substituted rubredoxin — Fe-containing protein with an active centre in the form of iron bound with Cys residues [$Fe^{II/III}(-S-Cys)_4$] — from aqueous thermophilic archaea *Pyrococcus furiosus*.[53] Natural iron(II) in the protein was replaced with Ni^{II}. A study of the obtained high-spin Ni^{II}-centre in oxidized and reduced forms of rubredoxin and model complex $[Et_4N]_2[^{61}Ni(SPh)_4]$ showed that SR-MbS is sensitive to the internal hyperfine magnetic field on nickel ions, as well as to the value and sign of the electric field gradient. Hence, one can gain information about the magnetic properties and local geometry of ^{61}Ni-sites. Thus, ^{61}Ni SR-MbS as an alternative to conventional measurement techniques with radioactive sources can be useful to study Ni-containing biocomplexes and enzymes, including those with heteronuclear bimetallic cofactors Ni – Fe in active centres.

Along with the conventional ^{57}Fe-MbS technique, both SR-MbS variants (nuclear resonant inelastic scattering and nuclear resonant forward scattering) were used to study an unusual enzyme: human acireductone dioxygenase (hARD), which is involved in the methionine recirculation path. This enzyme can catalyze various oxidative reactions with the same substrate, depending on the metal type (Fe or Ni) in the active centre, in the native form (Fe) and in the presence of the substrate.[54]

In recent study,[55] the techniques of NRFS and nuclear resonant inelastic scattering of 14.4-keV radiation from ^{57}Fe nuclei were applied to the oxidase of *Geobacillus kaustophilus* bacterium with introduction of only $^{57}Fe^{II}$ or Mn^{II} + $^{57}Fe^{II}$ to the apoenzyme in order to produce homo- or heteronuclear cofactors [Fe – Fe] or [Fe – Mn]. The use of isotopic substitution $^{16/18}$O and H/D in combination with quantum chemical calculations of nuclear resonance vibrational spectra yielded data on the state of cofactors and Mössbauer quadrupole splitting energies, molecular structural parameters and vibrational modes of cofactors, as well as on the specific features of O_2 activation processes.

It follows from the aforesaid that the scope of studies on diverse bioanalytical MbS applications, including both the analysis of fairly complex biochemical systems and the development of methodological procedures, has significantly expanded in the last years, and the data obtained should be generalized and systematized, with illustration of the rich and, in many respects, unique possibilities of MbS.

2. Low molecular weight biologically active compounds and biomacromolecules

2.1. Low molecular weight biologically active substances and biocomplexes, biomaterials and biocomposites

Many biologically active substances and pharmaceutical preparations are compounds containing Mössbauer isotopes. The MbS analysis of their structure and composition has a long-term history. The section of review[35] that is devoted to biomedical analyses contains, in particular, references to earlier studies (published prior to 2011) on [^{119}Sn]-MbS of organic tin(IV) compounds with cytotoxic activity in regard to the cells of human cervical adenocarcinoma (HeLa), complexes of organotin(IV) with heterocyclic

thioamides, which also exhibit anticancer activity; and some others, as well as on the [^{197}Au]-MbS of selenoauranofin, an analogue of auranofin — clinically applied gold(I)-containing antiarthritic preparation. A majority of Mössbauer studies of pharmaceutical products and food additives is related to iron-containing preparations. Some of those studies published before 2011, for example, investigations of a number of polysaccharide-containing models of ferritin, iron storage protein with a nanocore composed of iron(III) oxohydroxides; complexes with a protein or polygalacturonic acid; vitamin and food additives containing fumarate, gluconate and various iron(II) chelates, were also mentioned in review [35]. Mössbauer measurements made it possible to reveal and estimate quantitatively the presence of different amounts of oxidized impurities (Fe^{3+}) in Fe^{2+}-containing preparations and additives.[35]

To increase the accuracy of analysis of Fe-containing medical preparations, Arredondo *et al.*[56] calculated additionally the Lamb–Mössbauer factors for their components, which may somewhat differ in view of differences in the structure and dynamics of iron ions. A significant broadening of quadrupole doublet lines of high-spin Fe^{2+} in Mössbauer spectra of some medicines based on iron(II) fumarate at $T = 77$ K was found.[57] Due to this, it was necessary to introduce an additional Fe^{2+} doublet when fitting the spectra, whereas the room-temperature spectra were fitted using only one Fe^{2+} doublet. A comparative analysis of the Mössbauer data for iron(II) fumarate and iron(II) sulfate using Raman spectroscopy made it possible to explain the aforementioned effect by the presence of different labile hydrate forms of Fe^{2+}-containing components in the preparations. The 'fixation' of structures with different degrees of hydration at reduced temperatures allows one to distinguish them in a spectrum. It is noteworthy that the ratio of these two Fe^{2+}-containing components, detected at $T = 77$ K in three preparations with iron(II) fumarate, was very close to 1 : 1; they had similar isomer shifts ($\delta = 1.20-1.22$ mm s^{-1}) but different quadrupole splitting values ($\Delta E_Q \approx 2.2-2.3$ and $2.6-2.7$ mm s^{-1}).[57]

The Mössbauer data and dynamic properties of solid iron(II) gluconate lattices were discussed for amorphous [58] and crystalline [59] materials (including in both cases a minor Fe^{3+}-containing phase). Note that in both cases the Mössbauer spectra (measured in the constant acceleration mode with 1024 channels per spectrum) contained two Fe^{2+} components (making up in sum ~72% and 90–94% of the total spectrum area for the amorphous and crystalline phases, respectively). Their individual contributions were almost the same for the amorphous material but differed by a factor of two or more (at different temperatures) for the crystalline one.[58, 59] The presence of two Fe^{2+} components was explained [58] by the structural differences between the surface layers of fine-grained particles (having larger ΔE_Q values) and their core (with smaller ΔE_Q).

In the last decade a number of studies of pharmacological preparations were performed using MbS with a high velocity resolution (MbS-HVR), which makes it possible to fit and interpret complex spectra with higher accuracy and reliability (details of the MbS-HVR methodology can be found, for example, in the studies by Oshtrakh's research group [38–40, 60]), including the part of review [32] devoted to these preparations. As an example, Fig. 2 shows the Mössbauer spectra of preparation Ascofer®, whose main component is iron(II) gluconate.

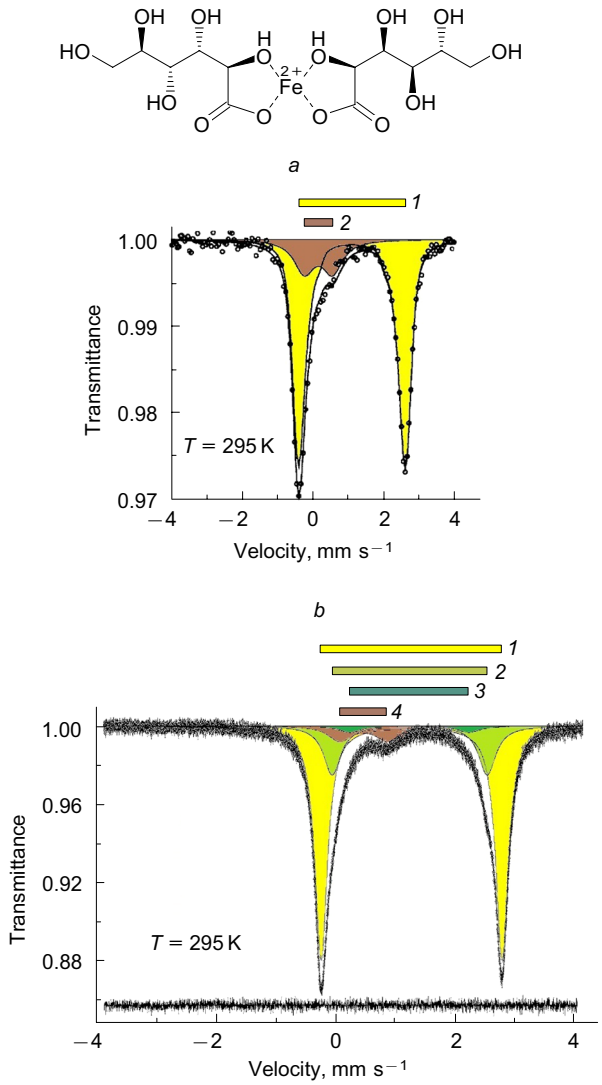


Figure 2. Structural formula and Mössbauer spectra of Ascofer® preparation, containing iron(II) gluconate as the main component. The spectra were recorded with (*a*) low (registration in 128 channels) and (*b*) high (4096 channels) velocity resolutions. The positions of spectral components *1*–*4* are indicated above the spectra (see text). There is a differential spectrum (experimental data (dots) minus the spectrum calculated as the sum of components *1*–*4*, obtained by fitting the experimental data) in the lower part of Fig. *b*. The figure was prepared by the authors using the data of Refs 32, 61.

One can see that the low-resolution spectrum is quite adequately described by one doublet of Fe^{2+} with the minor phase of oxidized iron(III) (Fig. 2 *a*, components *1* and *2*, respectively), whereas the high-resolution spectrum (see Fig. 2 *b*) even at room temperature reveals, along with the major and minor phases (components *1* and *4*, respectively), the presence of two more components: *2* and *3*. The Fe^{2+}-containing components *1*–*3* (see Fig. 2 *b*), having close δ values (~1.21, 1.18 and 1.17 mm s^{-1}), differ in both the ΔE_Q values (~3.02, 2.59 and 1.98 mm s^{-1}, respectively) and contributions (69.0, 19.6 and 3.5%, respectively).[61] Since similar components and differences between them were also found for pure iron(II) gluconate,[61] their presence is most likely due to the structural differences inherent in the iron(II) gluconate complex (different symmetries of the coordination environment of Fe^{2+} ions and degrees of

hydration), while the presence of Fe^{3+}-containing component is due to the oxidized impurity phase.[32, 61]

The Mössbauer analytical studies of Fe-containing pharmaceutical products or complexes with biomolecules, carried out in the last years, covered also the preparations based on iron(II) fumarate[62, 63] and iron(II) ascorbate,[63] polynuclear iron(III)-oxohydroxide-saccharose composites for intravenous injections in treatment of iron deficiency anemia,[64] anti-iron deficiency drugs — pharmaceutical analogs of ferritin: iron(III)-polymaltose preparations Ferrifol®,[65–67] Ferrum Lek[68–70] and Maltofer®;[70] complexes of iron(III) with ephedrine[71] and curcumin.[72]

Some previous studies of iron-, tin- and gold-containing drugs and pharmaceutical preparations using ^{57}Fe, ^{119}Sn and ^{197}Au MbS were briefly discussed in the corresponding section of Oshtrakh's review.[9]

Kuzmann *et al.*[73] used ^{119}Sn MbS (with a $Ba^{119m}SnO_3$ source) to analyze lyophilisates of X-ray-amorphous Sn-containing preparations for radiopharmaceutical studies — MULTIBONE (with the following composition: $SnCl_2 \cdot 2\,H_2O$, ethylenediamine tetramethylene phosphonate, NaCl) and PHYTON ($SnCl_2 \cdot 2\,H_2O$, myo-inositol hexaphosphate ester, NaCl), designed for monitoring therapy and imaging of tumours labelled by radionuclide ^{99m}Tc. It should be noted that labelling is performed using [^{99m}Tc]-pertechnetate(VII), which is reduced by tin(II), to obtain an acting radiopharmaceutical preparation; therefore, the stability of the latter and its analysis for the content of tin(II) and tin(IV) impurities are extremely important. The ^{119}Sn-Mössbauer measurements at $T = 80$ K for the MULTIBONE and PHYTON preparations showed the presence of two doublets in each spectrum: a major one, corresponding to the dominant tin(II) complex [$\delta \approx 3.01(1)$ and 3.12(1) mm s^{-1} (relative to $BaSnO_3$), $\Delta E_Q \approx 1.73(2)$ and 1.84(2) mm s^{-1}; $A \approx 97(2)$ and 81(2)%, respectively] and a minor one, corresponding to Sn^{IV} [$\delta \approx -0.08(4)$ mm s^{-1}, $\Delta E_Q \approx 1.0(2)$ mm s^{-1} for both preparations; $A \approx 3$ and 19% for MULTIBONE and PHYTON, respectively]. According to the ^{119}Sn-MbS data, the preparation composition remained relatively stable after storing for several months in air at 8 °C. This is sufficient for successful labelling of preparations with [^{99m}Tc]-pertechnetate(VII); the ^{119}Sn-MbS technique can be used to monitor their quality.[73]

The studies of a series of azo (−N=N−) and imino (−C=N−) carboxylate compounds of triphenyltin(IV) with antitumour and antibacterial activity, including ^{119}Sn-Mössbauer measurements, were reviewed recently.[74] Similar ^{119}Sn-MbS investigations of biologically active or medically important organic tin compounds, aimed at confirming the structure and type of coordination and bonds of central tin atoms, are widespread (see, *e.g.*, experimental studies[75–79] and references therein).

The informativeness of MbS in structural studies of macromolecules and their compositions that are used as biomaterials in medicine is related to introduction of iron ions or compounds both as components and as a doping additive (probe label) to detect structural features. Examples are the functionalized magnetic nanocarrier based on a biopolymer from xanthane resin with grafted glycidyl methacrylate inserts and incorporated Fe^{3+} ions (which is characterized, according to the MbS data, by superparamagnetic behaviour), used to immobilize and separate proteins,[80] and methylcellulose/alginate composite films, cross-linked by Fe^{2+} and Fe^{3+} ions, which increase the stability and mechanical strength of films.[81] Mössbauer measurements showed that the compositions of Fe-containing alginate cross-linkings in dried films with added ascorbic acid, serving both as a complexing agent and a reducing agent for Fe^{3+}, are stabilized at a level of ~3/4 Fe^{2+} (high-spin complexes with the coordination type O_6 and parameters $\delta = 1.21$ mm s^{-1}, $\Delta E_Q = 2.21$ mm s^{-1}) and ~1/4 Fe^{3+} (similar high-spin octahedral complexes; $\delta = 0.39$ mm s^{-1}, $\Delta E_Q = 0.73$ mm s^{-1} at ambient temperature) and do not change in air for up to half a year. In addition, in contrast to methylcellulose/alginate films without iron ion additives, the obtained composites remain stable in a physiological solution for up to two weeks.[81]

Examples of introduction of iron ions as Mössbauer probes into polymer materials can be found in the studies of poly(ether-urethane) derivatives;[82, 83] the latter are widely used (in the form of numerous modifications and composites) in industry, in particular, as medical materials, in view of their high biocompatibility and strength. The Mössbauer measurements on films of thermoplastic linear poly(ether-urethane) sulfonated ionomer {PEUSI; the degree of sulfonation of regular toluyl substituents in O−C(=O)−NH−Ar−NH segments, where Ar = [$C_6H_3(CH_3)$], is ~3%}, obtained by drying in air an aqueous emulsion with introduced iron(II) sulfate, were performed at $T = 78$ and 290 K.[82] The spectra exhibited a superposition of three quadrupole doublets, corresponding to two forms of high-spin iron(II), stabilized in coordination with the −C(=O)−NH− and −NH−NH− groups of the main macromolecular chain and the [$(C_2H_5)_3NH$]−[O−S(=O)$_2$] groups (the total spectral area percentage >40%), and to iron(III) with parameters typical of ultrafine-grained superparamagnetic (oxo)hydroxide. The latter was obviously formed as a result of oxidation of introduced Fe^{2+} during drying; very weak lines of the magnetic sextet ($B_{eff} = 44.6$ T, $A \approx 3$%), corresponding to the fraction of somewhat larger particles, were also observed at $T = 78$ K.

In a microheterogeneous system based on the same ionomer PEUSI (70%) with irregularly distributed copolymer (30%), composed of styrene (St) and acrylic acid (AA; St : AA = 45 : 55 mol.%; about 40% carboxyl groups in AA exist in the form of potassium salt),[83] after introducing Fe^{2+} into the initial emulsion and drying it, ~41% iron were also stabilized as two states of high-spin iron(II). However, the parameters of the latter differed significantly from those observed for PEUSI. In addition, both at 78 and 290 K, the iron(II)-doped PEUSI styrene acrylic system exhibited, along with the doublet of fine-grained Fe^{3+} (oxo)hydroxide (~40%), stronger lines of a broadened sextet of the magnetic phase ($A \approx 19$%) with $\delta = 0.45$ mm s^{-1} and $B_{eff} = 44$ and 39 T, respectively.[83]

Thus, the prime conclusion is as follows. In the aforementioned objects, in contrast to some other iron(II)-doped polymer systems,[82, 83] the coordination of introduced Fe^{3+} ions with the donor atoms of polar groups and polymer chain substituents leads to only their partial (of the order of 60%) oxidation in air to fine-grained iron(III) (oxo)hydroxide compounds. Obviously, the newly formed stabilized Fe^{2+} complexes are sensitive to constitutional changes in composite materials, which manifests itself in their Mössbauer parameters. In addition, basing on such systems one can implement a fairly simple one-step synthesis of polymer composites containing a magnetic phase of iron(III) (oxo)hydroxides, which is formed directly

during doping an aqueous emulsion and its subsequent drying.

There is an ever increasing number of MbS studies devoted to the development of methods of formation, physicochemical characterization, phase analysis and determination of the composition and properties of magnetic nanomaterials based on iron compounds (mainly oxides), including those entering the composition of biopolymers or their (nano)composites, for biomedical applications. Multifunctional biocompatible coatings composed of such nanoparticles were described in the review by Bychkova *et al.*[84] Mössbauer spectroscopic studies of Fe-containing nanomaterials based on feroxyhyte (δ-FeOOH) nanoparticles, including those doped with silver, copper or zinc ions; maghemite (γ-Fe_2O_3); metastable Fe_2S_3; as well as Fe_3C, α-Fe and γ-Fe nanoparticles, were considered in recent review.[85] Review[86] was devoted to the synthesis and investigation (in particular, by MbS) of magnetic iron carbides and nitrides, which are also widely applied in biomedicine and biosensorics. Tanaka *et al.*[87] noted in their review devoted to the nanoarchitecture of iron oxide particles for biomedical and other applications that Mössbauer measurements had revealed unusual magnetic properties of mesoporous γ-Fe_2O_3 and Fe_3O_4 nanoparticles, which manifest themselves up to temperatures of about 340 K, despite the fact that the pore wall thickness amounted to $\sim$7 nm. It should be noted that conventional nanoparticles of these oxides with sizes $<$8 nm lose magnetic ordering at much lower temperatures.[87]

Maghemite nanoparticles 10 nm in size, functionalized by hydrophilic molecules of pyrocatechol derivative — dopamine (neurotransmitter with hormonal functions) — and designed for medical applications, were investigated by physicochemical methods.[88] The MbS data made it possible to reveal the specific features of binding dopamine molecules on the surface of oxide nanoparticles, as was confirmed by model calculations.

Applying MbS in combination with X-ray diffraction analysis, Chistyakova *et al.*[89] investigated the particle sizes and superparamagnetic behaviour of nanocomposites composed of iron oxides and pectin, a plant carboxypolysaccaride (up to 10% of total composition), in the temperature range of 5–300 K. Rana *et al.*[90] studied the phase composition of superparamagnetic maghemite nanoparticles with sizes of 2–6 nm, also stabilized with pectin and exhibiting antimicrobial activity. Biopolymer capsules from modified chitosan (deacetylated derivative of chitin — poly-*N*-acetyl-D-glucosamine — natural nitrogen-containing polysaccharide) were obtained and investigated.[91] According to the MbS data,[91] the capsules contained superparamagnetic nanoparticles $\sim$15 nm in size with a wustite (FeO) core and a maghemite shell, having vacancies in the octahedral sites of its inverse spinel structure. Magnetic biocomposite nanoparticles based on poly(glycidyl methacrylate)xanthane resin with surface iminodiacetate groups as an adsorbent carrier for proteins, including magnetic iron oxides, were synthesized in the above-mentioned study,[80] where Mössbauer characterization of the magnetic properties, composition and structure of magnetic Fe-containing nanoparticles was also reported.

The results of studying the structure and behaviour of nanoparticles and nanocomposite materials exhibiting spin crossover (in particular, those incorporated into biopolymer matrices, such as chitosan and alginate), including MbS data, were discussed in review.[92]

The possibility of using MbS to study not only solid compounds but also solutions (in the frozen state; this issue was considered in monograph[93]) containing Mössbauer isotopes made it possible to apply Mössbauer measurements to complexing processes. As was noted above, fast freezing allows one to 'fix' a system in which almost all chemical processes are stopped at the instant of freezing.[27] From the point of view of bioanalytical applications, this possibility is important when considering the formation of coordination compounds with biomolecules and(or) their redox transformations. Primarily, one should begin consideration of the aforementioned processes as applied to small biomolecules.

Many fairly simple biomolecules (including secondary metabolites, synthesized and released by microorganisms into the environment) are known to serve as various 'chemical signals'. Obviously, any transformation of these biomolecules with participation of a metal may affect the exchange of signals (role of abiotic factors). Previous studies, proving (by the MbS technique) the possibility of oxidation of some secondary microbial metabolites (anthranilic (*o*-aminobenzoic) acid, indole derivatives — auxin phytohormones, tryptophan, cysteine, *etc.*) by iron(III) in acidic aqueous solutions, modeling widespread acidic soils, were mentioned in review.[35]

Chemical reactions with participation of iron(III) were investigateds[94–96] by MbS (measurements in frozen solutions). The objects of study were indole-3-acetic acid (IAA) and its analogues — auxin phytohormones, which are released and used by soil microorganisms for exchange of 'signals', including the exchange with higher plants (in the rhizosphere — the soil region in the vicinity of plant roots). Along with the confirmation of the occurrence of iron(III) complexes and study of their structural features, it was shown that these biomolecules in acidic solutions (with pH $\sim$ 3) undergo fairly rapid (within a few minutes for the most reactive IAA) oxidation with reduction of trivalent iron to Fe^{2+}, even in the presence of NO_3^- and under aerobic conditions. It was shown previously by MbS for IAA that drying a reaction solution (in which, under conditions of IAA excess, iron(III) was almost completely reduced to Fe^{2+} within two days) in air led to the inverse process: oxidation of iron(II) to Fe^{3+} (Ref. 35). This finding indicates that a cyclic process with oxidative transformation of auxins may occur in acidic soils with a change in periods of humidity and aridity.

Mössbauer spectroscopy studies (with measurements in frozen solutions) of the interaction of alkylresorcinols (alkylated *m*-dihydroxyphenols), widespread low-molecular extracellular autoregulators of microorganisms, with iron(III) under similar conditions also showed their rapid oxidation. However, when drying these reaction mixtures in air, the inverse process [oxidation of iron(II)] was not observed.[97,98] The latter circumstance indicates a much higher reducing potential of these biomolecules in comparison with indole-3-alkanoic acids and, possibly, a stronger binding of iron(II) by their oxidized derivatives — corresponding trihydroxylated alkylbenzenes (or hydroxylated quinones).[98] It was shown[99] for 4-n-hexylresorcinol — the most reactive alkylresorcinol among the studied ones — that the iron(III) reduction rate depends strongly on pH. At pH above $\sim$3–3.5 the reaction practically stops; with a further decrease in pH to values $<$3 the reduction of Fe^{3+} (which is obviously present in solution in the form of hydroxopolynuclear colloidal

particles under these conditions) is resumed, although more slowly.

According to the MbS data reported,[100] a comparative study of the reduction in a series of alkylresorcinols 5-methylresorcinol (5-MR, with a trivial name of orcinol), 5-n-propylresorcinol (5-n-PR), 4-n-hexylresorcinol (4-n-HR) by iron(III) in aqueous solutions (pH 3) revealed significant differences in the process rate, depending on the biomolecular structure, specifically, the length of alkyl substituent and its position (Fig. 3). In the case of 4-n-HR an ethanol aqueous solution (20 vol.%) was used to increase its solubility [special experiments for 5-MR in aqueous and water–ethanol (20 vol.%) solutions showed that ethanol with this concentration insignificantly affects the redox process kinetics]. A general kinetic scheme was proposed, which describes well the experimental data on the time dependence of the relative concentration of newly formed Fe^{2+} (determined from the Mössbauer spectra of solutions frozen at certain instants; see Fig. 3 and Table 1); this scheme allows one to estimate the reaction rate constants for structurally different alkylresorcinols.[100] The Mössbauer parameters (see Table 1) for Fe^{3+} ($\delta \approx 0.47$ mm s^{-1}, $\Delta E_Q \approx 0.7-0.8$ mm s^{-1}) correspond to hydroxopolynuclear complexes formed during the hydrolysis of iron(III) at pH ~ 3; the parameters for Fe^{2+} ($\delta \approx 1.3-1.4$ mm s^{-1}, $\Delta E_Q \approx 3.2-3.4$ mm s^{-1}) are characteristic of its hydrated ions.[93] The increase in the linewidth (in some cases to $\Gamma > 0.5$ mm s^{-1}) may be due to some extent to the heterogeneity of the hydrolysis products (for Fe^{3+}) and, possibly, the influence of the coordination of the newly formed alkylresorcinol oxidation products. The difference in the oxidation rates of the aforementioned alkylresorcinols, determined experimentally based on MbS data, was explained[100] with allowance for the results of quantum chemical calculations and the influence of kinetic parameters, related to the differences in the hydrophobicity and diffusion coefficients of the molecules.

The aforementioned studies illustrate the MbS potential for studying the reactivity of important signalling biomolecules and low-molecular autoregulators of microorganisms, as well as the kinetics of their transformations in acidic media, modelling ecological conditions in soils and water-bearing beds.

The Mössbauer analysis of the state of iron in soil, along with Fe-bearing minerals (for which it is widely used, being of great interest for mineralogy and soil science), is also important from the point of view of the influence of its bioorganic component.[101, 102] Sorkina *et al.*[103] synthesized (by coprecipitation of potassium humate and iron(II) sulfate with controlled mixing rate and pH conditions) Fe-containing derivatives of humic acids (natural soil components), which demonstrated the effectiveness of preventing iron deficiency (chlorosis) for plants (under hydroponic conditions). Mössbauer analysis at 298, 78 and 5 K, in combination with other instrumental techniques, showed that the obtained bioactive composites consist of microcapsules formed by humic materials. The latter contain fine-grained iron(III) oxohydroxides and iron(II,III) hydroxosulfates (in total up to 30% Fe^{2+}), where iron turned out to be quite biologically available for plant growth.

In recent study[104] the ^{57}Fe-MbS technique was used to analyze the soil composition for different rice fields located at a distance of 60 km from the Fukushima Daiichi Nuclear Power Plant (Japan) in order to explain the enhanced accumulation of radioactive caesium (^{134}Cs and ^{137}Cs) in rice grain in one of the fields after the nuclear accident. According to the MbS data, the soils contained somewhat different amounts of Fe^{2+} and Fe^{3+} compounds (quadrupole doublets); hematite (α-Fe_2O_3) and, in some cases, magnetite (Fe_3O_4) (sextets). The analysis showed that the

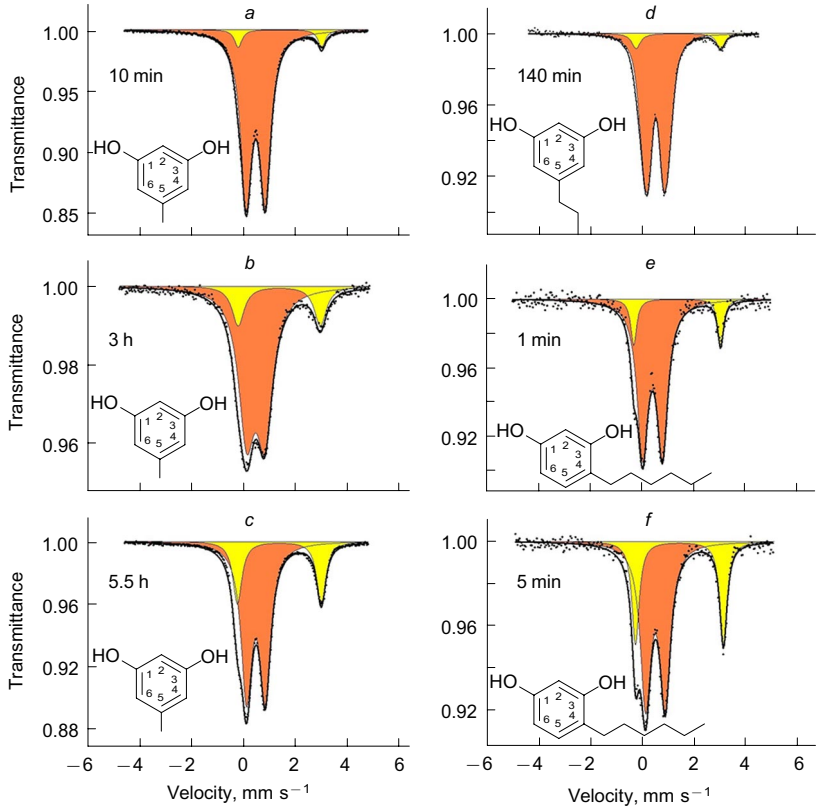


Figure 3. Mössbauer spectra of $^{57}Fe^{III}$-containing aqueous solutions of (*a*–*c*) 5-MR, (*d*) 5-n-PR and (*e*, *f*) 4-n-HR (containing 20% ethanol) with pH ~ 3 (total concentration 16 ± 1 mM; molar ratios Fe : alkylresorcinol = 1 : 3), rapidly frozen after different time intervals (indicated in Figs) after mixing reagents. The spectral components coloured brown (Fe^{3+}) and yellow (Fe^{2+}) make up the total spectrum (envelope), which was obtained by fitting the experimental data (dots). The Mössbauer parameters of spectral components are given in Table 1. The Figure was prepared by the authors using the data of Ref. 100.

Table 1. Mössbauer parameters for $^{57}Fe^{III}$-containing aqueous solutions of 5-MR, 5-n-PR and 4-n-HR at pH ~ 3, rapidly frozen at different times (indicated) after mixing reagents (according to the data of Ref. 100).

Alkylresorcin (mixed with $^{57}Fe^{III}$ in solution)	Reaction time [a]	Oxidation state of iron	δ, mm s^{-1}	ΔE_Q, mm s^{-1}	Γ, mm s^{-1}	A (%) (see [b])
5-MR (see Figs 3 *a*–*c*)	10 min	+3	0.48(1)	0.74(1)	0.52(1)	93.3
		+2	1.41(1)	3.22(1)	0.34(1)	6.7
	3 h	+3	0.478(3)	0.70(1)	0.75(1)	82.1
		+2	1.39(1)	3.17(1)	0.56(2)	17.9
	5.5 h	+3	0.48(1)	0.72(1)	0.50(1)	74.1
		+2	1.38(1)	3.23(1)	0.42(1)	25.9
5-n-PR (see Fig. 3 *d*)	140 min	+3	0.47(1)	0.80(2)	0.25(2)	92.0
		+2	1.35(1)	3.26(1)	0.40(2)	8.0
4-n-HR (see Figs 3,*e*, *f*)	1 min [c]	+3	0.4(1)	0.77(3)	0.51(3)	85.6
		+2	1.31(1)	3.35(1)	0.27(2)	14.4
	5 min [c]	+3	0.475(3)	0.757(4)	0.49(1)	68.8
		+2	1.402(3)	3.388(5)	0.34(1)	31.2

[a] Time passed from the instant of mixing reagents to the instant of fast freezing of reaction mixtures. [b] The relative errors for A do not exceed ±4% of the aforementioned values. [c] In aqueous solutions with 20 vol.% ethanol.

decrease in the Fe^{2+} content in soil (more oxidative conditions) and the presence of larger soil particles, containing on the whole a larger amount of iron and smaller amount of clay, correlated with the enhanced accumulation of radioactive caesium in rice grain.

We should also note the results of the emission (^{57}Co) studies‡ of rapidly frozen diluted aqueous solutions and dried complexes of divalent [^{57}Co] with simple biomolecules: indole-3-acetic, anthranilic (*o*-aminobenzoic) acids and tryptophan.[105–107]

In all cases (except for tryptophan) the emission spectra exhibited superpositions of the quadrupole doublet of the daughter high-spin complex of $^{57}Fe^{2+}$ (characterizing the state of the initial complex of $^{57}Co^{2+}$) and the lower intensity doublet of the nucleogenic $^{57}Fe^{3+}$ (as the results of post-effects). An unusual feature is that the spectrum cointained only one $^{57}Fe^{2+}$ doublet (without post-effects) for the complex with tryptophan,[105] although the nature of the coordination of cobalt(II) with the aforementioned amino acids is of the same type (they both coordinate metal with participation of a carboxyl group and neighboring α-amino group). Note that the Mössbauer parameters of the $^{57}Fe^{2+}$ doublet for the complexes with tryptophan [(δ = 0.88(6) mm s^{-1}, ΔE_Q = 2.8(1) mm s^{-1}] and anthranilic acid [δ = 1.10(2) mm s^{-1}, ΔE_Q = 2.71(5) mm s^{-1}] at T = 80 K and, in particular, small isomer shifts are indicative of tetrahedral coordination (T_d) of cobalt(II) in them. For comparison, the anthranilate complex of iron(II) with octahedral coordination (O_h) yields δ = 1.25(1) mm s^{-1} in the absorption spectrum at T = 80 K.[105]

Similar parameters were observed[108] for $^{57}Co^{2+}$ complexes in aqueous solutions and in the dried state with other biomolecules: low-molecular extracellular microbial autoregulators 4-n-hexylresorcinol and homoserine lactone (HL). In particular, the δ values at 80 K did not exceed 0.9 mm s^{-1} (Table 2), which indicates tetrahedral coordination of cobalt(II) in these biocomplexes (note that in all cases the ligand concentration exceeded significantly the $^{57}Co^{2+}$ concentration while preparing a solution).

It is of interest that in the case of another amino acid — aspartic acid (AspA) — the emission spectra of its $^{57}Co^{2+}$-containing frozen solution and dried sample exhibited, along with the nucleogenic $^{57}Fe^{3+}$ doublet (due to post-effects), which amounted less than 10% spectrum area, a superposition of two $^{57}Fe^{2+}$ doublets (Table 2) with significantly differing parameters. This is obviously related to the fact that aspartic acid HO(O=)C−CH$_2$−CH(NH$_2$)−C(=O)OH can coordinate metal ion both by a carboxyl group, jointly with the neighboring α-amino group (which is typical of free amino acids), and by the hydroxyl group located at the opposite side of the acid molecule. It is most likely that, when the amino acid is in excess in comparison with the $^{57}Co^{2+}$ ion,

Table 2. Mössbauer parameters [a] of the main doublets for high-spin nucleogenic $^{57}Fe^{2+}$ in the emission (^{57}Co) spectra of $^{57}Co^{2+}$ complexes with biomolecules (according to the data of Ref. 108).

Biomolecules (state)	Multiplet [a]	δ,[b] mm s^{-1}	ΔE_Q, mm s^{-1}	Γ, mm s^{-1}	A (%)
4-n-HR (s-n)	Doublet	0.91(5)	2.7(1)	0.87(5)	64
4-n-HR (s-d)	Doublet	0.80(1)	2.48(3)	0.77(1)	75
HL (s-n)	Doublet	0.90(1)	2.89(1)	0.78(2)	71
HL (s-d)	Doublet	0.8(1)	2.7(2)	1.02(7)	78
AspA (s-n)	Doublet 1	1.21(2)	2.82(3)	0.60(3)	72
	Doublet 2	0.96(7)	2.3(1)	0.7(1)	19
AspA (s-d)	Doublet 1	1.15(1)	2.60(1)	0.59(2)	68
	Doublet 2	0.80(3)	2.37(5)	0.63(7)	24

Note. Measurements were performed at T = 80 K in aqueous solutions (s-n) after their fast freezing and in dried samples (s-d). [a] The main doublets of $^{57}Fe^{2+}$ forms stabilized after the nuclear transformation $^{57}Co \rightarrow {}^{57}Fe$ (residual doublets of the forms $^{57}Fe^{3+}$ with $\Gamma \approx 0.7–1.0$ mm s^{-1}, which manifest themselves in emission spectra, are due to post-effects; the A values for them are 100% minus the A values for the main doublets corresponding to the $^{57}Fe^{II}$ forms). [b] Isomer shift (relative to α-Fe at room temperature) is converted to the form compatible with the values for transmission measurements.

‡ For emission measurements the values of isomer shift in sign are converted to a form comparable with that for transmission measurements. In this case, if the coordinations of cobalt(II) and iron(II) in complexes of the same type completely coincide, the δ values in the emission and transmission spectra are identical. As was noted above, the reason is that in an emission spectrum, the parameters for the nucleogenic ^{57}Fe ion in the microenvironment of the initial ^{57}Co ion are measured.

chelation of two AspA molecules by the carboxyl group jointly with the α-amino group leads to the formation of tetrahedral coordination (doublet 2; see Table 2; $\delta < 1.0$ mm s^{-1} at $T = 80$ K), whereas the coordination by only terminal carboxyl groups (and, possibly, water molecules) gives rise to octahedral coordination (doublet 1, see Table 2; $\delta \geqslant 1.15$ mm s^{-1} at $T = 80$ K). It should be noted that the coordination number 4 and T_d symmetry for cobalt(II) complexes are widespread, especially in the composition of enzyme active centres.[10, 36]

Of great importance is the study of the production and transformations of biologically active NO molecule, whose functions in mammal tissues are fairly diverse (from nervous signal transfer in nanomolar concentrations to immune protection in micromolar concentrations). Joint application of Mössbauer spectroscopy and other techniques helped in many respects to reveal the mechanisms of NO formation and transformation processes and determine the structure of NO-binding sites both in heme-containing redox-active centres of biomolecules (whose coordination chemistry has been thoroughly studied; see, *e.g.*, publications [109–112] and references therein) and in model nonheme Fe-nitrosyl complexes.[109, 113–115]

Speelman *et al.*[109] applied MbS (along with other techniques) to study a series of nonheme high-spin Fe–nitrosyl complexes where iron exists in different oxidation states: [Fe^{II}–NO$^-$], [Fe^{III}–NO$^-$] and [Fe^{IV}–NO$^-$]; these complexes have been relatively poorly studied (except for the Fe^{III} complexes). The authors [109] used a ligand based on permethylated guanidine, which forms iron-nitrosyl complexes with the same coordination sphere, independent of the iron oxidation state. The electronic structures of these complexes were considered in detail; it was shown that, for the reduced form [Fe^{II}–NO$^-$], protonation in the presence of weak acids occurs over ligand (in view of the high basicity of guanidine groups, which impedes the generation of the protonated HNO form) rather than over the nitrosyl centre. Figure 4 shows schematically the structures of complexes formed and presents some parameters obtained as a result of their spectroscopic studies.[109]

In the series of studied high-spin complexes, when passing from [Fe^{II}–NO$^-$] to [Fe^{III}–NO$^-$] and then to [Fe^{IV}–NO$^-$], one could observe significant changes in the isomer shift in Mössbauer spectra (by ~0.4 mm s^{-1} in each oxidation stage) and relatively small changes in the frequency of nitrosyl-group stretching vibrations (by ~130 cm^{-1}; see Fig. 4). For classical low-spin nitrosyl complexes, the corresponding series involved in single-electron oxidation with preservation of low-spin Fe^{II} ($S = 0$, 1/2 and 0) is characterized by transformations of coordinated nitrosyl group from O=N$^{(-)}$ to O=N$^{(\bullet)}$ and then to O≡N$^{(+)}$ with the corresponding much larger increase in ν_{NO} (of the order of 300 cm^{-1} at each oxidation stage) and smaller corresponding changes in δ (by ~0.2 mm s^{-1}).[109] Thus, the MbS data in combination with the results obtained by other techniques show that redox processes in high-spin nitrosyl complexes occur on the iron ion, whereas in low-spin complexes they occur on the NO group.

Dong *et al.*[116] synthesized (as a model for flavodiiron NO reductases, which are important enzymes of NO-molecule transformation) a high-spin binuclear complex of iron(II) with 2,6-bis[[(2-pyridylmethyl)-(2-phenylmethyl)-amino]methyl]-4-methylphenol and two propionate bridging ligands coordinated with iron ions (Fig. 5*a*). When contacting with the NO gas phase at room temperature, this complex (in the form of a solution in CH_2Cl_2) instantaneously changed its colour from dark orange to red. Then in a few minutes the entire amount of NO transformed into N_2O according to the scheme shown in Fig. 5*b*, with the formation of a μ-oxo-bridging bond between iron(III) ions. The Mössbauer parameters of the complex after its reaction with NO correspond to two quadrupole doublets observed in the spectrum (yielding in total ~93% of the spectrum area) of a pair of antiferromagnetically coupled Fe^{III} ions. The difference in the ΔE_Q values is obviously due to the difference in the coordination symmetries of Fe^{III} centres (see the bottom spectrum in Fig. 5*d*). Note that low-temperature experiments (in which the reaction of this complex with NO occurred at −80 °C with a lower rate) made it possible to reveal the presence of an intermediate with a [Fe^{II}NO]$_2$ structure in the Mössbauer spectra (see the transformation scheme 1 → 2 in Fig. 5*d*). The presence of a weak magnetically split component (~7%) in the Mössbauer spectrum after the reaction (see Fig. 5*b*, lower spectrum) is explained by the formation of a ferromagnetically coupled mixed-valence cluster (Fe^{II}/Fe^{III}).[116] These results can be considered as the first demonstration of the possibility of direct reduction of NO to N_2O by nonheme di-Fe^{II}-containing centres, indicating that a similar process may occur for flavodiiron NO reductases without participation of flavin cofactor in the reaction.

The Mössbauer studies [117] (along with other spectroscopic techniques and X-ray diffraction analysis) of the

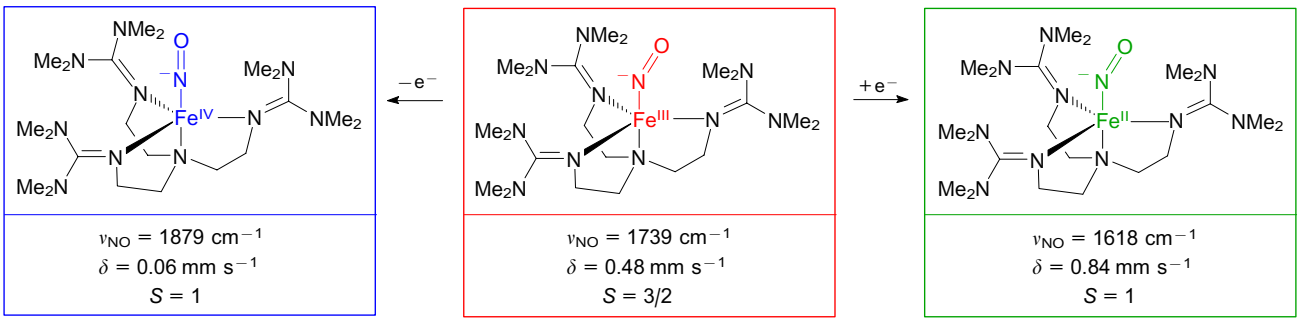


Figure 4. Structures of high-spin nitrosyl iron(IV,III,II) complexes with ligands based on permethylated guanidine and their spectroscopic parameters; S is the spin in the ground state, δ is the isomer shift of the quadrupole doublet in the Mössbauer spectrum at $B_{ext} = 0.053$ T; and ν_{NO} is the frequency of nitrosyl group stretching vibrations in the IR spectra of complexes. The Figure was prepared by the authors using the data of Ref. 109.

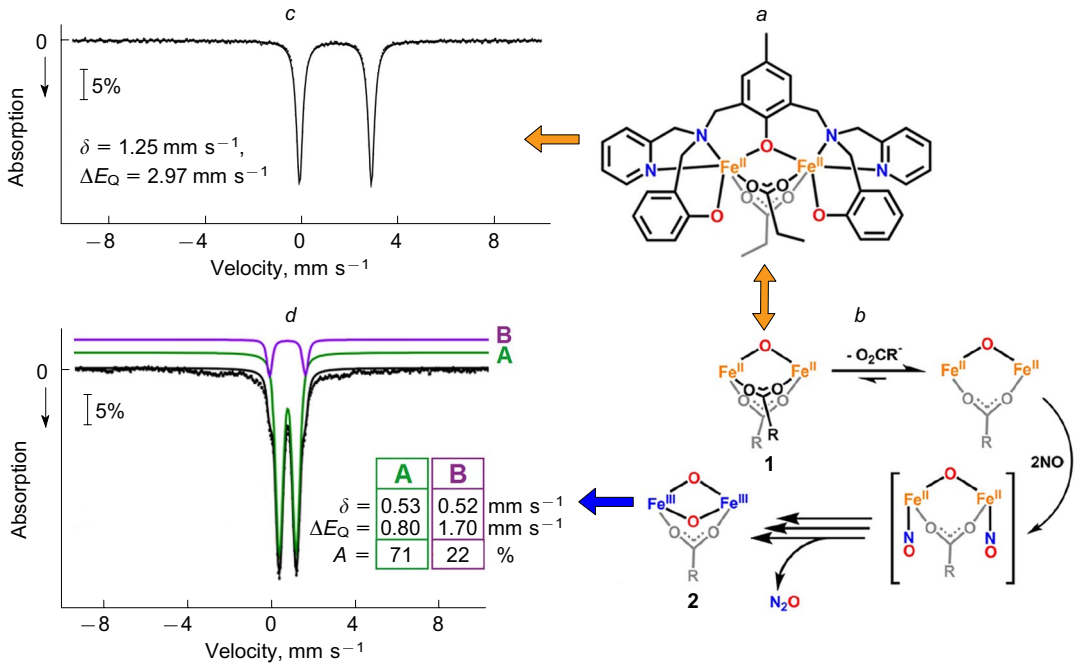


Figure 5. (*a*) Structure of the model high-spin binuclear iron(II) complex with coordinated propionate ions and (*b*) schematic diagram of the catalytic reduction of NO to N_2O with the corresponding transformations of its active centre with the formation of an μ-oxo-bridge between Fe^{III} ions, as well as their Mössbauer spectra (*c*, *d*; $T = 4.2$ K, $B_{ext} = 0.053$ T). **1** and **2**: see text. The solid black line in Fig. *d* corresponds to the sum of spectral components A and B. The figure was prepared by the authors using the data of Ref. 116.

nonheme iron-nitrosyl complex with tris(2-pyridylmethyl)-amine (TPA) — a model complex for flavodiiron NO reductases — made it possible to reveal for the first time the unusual binuclear structure of the $[Fe_2(NO)_2]$ centre. This structure was stabilized due to the change in the spin state (spin-crossover) of Fe centres with the formation of low-spin Fe^{2+}; a single quadrupole doublet with characteristic parameters ($\delta = 0.31$ mm s^{-1}, $\Delta E_Q = 1.40$ mm s^{-1} at $T = 4.2$ K) was observed in the Mössbauer spectrum of the complex. The use of a TPA derivative with a weaker ligand field (incapable of maintaining the spin transition) for complexing led to the formation of a more conventional mononuclear dinitrosyl centre $[Fe(NO)_2]$.

Spectroscopic studies (including MbS) of NO binding and transformation were performed [118, 119] on samples of flavo-diiron proteins [which reduce both O_2 (to H_2O) and NO (to N_2O)] from the bacteria *Thermotoga maritima* and *Desulfovibrio vulgaris* (isolated after expression in cells of genetically transformed *E. coli*). Two doublets of identical intensity were observed in the Mössbauer spectrum of the nonheme centre of the protein after the reaction with one NO equivalent {calculated per $[Fe^{2+}-(\mu\text{-}OH)-Fe^{2+}]$ centre when binding an NO molecule with one of the Fe ions}: one doublet for Fe^{2+} ($\delta = 1.5$ mm s^{-1}, $\Delta E_Q = 2.05$ mm s^{-1}) and one for $Fe^{3+}-NO^-$ ($\delta = 0.68$ mm s^{-1}, $\Delta E_Q = 1.56$ mm s^{-1} at $T = 50$ K). The spectrum recorded after the reaction with two NO equivalents contained a main doublet ($A = 85\%$) with the parameters $\delta = 0.71$ mm s^{-1}, $\Delta E_Q = 1.85$ mm s^{-1} for $[Fe^{3+}-NO^-]_2$. The Mössbauer parameters (including those measured in an external magnetic field) and results of DFT calculations showed the formation of a mononitrosyl complex of diiron centre with a half-bridging NO^- ligand in the first stage: $[Fe^{3+}-NO^-\cdots Fe^{2+}]$ (with preservation of μ-OH-bridge between Fe ions).[119] In the second stage the interaction with the second NO molecule leads to the formation of $[Fe^{3+}(^-O{=}N\cdots N{=}O^-)Fe^{3+}]$ intermediate (also with preservation of μ-OH-bridge between Fe ions), which provides an N_2O molecule and the oxidized form $[Fe^{3+} < (\mu\text{-}OH)_2 > Fe^{3+}]$ upon protonation. The reduction of the latter ($+2e^-$, $-H_2O$) closes the catalytic cycle with occurrence of the initial form $[Fe^{2+}-(\mu\text{-}OH)-Fe^{2+}]$.

Despite the above-mentioned progress in studying the heme-containing NO-binding complexes, in particular, microbial cytochrome P450 NO reductase, reducing two NO molecules to N_2O (one of the most important paths of nitrogen cycle, with release of N_2O from soil), the nature of the electronic structure of the so-called intermediate I, which is responsible for the stage of N–N coupling in this enzyme, has been revealed only recently.[120] A heme model complex with tetra[2,6-bis(3,5-dimethylphenoxy)-phenyl]porphyrin dianion was synthesized; this complex contains a methylhydroxylamide ligand, which is bound with a high-spin iron(III) ion — $[Fe^{III}-NH-OMe^-]$ ($\delta = 0.50$ mm s^{-1}, $|\Delta E_Q| = 0.41$ mm s^{-1}). Upon single-electron oxidation this complex, according to the data of MbS and other spectroscopic techniques, formed an intermediate high-spin form $[Fe^{III}-(NH-OMe)^{\bullet}]$ ($\delta = 0.43$ mm s^{-1}, $|\Delta E_Q| = 0.75$ mm s^{-1} at $T = 4.2$ K) but not a Fe^{IV}-containing product, for which the δ values are much smaller (generally < 0.2 mm s^{-1}). This model (synthesized for the first time) of intermediate I of cytochrome P450 NO reductase reacted with NO within several seconds even at −80 °C *via* radical–radical binding of NO molecule with the ligand $(NH-OMe)^{\bullet}$. The reaction product HON–NOMe could not decompose (as HON–NOH does, which occurs in the NO reductase) into N_2O and H_2O; however, it was important to confirm the formation pathway and electronic structure of the 'intermediate I'. The

results[120] indicate possible existence of specifically this electronic structure of the 'intermediate I' of cytochrome P450 NO reductase, which facilitates generation of the N–N bond with further formation of N_2O molecule.

The formation of a new mononuclear nonheme Fe^{II}-complex with cyclam (1,4,8,11-tetraazacyclotetradecane) — tetradentate ligand — and two *trans*-coordinated ligands CH_3CN ($\delta = 0.53$ mm s^{-1}, $\Delta E_Q = 0.61$ mm s^{-1} at $T = 14$ K; low-spin configuration Fe^{II}, $S = 0$) was described in recent study.[121] It was shown by MbS that this complex activates O_2 with replacement of one of the CH_3CN ligands and formation of a $Fe^{IV}{=}O$ complex ($\delta = 0.05$ mm s^{-1}, $\Delta E_Q = 2.49$ mm s^{-1} at $T = 80$ K; $S = 1$) according to a mechanism similar to oxygen activation by di-Fe^{II}-centres of enzymes — soluble methane monooxygenases.

2.2. Metalloproteins and metalloenzymes

One of the most interesting and important bioanalytical applications of MbS is the analysis of proteins, including enzymes: biological catalysts whose metal-containing centres play a leading role in diverse biocatalytic processes. It should be noted that the bioorganic 'shell' of protein compounds is transparent for Mössbauer γ-radiation. In many cases due to this circumstance one can obtain selectively unique structural information about metal-containing active centres, which are often inaccessible or hard-to-reach when using other techniques.[7, 10, 14, 27]

A number of reviews concerning the MbS study of proteins have been published in the last decade. They include Mössbauer studies of various metalloproteins — ferritins with a nanoscale core composed of particles of oxohydroxide iron(III) compounds;[29] iron–sulfur proteins;[11, 33] generalizing works on Mössbauer analysis of other Fe-containing proteins;[10, 32] and reviews devoted to individual proteins, with sections concerning MbS applications.[30, 31, 122] Here, we consider the most interesting latest publications containing Mössbauer data on different proteins, illustrating the bioanalytical applications of MbS.

An MbS-HVR analysis performed recently by Oshtrakh *et al.*[123] showed that the differences in the stereochemical environment of heme iron(II) ions and Fe(II)–O_2 bond geometry in α- and β-subunits of tetrameric rabbit hemoglobin (HbR) in the oxygenated form (HbR-O_2) manifest themselves in a high-resolution Mössbauer spectrum (Fig. 6). In the HbR-O_2 structure, which is included in the Protein Data Bank (PDB, code 2RAO), the distances between the O(2) atom of oxygen molecule and the nitrogen atom N_ε of the imidazole ring of distal histidine residue (His E7) in the α- and β-subunits are, respectively, 2.75 and 3.76 Å. This may indicate the absence of H-bond between O(2) and N_ε (His E7) and free rotation of the terminal atom O(2) in the β-subunit (see Fig. 6 *b*). In correspondence with this, in the Mössbauer spectrum (see Fig. 6 *d*) recorded at $T = 90$ K the best fit yielded a superposition of two doublets of identical intensity (area), one of which (component 1 in Fig. 6 *d*; $\delta = 0.267(3)$ mm s^{-1}, $\Delta E_Q = 2.224(5)$ mm s^{-1}, $\Gamma = 0.29$ mm s^{-1}; $A = 50\%$) had narrow lines (α-subunits), whereas the other [$\delta = 0.267(3)$ mm s^{-1}, $\Delta E_Q = 1.90(2)$ mm s^{-1}, $\Gamma = 0.48$ mm s^{-1}; $A = 50\%$] exhibited broader lines, displaying the distribution of the orientations of O(2) atom around the sites with energy minimum in β-subunits.[123] Similar results of the analysis of HVR Mössbauer spectra were obtained previously by Oshtrakh *et al.*[124, 125] when they compared the stereochemistry of heme environment (based on the PDB data) of human, rabbit and pig oxyhemoglobins. Along with the revealed differences in the Mössbauer parameters for the aforementioned proteins, a correlation of ΔE_Q values with the affinity of hemoglobins to oxygen was established.

For the deoxygenated form of HbR (after treating erythrocytes with sodium dithionite), the authors of

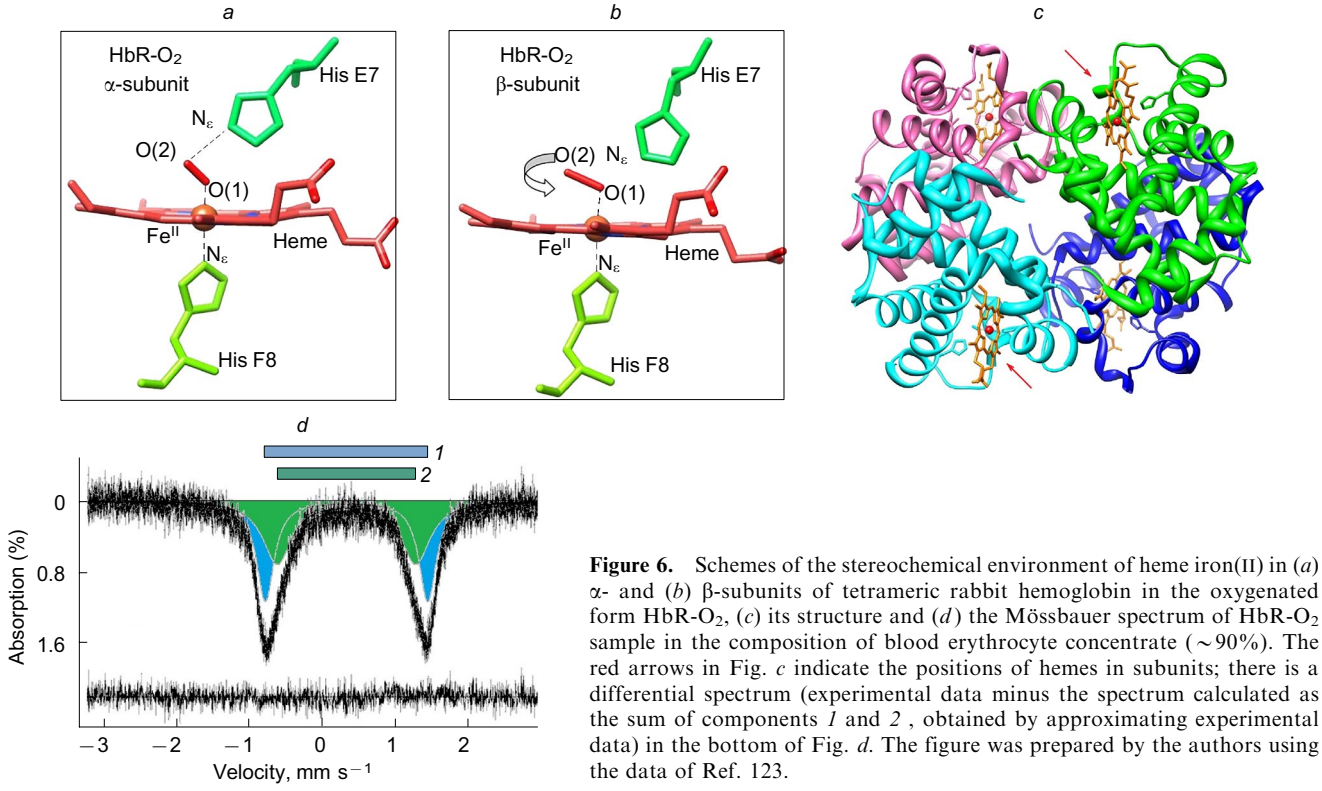


Figure 6. Schemes of the stereochemical environment of heme iron(II) in (*a*) α- and (*b*) β-subunits of tetrameric rabbit hemoglobin in the oxygenated form HbR-O_2, (*c*) its structure and (*d*) the Mössbauer spectrum of HbR-O_2 sample in the composition of blood erythrocyte concentrate (~90%). The red arrows in Fig. *c* indicate the positions of hemes in subunits; there is a differential spectrum (experimental data minus the spectrum calculated as the sum of components *1* and *2* , obtained by approximating experimental data) in the bottom of Fig. *d*. The figure was prepared by the authors using the data of Ref. 123.

Ref. 123 observed two quadrupole doublets of identical intensity in the Mössbauer spectrum (with identical linewidths), with the following parameters: $\delta = 0.864(4)$ mm s^{-1}, $\Delta E_Q = 2.307(4)$ mm s^{-1}, $\Gamma = 0.26$ mm s^{-1} and $\delta = 0.962(4)$ mm s^{-1}, $\Delta E_Q = 2.256(4)$ mm s^{-1}, $\Gamma = 0.26$ mm s^{-1} (correspondingly, α- and β-subunits with high-spin Fe^{2+} ions), which gave in total 95.4% of the spectrum area. The additional minor doublet [$\delta = 0.50(1)$ mm s^{-1}, $\Delta E_Q = 1.11(2)$ mm s^{-1}, $\Gamma = 0.26$ mm s^{-1}; $A = 4.6\%$] of low-spin Fe^{2+} corresponded to hemochrome: complex with distal His E7 as the sixth ligand, formed in deoxyhemoglobins at low temperatures. The data obtained are in agreement with the results of previous Mössbauer studies of other hemoglobins.[123]

In the same study Oshtrakh *et al.*[123] investigated for comparison the soybean leghemoglobin *a* (Lba). This is a protein from the group of monomeric O_2-binding hemoproteins, which are present in root nodules of leguminous plants; its tertiary structure and heme environment are similar to those of myoglobin or subunits of mammal hemoglobin with a pentacoordinated iron ion. Due to the high resolution of Mössbauer spectra, the existence of different conformations of the heme centre in deoxy- and oxy-forms of Lba was revealed. The most likely of these conformations are fixed when the protein is rapidly frozen and manifest themselves in spectra (at $T = 90$ K) as superpositions of doublets, differing mainly in the ΔE_Q values (for Lba-O_2: $\delta = 0.25-0.27$ mm s^{-1}, $\Delta E_Q = 2.26-2.11$ mm s^{-1}, $\Gamma = 0.26$ mm s^{-1}; for deoxy-Lba: $\delta = 0.88$ mm s^{-1}, $\Delta E_Q = 2.34-1.75$ mm s^{-1}, $\Gamma = 0.26$ mm s^{-1}). Proceeding from the relative areas of these doublets, the probability of their stabilization at $T = 90$ K was estimated.[123]

Khan *et al.*[126] described the biophysical and structural characteristics of the new heme-containing protein Sfh5 (typical of the fungi kingdom), with pentacoordinated redox-active high-spin Fe^{3+} and unusual heme-binding properties. This protein is presumably involved in the formation of responces to stresses induced by organic oxidants. To carry out MbS, the recombinant protein Sfh5 was expressed and isolated from the biomass of *E. coli* grown on a medium with 0.04 mM $^{57}FeCl_3$. The Mössbauer spectra measured at $T = 5$ K and $B_{ext} = 0.05$ T (for 0.8 ml of 1.5 mM recombinant [^{57}Fe]-labelled protein), showed the presence of two different magnetic states of high-spin ($S = 5/2$) heme Fe^{III}, reduced by dithionite to high-spin Fe^{II}. The latter fact, along with the data obtained by other spectroscopic techniques, confirms the redox activity of Fe^{III}.

The authors of Ref. 127 used a complex of spectroscopic and biochemical methods to characterize for the first time the oxygen-binding diiron protein (ODP) of the pathogenic bacterium *Treponema denticola*, which is genetically related to cytoplasmic chemoreceptors. It was shown that ODP functions as a 'sensor' of iron ions and O_2 molecules and mediates chemotaxis, promoting (in the O_2-bound form) phosphate release from the phosphorylated form of histidine kinase CheA. Mössbauer studies of ODP from *T. denticola* (obtained by expression in *E. coli*, grown on a medium with $^{57}Fe^{2+}$) showed reversible oxygen binding by the diiron protein centre (Fig. 7). The oxygenated form of ODP, containing two equivalent antiferromagnetically coupled high-spin ($S = 5/2$) Fe^{III}-centres with a peroxo bridge ($\delta = 0.58$ mm s^{-1}, $\Delta E_Q = 1.01$ mm s^{-1}, $\Gamma = 0.33$ mm s^{-1}; Fig. 7 *a*), can release spontaneously oxygen upon interaction with oxidase–catalase system (Fig. 7 *b*) and under anaerobic conditions (Fig. 7 *c*). In this case, along with the residual fraction of the peroxo-di-Fe^{III} form, in contrast to other nonheme flavo-diiron and O_2-binding proteins (in which this peroxy-form decomposes into O_2 and the di-Fe^{III} form in the absence of a reducing substrate), the di-Fe^{II} form with high-spin ($S = 2$) centres ($\delta = 1.20$ mm s^{-1}, $\Delta E_Q = 2.60$ mm s^{-1}, $\Gamma = 0.35$ mm s^{-1}; Figs. 7 *b*,*c*) is also accumulated. The Mössbauer data were confirmed by the results obtained with other techniques, in particular, resonant Raman spectra with characteristic stretching vibration bands O–O (828 cm^{-1}) and Fe–O (469 cm^{-1}) for [$Fe^{III}_2(O-O)^{2-}$]. These bands shifted due to the isotopic effect upon interaction with the di-Fe^{II} form instead of $^{16}O_2$ of a buffer solution $^{18}O_2$ (with occurrence of bands at 783 and 436 cm^{-1}, respectively).[127]

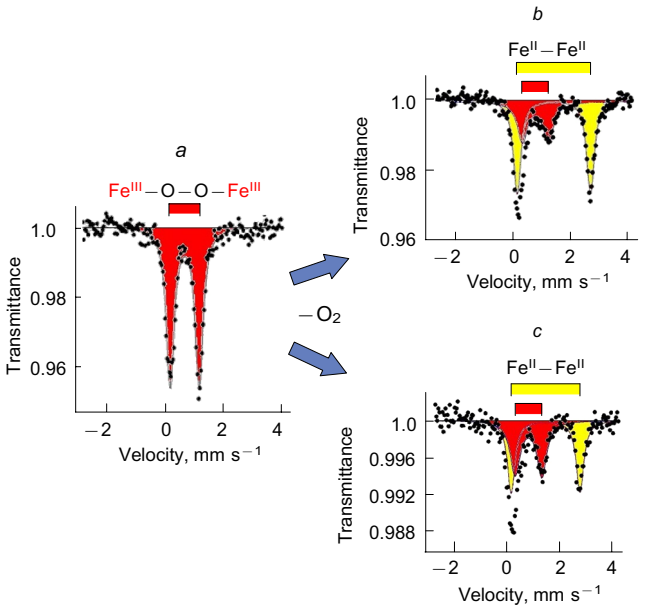


Figure 7. Mössbauer spectra of the ODP of *Treponema denticola* bacterium (*a*) in the oxidized form with oxygen-binding centre [$Fe^{III}_2(O-O)^{2-}$] and after partial oxygen removal (*b*) upon interaction of the oxidized protein form with the enzyme system glucose oxidase–catalase in the presence of glucose (1 h under anaerobic conditions) or (*c*) by 12-h exposure under anaerobic conditions; $T = 4.2$ K. The figure was prepared by the authors using the data of Ref. 127.

Kutin *et al.*[128] investigated the binding of Mn^{2+} and Fe^{2+} ions in sites of manganese–iron cofactors of bacterial enzymes (ribonucleotide reductases and ligand-binding oxidases), involved in redox processes as electron carriers. For metal-containing sites of ligand-binding oxidase (R2lox) of the *Geobacillus kaustophilus* bacterium (Fig. 8 *a*), Mössbauer spectra were recorded for sites filled with only iron ions (Fe/Fe homodimer) or Mn^{2+} and Fe^{2+} ions (Figs. 8 *b–d*). For the reduced form (Red), which arises under anaerobic conditions, the spectra of both Fe/Fe homodimer and Mn/Fe heterodimer contain a symmetric quadrupole doublet of high-spin Fe^{2+} ($\delta = 1.26$ mm s^{-1}, $\Delta E_Q = 2.98$ mm s^{-1} at $T = 80$ K; $S = 2$; Fig. 8 *b*). Its intensity for Mn/Fe is ~2 times lower (half of the sites are occupied by Mn^{2+} ions, which do not contribute to the spectrum). Under aerobic conditions (Ox), there is a doublet of high-spin Fe^{3+} in both cases ($\delta = 0.51$ mm s^{-1},

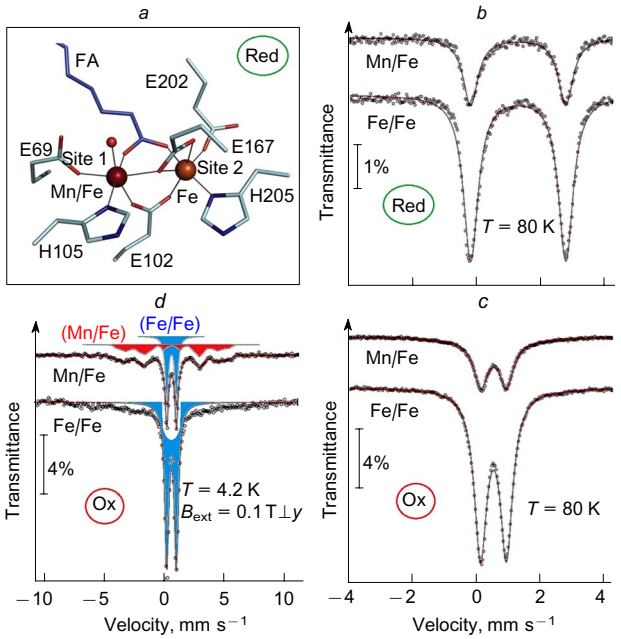


Figure 8. (*a*) Structure of the reduced form (R2lox) of *Geobacillus kaustophilus* bacterium with sites 1 and 2, occupied in approximately equal ratios with Mn^{2+} and Fe^{2+} ions and (*b*–*d*) Mössbauer spectra of R2lox with sites occupied by only $^{57}Fe^{II}$ (Fe/Fe) or Mn^{II} and $^{57}Fe^{II}$ (Mn/Fe) in (*b*) anaerobic and (*c*, *d*) aerobic conditions; FA is a μ-carboxylate-coordinated fatty acid ligand. The solid lines in Figs. *b* and *c* and at the bottom of Fig. *d* are the results of fitting by Lorentzian doublets. The spectrum with a magnetic structure at the top of Fig. *d* is presented by a superposition of the heterodimer Mn^{III}/Fe^{III} fitted with a spin Hamiltonian (red Mn/Fe component) and a doublet of the homodimer Fe^{III}/Fe^{III} (blue Fe/Fe component); *y* is the γ-radiation propagation direction. The figure was prepared by the authors using the data of Ref. 128.

ΔE_Q = 0.81 mm s^{-1} at T = 80 K; S = 5/2), which also has a lower intensity for the Mn/Fe form (Fig. 8 *c*). The measurements for the Ox-form of Mn/Fe at T = 4.2 K in an external magnetic field with induction B_{ext} = 0.1 T showed that the spectrum contains a contribution from paramagnetic (ESR-active) magnetically split heterodimer Mn^{III}/Fe^{III} and a doublet of diamagnetic homodimer Fe^{III}/Fe^{III} with antiferromagnetic coupling (Fig. 8 *d*, upper spectrum). The contribution of the latter (calculated using the relative areas of the Fe^{III} components on the assumption of identical Lamb–Mössbauer factors) is 55%; this value corresponds to a ratio of 62 : 38 for Mn^{III}/Fe^{III} and Fe^{III}/Fe^{III} clusters, which indicates preferred formation of heterodimer clusters.[128]

After the publication of the informative review by Papaefthymiou[29] on the Mössbauer studies and magnetic properties of ferritin Fe^{3+}-oxohydroxide cores (where mammal ferritins were mainly considered) in 2010, these questions were also discussed in later reviews, devoted to other ferritins[30,31] and various proteins, including ferritins.[9,10,35] Ferritin-like proteins in all organisms, from mammals to unicellular organisms, are a unique 'storage' of iron(III), which is necessary for biosynthesis of other numerous Fe-containing proteins and enzymes with diverse functions. With a sufficient amount of iron(III), there is less need for more soluble iron(II), whose elevated concentrations are hazardous due to the formation of reactive oxygen species (Fenton reaction), because the iron(III) stored in the ferritin core can be used for selective reduction and translocation of Fe(II).[10] Human and animal ferritins are 24-subunit protein shells with an internal cavity 10–12 nm in diameter, containing up to ~4500 iron atoms. The cores of these ferritins are generally characterized by a higher degree of crystallinity than those of microbial ferritins. Bacteria possess ferritin-like proteins of three types:[10,30]

— bacterial ferritin with a 24-subunit shell, similar to the ferritin of eukaryotes, with a cavity diameter of ~7.9 nm (up to 2500 iron atoms);

— bacterioferritin with 24 subunits of smaller size, bound with 12 heme groups, and a cavity diameter of ~6 nm (up to 1800 iron atoms);

— DNA-binding dodecameric ferritin with a cavity diameter of ~4.5 nm (up to ~500 iron atoms).

Mössbauer studies of ferritins,[9,10,29–31,35,70,129] including HVR measurements,[9,35,70] revealed not only structural and compositional differences between the cores of different ferritins but also structural inhomogeneities within the ferritin nanocore. In particular, five quadrupole doublets of different intensity (with different relative areas) were observed in the spectra measured with a high velocity resolution (4096 channels) and subjected to the best fitting (minimum number of components) for a ferritin sample from human liver; these doublets were characterized by close δ (~0.36–0.38 mm s^{-1}) values but significantly different ΔE_Q values (~0.37–1.37 mm s^{-1} at T = 295 K),[70] which corresponds to the model of heterogeneous ferritin core. The successive increase in ΔE_Q corresponds to the transition from more closely packed internal regions in iron(III) oxohydroxide crystallites to more loosely packed regions, close to the particle surface layer.[10,70] Anomalous temperature behaviour of the Mössbauer parameters of some components because of the low-temperature structural transformations of Fe–O packing in different crystallite regions was also found.[70]

Hartmann *et al.*[129] compared the informativeness of Raman microspectroscopy and MbS when studying ferritin and materials [magnetite, maghemite and ferrihydrite — hydrated iron(III) oxide with crystallites sizes < 10 nm] whose composition is similar to that of the iron(III) hydroxo compounds present in the ferritin core. It was shown that the spectroscopic data for the horse spleen ferritin correspond to the data for ferrihydrite.[129] In particular, at T = 4.2 K similar asymmetrically broadened spectra with a dominant magnetically split sextet characterized by δ = 0.24 mm s^{-1} and Gaussian distribution of B_{eff} from ~48.6 to ~50.4 T were observed for the aforementioned ferritin and ferrihydrite.

Specialized reviews devoted to the MbS of iron–sulfur protein clusters have been published recently by Bill,[33] Pandelia *et al.*,[11] and Garcia-Serres *et al.*;[130] there is a section devoted to these interesting and diverse compounds in reivew[10] of the Mössbauer studies of proteins. There is also a section devoted to MbS applications in the review chapter presenting the results of spectroscopic studies of iron–sulfur proteins.[131] The Mössbauer spectra of iron–sulfur clusters ([2Fe–2S], [3Fe–4S], [4Fe–4S], [4Fe–3S]), which are responsible for the electron transfer in many enzymes in organisms of all domains of life, are generally characterized by small isomer shifts for both Fe^{2+} and Fe^{3+} in view of the high covalency of the Fe–S bond (Fe–S clusters may also contain ions in mixed oxidation states ($Fe^{2.5+}$), with intermediate δ values).[10,11]

Müller *et al.*[132] used MbS to study the $[2Fe-2S]^{2+}$ cluster of the so-called Rieske protein from the *Thermus thermophilus* bacterium. Rieske proteins are components of cytochrome complexes in many organisms; they are responsible for the electron transfer in a wide range of redox potentials. Their distinctive feature is the existence of the [2Fe–2S] cluster, in which one iron ion is coordinated by four sulfur atoms (two S^{2-} ions of the cluster and two S atoms from the coordinated Cys residues), while the other Fe ion is coordinated, along with $2S^{2-}$ ligands, by two nitrogen atoms of His residues. Changes in the Mössbauer parameters of the oxidized cluster $[2Fe-2S]^{2+}$ as a function of pH with an increase in pH from 6 to 10.5 were traced.[132] This increase is obviously accompanied by a transition from the completely protonated state of His residues to deprotonation of the imidazole ring (in view of the decrease in pK_a of the NH group of the imidazole ring from ~14.6 for free His to ~7.5 and ~10.1 for two coordinated His residues due to the coordination of the ring with Fe^{3+}).[132] Table 3 contains the Mössbauer parameters of the $[2Fe-2S]^{2+}$ cluster for different pH values. Note that a significant decrease in the isomer shift (from 0.34 to 0.28 mm s^{-1}) is observed in the case of His deprotonation for only the Fe^{3+} ion, coordinated with His residues (see Table 3). The latter is due to the fact that the anionic (imidazolate) form of the His ring is a good σ-donor; therefore, the electron density on the Fe^{3+} ion coordinated with the His cycle increases, which is accompanied by a decrease in δ.

Among the samples of bioinorganic compounds that were analyzed in early studies by MbS and considered in review,[133] there are oxidized and reduced states of ferredoxin — Fe-containing protein including Fe–S clusters of different structure and composition — that serve as electron carriers in many biological redox processes. A protein with the [2Fe–2S] cluster (after replacing native iron with ^{57}Fe isotope) was extracted from green algae *Scenedesmus*. Its oxidized form was approximated by one doublet (δ = 0.20 mm s^{-1}, ΔE_Q = 0.60 mm s^{-1} at T = 195 K), which corresponded to two high-spin Fe^{3+} ions with antiferromagnetic coupling. (As was noted in the review by Semenov *et al.*,[8] later studies showed that in the case of plant ferredoxin these Fe^{3+} ions are not quite equivalent and yield two overlapping doublets of equal intensity but with slightly different parameters: δ = 0.22–0.25 mm s^{-1}, ΔE_Q = 0.6–0.7 mm s^{-1} at T = 195 K.) Two doublets of the same intensity were observed for reduced forms: for the Fe^{2+} ion with much larger parameters (δ = 0.56 mm s^{-1}, ΔE_Q = 2.75 mm s^{-1}) and Fe^{3+} ion (δ = 0.22 mm s^{-1}, ΔE_Q = 0.59 mm s^{-1}).[133]

In recent study[134] (Ref. 135 for corrections) Müller *et al.* performed an MbS characterization of isolated and purified ferredoxin of the pathogenic bacterium *Mycobacterium tuberculosis*, expressed in *E. coli* cells (with medium enrichment in ^{57}Fe); the knowledge of the structure and properties of this protein is important for target development of antituberculous preparations. The Mössbauer spectrum of the Fe–S cluster in purified ferredoxin at T = 77 K (in the absence of external magnetic field) is a superposition of two doublets:

— with the parameters δ = 0.27(2) mm s^{-1}, ΔE_Q = −0.53(3) mm s^{-1} (A = 33%), which are typical of 4S-tetrahedrally coordinated high-spin (S = 5/2) Fe^{III} ion,

— with the parameters δ = 0.44(2) mm s^{-1}, ΔE_Q = 1.47(3) mm s^{-1} (A = 67%), which are characteristic of a pair of $Fe^{2.5+}$ ions of mixed valence.

In the absence of diamagnetic centres, as was confirmed by the paramagnetic splitting of the spectrum in an external magnetic field at T = 4.2 K, and with allowance for the distribution of doublet areas, the cluster under study was characterized as a reduced form $[3Fe-4S]^0$, in agreement with the DFT calculations.[134]

In the detailed work[136] MbS was successfully applied to determine the role, structural features and transformation of the so-called auxiliary clusters [4Fe–4S] in the composition of bacterial enzyme methylthiotransferase (MiaB). To carry out the experiments, the enzyme was extracted from biomass of *Bacteroides thetaiotaomicron* bacteria grown on a medium with $^{57}FeCl_3$ (an iron source, introduced to increase the intensity of Mössbauer lines), chromatographically purified and identified by analytical and biochemical methods. It was shown experimentally that the auxiliary enzyme cluster $[4Fe-4S]^{2+}$, composed of four equivalent mixed-valence sites $Fe^{2.5+}$, is transformed during a catalytic event into a cluster of the $[3Fe-4S]^0$ type. The latter, in contrast to typical cuboid clusters $[3Fe-4S]^0$ with identical parameters of two mixed-valence iron centres, is characterized by unusual Mössbauer parameters, in particular, different ΔE_Q values for two Fe^{3+} centres (Fig. 9; the indicated δ values are characteristic of the corresponding 4S-coordinated Fe^{2+} and Fe^{3+} ions). The corresponding fraction of high-spin $(O/N)_6$-coordinated complex of Fe^{2+} is also fixed in the reaction medium (Fig. 9, on the right). Based on the

Table 3. Mössbauer parameters for the $[2Fe-2S]^{2+}$ cluster of the Rieske protein from *Thermus thermophilus* bacterium at different pH values and T = 77 K (according to the data of Ref. 132).

pH (state of His residues)	Cluster fragment	δ, mm s^{-1}	ΔE_Q, mm s^{-1}	Γ, mm s^{-1}
6.0 (protonated)	$2S > Fe^{3+} < (S-Cys)_2$	0.23(1)	0.57(1)	0.26(1)
	$2S > Fe^{3+} < (N-His)_2$	0.34(1)	1.05(1)	0.27(1)
10.5 (almost completely deprotonated)	$2S > Fe^{3+} < (S-Cys)_2$	0.24(1)	0.44(1)	0.25(1)
	$2S > Fe^{3+} < (N-His)_2$	0.28(1)	0.71(1)	0.27(1)

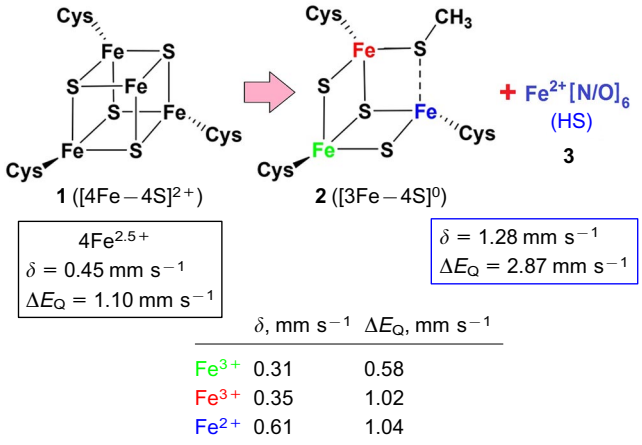


Figure 9. Structures of the auxiliary cluster $[4Fe-4S]^{2+}$ of methylthiotransferase of *Bacteroides thetaiotaomicron* bacterium (**1**), an intermediate product of its catalytic transformation (**2**) with a splitted-off high-spin (HS) $(N/O)_6$-coordinated Fe^{2+} complex (**3**), and their Mössbauer parameters at T = 4.2 K. The figure was prepared by the authors using the data of Ref. 136.

data obtained, in particular, the results of Mössbauer measurements performed under different conditions to confirm the conclusions drawn, a mechanism was proposed, according to which the auxiliary cluster $[4Fe-4S]^{2+}$ is the direct donor of a sulfur atom, incorporated into the fimal product during catalytic transformation. The intermediate transformation product is a cluster of the $[3Fe-4S]^{0}$ type with an unusual structure (see Fig. 9, structure **2**).[136]

Note that the results of fundamental structural analytical studies of complex biochemical systems by MbS may be useful when searching ways to develop drugs. In particular, the synthesis of isoprenoids in many pathogenic microorganisms, including unicellular parasites from the plasmodium species (*Plasmodium falciparum*), malaria agents, occurs according to the methylerythritol phosphate (MEP) pathway. The latter, being absent in humans, is a target one for developing antimicrobial preparations that can block this pathway.[137] The last stage of this biosynthetic pathway is the transformation of 1-hydroxy-2-methyl-2-butenyl-4-diphosphate (HMBPP; or 4-hydroxy-3-methylbut-2-en-1-yldiphosphate) into isoprenoid precursors; this transformation is catalyzed by the $[4Fe-4S]^{2+}$ cluster of homodimeric enzyme LytB (which is sometimes also referred to as IspH; M = 72 kDa) with an unusual structure (Fig. 10 *a*). This cluster, being diamagnetic, does not generate an ESR signal; however, MbS studies of an isolated LytB revealed[138] that the iron ions in it are not equivalent (in contrast to conventional $[4Fe-4S]^{2+}$ clusters of ferredoxins). One of the four iron ions has parameters unusual for iron–sulfur proteins: δ = 0.89 mm s^{-1}, ΔE_Q = 1.97 mm s^{-1} at T = 77 K (see Fig. 10 *b* and Table 4, component *3*; A = 25%).

Similar parameters, observed in Fe–S clusters of some other enzymes,[137,138] correspond to the coordination of high-spin (in the absence of substrate) Fe^{2+} (see Fig. 10 *a*, indicated by black arrow) by three sulfur atoms of the cluster and, additionally, two or three donor oxygen or nitrogen atoms. In the presence of HMBPP substrate, the Mössbauer parameters of specifically this site change significantly (see Fig. 10 *c* and Table 4, component *3*). The drop of the isomer shift from 0.89 to 0.64 mm s^{-1} is explained by the substrate binding *via* its hydroxo-group with the cluster Fe^{2+} site (see Fig. 10 *a*); the other O/N ligands dissociate under these conditions (which is confirmed by structural studies[137]). The parameters of spectral component *1* (see Table 4) correspond to the centres tetrahedrally coordinated by sulfur atoms — the pair of mixed-valence $Fe^{2.5+}$ ions (A = 50%); the low value δ = 0.37 mm s^{-1} for component *2* (A = 25%) corresponds to 4S-coordinated high-spin cation Fe^{3+}. Ahrens-Botzong *et al.*[137] proposed also potential LytB inhibitors — analogues of HMBPP with NH_2 and HS groups (replacing the OH group), which possess high inhibiting ability and, according to the Mössbauer data, exhibit strong binding with the aforementioned LytB Fe-site.

The application of MbS was discussed in review,[139] devoted to the methods for determining the functional activity of the isoenzymes of cytochrome P450 — heme-thiolate monooxygenases, which are involved in the bio-

Table 4. Mössbauer parameters for the $[4Fe-4S]^{2+}$ cluster of LytB protein in the absence and in the presence of HMBPP substrate.[137]

Spectral component	Mössbauer parameters			
	δ [a]	ΔE_Q (see [a])	Γ [a]	A (%)
Without substrate (spectrum in Fig. 10 b)				
1	0.42(2)	1.21(3)	0.44(2)	50(3)
2	0.37(3)	0.89(2)	0.42(2)	25(3)
3	**0.89(3)**	**1.97(3)**	**0.61(2)**	**25(3)**
After addition of HMBPP substrate (spectrum in Fig. 10 c)				
1	0.42(1)	1.33(2)	0.32(2)	50(2)
2	0.38(2)	0.92(4)	0.30(5)	25(2)
3	0.64(2)	1.22(4)	0.29(1)	25(3)

Note. The parameters for the site with unusual iron coordination are in bold. The calculation errors in the last significant digit (according to the data of[137]) are given in parentheses. [a] In mm s^{-1}.

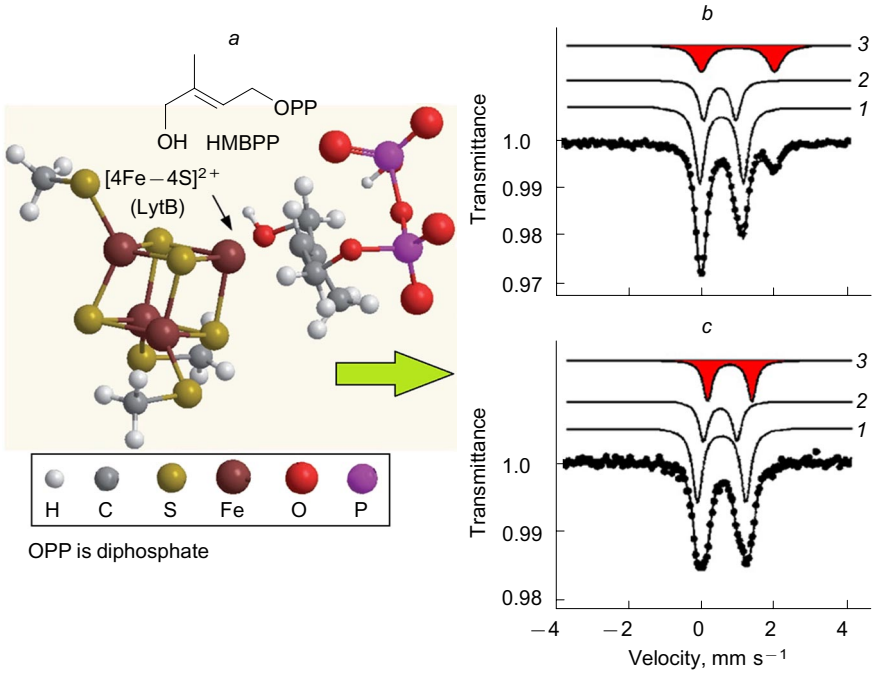


Figure 10. (*a*) Structure of the $[4Fe-4S]^{2+}$ cluster of LytB protein and the HMBPP substrate bound with it and (*b*, *c*) the Mössbauer spectra of ^{57}Fe-LytB in the absence (*b*) and in the presence (*c*) of HMBPP (T = 77 K, B_{ext} = 0). The protein was isolated from the cells of recombinant *E. coli* strain, superproducing ^{57}Fe-LytB (in a medium with added $^{57}FeCl_3$), and purified under anaerobic conditions. The Mössbauer parameters of spectral components *1–3* are listed in Table 4. The figure was prepared by the authors using the data of Ref. 137.

transformations of most of xenobiotics and pharmacological agents, as well as a number of endogenous components. The structure and transformations of nonheme di-Fe-centres of monooxygenases, which have only recently attracted the attention of researchers by their participation in biosynthetic pathways of the formation of natural compounds, were considered in review by Komor *et al.*,[140] jointly with analysis of MbS data. Similar reviews devoted to binuclear Fe-containing enzymes have also been published; they summarize the existing spectroscopic data, including the results of Mössbauer measurements. In those reviews a particular attention is paid to di-Fe^{III}-peroxo intermediates in biological and model systems,[141] as well as to the processes of formation and breaking of $-O-O-$ bonds in enzymes with Fe-containing centres, which are important both for key biological systems and for catalytic and synthetic reactions.[142] There is a section considering the use of Mössbauer measurements (including the SR-MbS variant) in review,[143] devoted to the spectroscopy of nitrogenases.

Numerous enzymes with nonheme di-Fe-centres (hemerythrin, various oxygenases, ferroxidases, hydrolases, *etc.*), which form association products of the O_2 molecule, were considered in detailed review.[122] The subsequent activation of the associated O_2 molecule is accompanied by the formation of more reactive active sites [di-$Fe^{II,III}$-superoxo- (with a ligand $-O-O^{\bullet}$), di-$Fe^{III,III}$-peroxo- ($-O-O-$), di-$Fe^{III,IV}$-oxo-, di-$Fe^{IV,IV}$-oxo-centres, *etc.*]; as a result, the substrates are oxidized to certain products. Data on the structure and electronic properties of reaction centres, intermediates and model complexes, obtained by a number of instrumental techniques (among which MbS plays an important role for gaining and confirming these data, including the spin state and degrees of oxidation of iron ions in binuclear centres), are discussed.

Pan *et al.*[144] combined spectrophotometric measurements (the stopped-flow method) and the rapid freeze-quench MbS methodology to investigate the successive reactions of hydroxylation and oxacyclization with participation of Fe- and 2-oxoglutarate-dependent oxygenase, which is involved in the biosynthesis of alkaloids of the class of saturated pyrrolizidines. The enzyme of endophytic fungus *Epichloë uncinata* was isolated after expression in genetically modified culture of *E. coli* and purified; native iron was removed by the EDTA treatment and dialysis; before the experiments, $^{57}Fe^{II}$ was introduced into the apoenzyme. Kinetic and spectroscopic measurements in enzyme solution in the presence of 2-oxoglutarate, substrate (1-*exo*-acetamidopyrrolizidine) and dissolved O_2 showed that the splitting of the C(2)–H bond in the substrate occurs with direct participation of intermediate in the form of a ferryl ($Fe^{IV}=O$) complex ($\delta = 0.28$ mm s^{-1}, $\Delta E_Q = -0.89$ mm s^{-1} at $T = 4.2$ K, $B_{ext} = 0.053$ T).

A combination of spectroscopic techniques, including MbS, was used to study the formation of Fe-site intermediates for the α-ketoglutarate-dependent nonheme Fe^{II}-enzyme deacetoxy-C-cephalosporin synthase (DAOCS), which catalyzes oxidative ring expansion of penicillin substrates in cephalosporin biosynthesis.[145] It has been shown that, in contrast to other α-ketoglutarate-dependent enzymes (in which iron is hexacoordinated when binding α-ketoglutarate), α-ketoglutarate binding for DAOCS leads to the formation of pentacoordinated (*i.e.*, coordinatively unsaturated) Fe^{II}-sites ($\delta = 1.24$ mm s^{-1}, $\Delta E_Q = 2.47$ mm s^{-1} at $T = 6$ K). The latter, in contrast to other hexacoordinated Fe^{II}-sites ($\delta = 1.22$ mm s^{-1}, $\Delta E_Q = 2.17$ mm s^{-1}), bind selectively O_2 and, forming a short-lived (nonaccumulating) ferryl-intermediate $Fe^{IV}=O$, in the presence of the substrate (penicillin) oxidize it to cephalosporin, being transformed into Fe^{III}. A component ($A = 40\%$) in the form of a doublet ($\delta = 0.43$ mm s^{-1}, $\Delta E_Q = 0.50$ mm s^{-1}) of high-spin Fe^{III} is fixed in the Mössbauer spectrum within a few seconds. In this case, α-ketoglutarate is decarboxylated to succinate, coordinated with the newly formed Fe^{III}-centre. Addition of α-ketoglutarate leads to reduction of Fe^{III} to Fe^{II}, making it possible to form a new enzymatic cycle.[145]

Spectroscopic (including MbS), crystallographic and biochemical studies[146] were carried out for the Fe-dependent oxidase UndA from the *Pseudomonas fluorescens* bacterium, which splits the C(3)–H and C(1)–C(2) bonds in dodecanoic (lauric) acid with the formation of 1-undecene and CO_2. It was shown that the cofactor is binuclear ($Fe^{II}-Fe^{II}$) and the substrate binding implies rapid attachment of an O_2 molecule with the formation of intermediate peroxo-$Fe_2^{III/III}$ detected using the rapid freeze-quench method. In the Mössbauer spectrum of a mixture of substrate with ^{57}Fe-substituted UndA (in the presence of O_2), frozen 0.01 s after mixing the reagents, the line intensity for the initial $Fe_2^{II/II}$ cluster decreases, and two overlapping quadrupole doublets of intermediate peroxo-$Fe_2^{III/III}$ arise ($\delta = 0.59$ and 0.56 mm s^{-1}, $|\Delta E_Q| = 1.07$ and 0.67 mm s^{-1}, respectively, at $T = 4.2$ K, $B_{ext} = 0.053$ T). This intermediate, according to the data obtained by the stopped-flow method, decomposes within 1 s; 5 s after, the Mössbauer spectrum of the mixture exhibits a doublet of the $Fe_2^{III/III}$ cluster ($\delta = 0.52$ mm s^{-1}, $|\Delta E_Q| = 0.97$ mm s^{-1}) against the background of $Fe_2^{II/II}$-cluster spectral signs.

Mössbauer spectroscopy was also used to study the Fe-containing clusters of special proteins, which implement synthesis of methanobactins — peptide compounds, which are secreted by methanotrophic bacteria to chelate copper (necessary for methane monooxygenase synthesis) and by other bacteria.[147]

The emission MbS studies of $^{57}Co^{2+}$-containing samples, mentioned in Subsection 1.2.2, after unsuccessful experiments of the 1970s with [$^{57}Co^{2+}$]-cobalamin as a coenzyme of ethanolamine ammonia lyase,[36] were resumed for the first time (as applied to the $^{57}Co^{2+}$-substituted active centre (AC) of metalloenzyme) only in the beginning of the XXI century.[148–151] An important step that confirmed the applicability and informativeness of the emission variant was the choice of the object of study — glutamine synthetase (GS, EC 6.3.1.2) from the *Azospirillum brasilense* bacterium — one of the key enzymes of nitrogen metabolism in living organisms (from mammals to bacteria). The molecule of this 12-subunit protein is composed of two hexameric rings aligned by planes (Fig. 11 *a*), with 12 ACs in intersubunit spaces, for which the main data on their structure (constant for bacterial GSs) were known.[36] The enzyme catalyzes biosynthesis of L-Gln from L-Glu and ammonium with participation of ATP. Each AC contains two main metal binding sites — n1 and n2, differing in amino acid residues (the n1 site contains three Glu residues, and the n2 site has two Glu residues and one His residue) — with possible coordination of H_2O molecules. Adenosine triphosphoric acid and Glu (substrate) penetrate from different sides of the AC 'double funnel'; there is an individual binding site for NH_4^+ (Fig. 11 *b*). Conventional

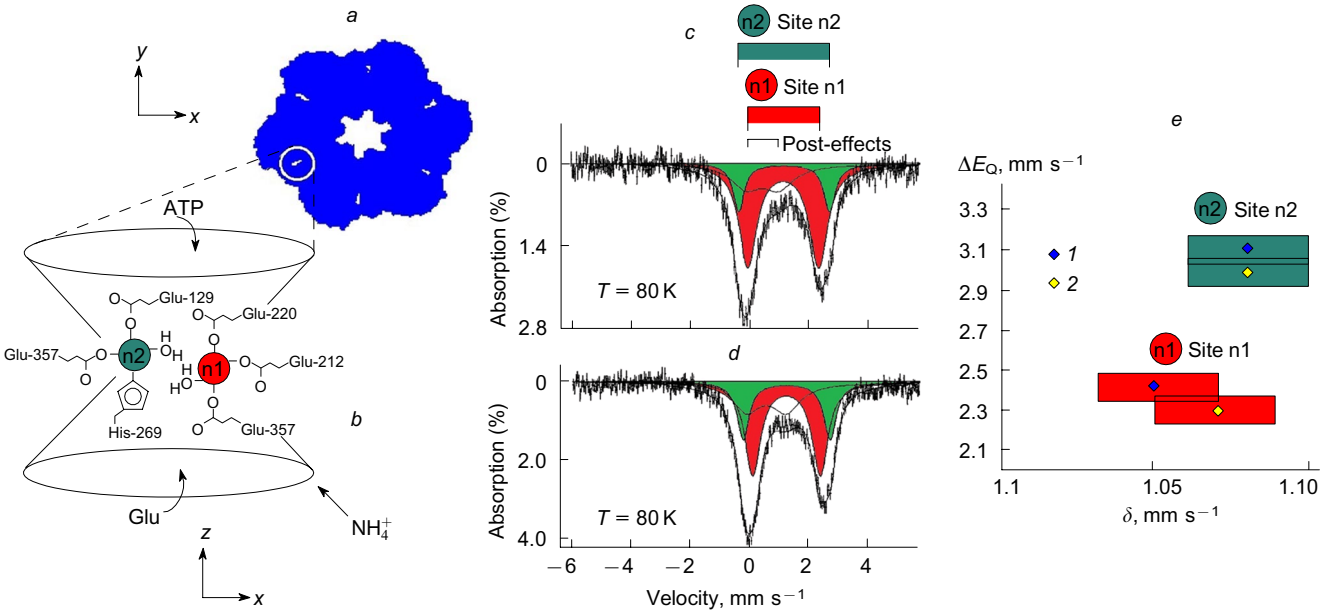


Figure 11. Schematic image (top view) of the (*a*) GS macromolecule of *Azospirillum brasilense* bacterium and (*b*) the structure of its active centre with the main cation binding sites n1 and n2, emission Mössbauer spectra of GS in a rapidly frozen solution (*c*) and after drying (*d*), and (*e*) the Mössbauer parameters (with an indication of the range of values), calculated for sites n1 and n2 in the frozen (*1*) and dried (*2*) samples. An enzyme with a degree of adenylylation of 18% after EDTA treatment and purification by dialysis, incubated with $^{57}Co^{2+}$ for 1 h at 295 K, was investigated. The lower envelope in Figs *c* and *d* is the total spectrum, obtained by fitting the experimental points as the sum of spectral components: quadrupole doublets corresponding to sites n1 and n2 and the doublet of nucleogenic $^{57}Fe^{3+}$ (due to post-effects); the positions of components are given above the spectrum. The data in Figs *c*–*e* are presented in the form comparable with the results of transmission measurements for ^{57}Fe. ATP is adenosine triphosphoric acid. The figure was prepared by the authors using the data of Refs 10, 149, 151.

activating cations for bacterial GSs are Mn^{2+} and Mg^{2+}; Co^{2+} can also play the role of an activating cation. In emission experiments one can use $^{57}Co^{2+}$ to replace native cations, because the Co^{2+} ion is 'physiological' for this enzyme (in contrast, for example, to Fe^{2+}).[149,151] The differences in the cation coordination in sites n1 and n2 predetermine possible differences in the emission Mössbauer spectra when binding $^{57}Co^{2+}$ in both AC sites of apoenzyme (the latter can be obtained by binding native cations from the AC with EDTA and subsequent removal of their EDTA complexes by dialysis).[149] With allowance for the presence of 24 main cation-binding sites (n1 and n2) in twelve ACs of the GS molecule, there is another important condition: the molar ratio $^{57}Co^{2+}$: GS must be less than 24 : 1. This condition corresponds to cation binding in only AC sites n1 and n2 (whose affinity to cations is many times higher than that of other functional protein groups) in order to avoid binding of an excess amount of $^{57}Co^{2+}$ with the protein (along with the AC) and corresponding complication of spectra.[151]

The emission Mössbauer spectra of $^{57}Co^{2+}$-doped GS sample in a frozen solution and in the dried state are similar (Figs. 11 *c*,*d*). The spectra demonstrate a superposition of three quadrupole doublets, corresponding to $^{57}Co^{2+}$ binding in two sites of the enzyme AC (the additional narrow doublet in both cases corresponded to the nucleogenic $^{57}Fe^{3+}$ as a result of the post-effects). The parameters of both forms for the initial $^{57}Co^{2+}$ in each site for the frozen solution and dry GS sample were close (Fig. 11 *e*), which can be interpreted as the preservation of the physiological enzyme activity (and, obviously, the AC site conformation) during drying. The insignificant variations could be caused by the change in the degree of hydration and small conformational differences in the solution and dry enzyme.[10] The assignment of the two doublets of nucleogenic $^{57}Fe^{2+}$ to site n1 (δ = 1.05–1.07 mm s^{-1}, ΔE_Q = 2.3–2.4 mm s^{-1}) and site n2 (δ = 1.08 mm s^{-1}, ΔE_Q = 3.0–3.1 mm s^{-1}; see Figs 11 *c*–*e*) corresponds to a higher symmetry of the coordination environment of site n1 (three Glu residues and H_2O) and, correspondingly, a smaller ΔE_Q value (site n2 contains, along with Glu, a coordinated His residue; see Fig. 11 *b*). Along with this, it is known[151] that for bacterial GS site n1 has a much higher affinity to cation than site n2, which is consistent with the higher relative intensity of doublets for site n1 (see Figs. 11 *c*,*d*). Note that fairly low δ values (< 1.1 mm s^{-1} for high-spin nucleogenic $^{57}Fe^{2+}$ at T = 80 K) correspond to the tetrahedral coordination of initial cations $^{57}Co^{2+}$ in both sites; this coordination, as was mentioned above, is typical of cobalt(II) in enzyme AC.[10] These results demonstrate informativeness of the emission MbS variant (in particular, when studying complex biological objects) and may serve as a starting point for further development of bioanalytical applications of the technique, in particular, with allowance for the possibility of using $^{57}Co^{2+}$ cations as an isostructural substituent in Zn-containing proteins.[36]

3. Supramolecular structures, biological tissues and organisms

3.1. Supramolecular structures and biological tissues of higher organisms

Specialized reviews on MbS applications in cellular biology of eukaryotes and physiology of animals can be found in the

chapters of monographs devoted to Fe–S clusters in biological systems.[152,153] The results of biophysical methods used to study the iron metabolism in mitochondria, considered in review[154], include also Mössbauer data.

MbS, ESR and biochemical methods were applied in a number of works[155–157] to investigate the state of iron in mitochondria (polymorphic cellular structures in which assembly of Fe–S clusters and biosynthesis of heme complexes occur) isolated from *Saccharomyces cerevisiae* yeast cells. Miao *et al.*[155] investigated the cells of *S. cerevisiae*, defective in synthesis of [2Fe–2S]-containing ferredoxin Yah1p of the mitochondria matrix, which is responsible for the biosynthesis of Fe–S clusters and heme prosthetic groups. Mössbauer measurements showed that, under aerobic conditions (O_2 bubbling), the mitochondria free of ferredoxin Yah1p accumulated excessive Fe^{III} (up to 10 mM) in the form of phosphate nanoparticles 2–4 nm in diameter with superparamagnetic relaxation. Treatment with dithionite led to reduction of Fe^{III} to Fe^{II} and its extraction from mitochondria. At the same time, iron was not accumulated in an anaerobic (argon) medium; a significant fraction of it was present in the form of high-spin Fe^{2+} ions. In correspondence with the results obtained, it was suggested that the accumulation of Fe^{III}-phosphate nanoparticles is due to either the absence of ligands impeding their formation in the mitochondria of wild-type (WT) yeast or the influence of oxygen in ferredoxin-free mitochondria.

Miao *et al.*[156] used a number of techniques (including MbS) to perform a complex biophysical characterization of the mitochondria isolated from the *S. cerevisiae* cells defective in synthesis of ATP-binding cassette (ABC) transporter Atm1p, which is involved in cellular metabolism of iron. In comparison with the mitochondria from WT cells of *S. cerevisiae*, the amount of Fe–S clusters and heme compounds in Atm1p-free mitochondria from aerobically grown cells was significantly reduced; the accumulation of nonheme Fe^{II} made oxidative damage stronger. In contrast, in Atm1p-free mitochondria from the cells grown in the absence of O_2, no excess iron was accumulated, and the level of Fe–S-clusters and heme compounds corresponded to that observed for WT mitochondria. These data of Mössbauer measurements and other techniques[156] show that the ABC transporter Atm1p is not involved in the assembly of Fe–S clusters of mitochondria, and the export of compounds performed with its assistance is necessary for assembly of Fe–S clusters in cytosol. In Atm1p-deficient mitochondria, accumulation of phosphate nanoparticles and damage of Fe–S clusters are secondary effects for only aerobically growing Atm1p-deficient cells as a result of the impact of reactive oxygen species. The latter can destroy Fe–S clusters and diminish the heme content in organelles.

In the next study[157] it was shown (using Mössbauer measurements) that the iron inside the mitochondria isolated from fermenting yeast exists in the form of nonheme high-spin Fe^{II}, Fe^{III} nanoparticles and mononuclear high-spin Fe^{III}. The content of these compounds in mitochondria did not decrease when treating the latter by Fe^{II}-chelating agents (not penetrating through the membrane), whereas 1,10-phenanthroline penetrating through the membrane bound Fe^{II} in mitochondria. Chelation of Fe^{II} occurred after ultrasonic destruction of mitochondria; dithionite, which did not reduce Fe^{III}-containing components of intact mitochondria, reacted with them after the membrane destruction by detergent. The Mössbauer spectra of intact yeast cells (see also Subsection 3.2), along with the spectral signs typical of isolated mitochondria, exhibited dominance of high-spin Fe^{III}-containing components;[157] this circumstance indicates that iron exists in yeast cells in two states: as dominant high-spin Fe^{III} beyond mitochondria and as their internal components.

A biophysical characterization of the mitochondria isolated from respiring (using O_2 for breathing) and fermenting yeast (in an oxygen-free environment), applying MbS and some other techniques, showed[158] that the distribution of mitochondrial iron in mitochondria (provided that its concentration is the same) was significantly different. When passing from respiring to fermenting cells, the amount of Fe-containing respiratory proteins in mitochondria decreased from ~40% of the total amount of iron by a factor of ~3, whereas nonheme high-spin iron(II), nonheme mononuclear high-spin iron(III) and Fe^{III} nanoparticles dominated. Based on these data, it was suggested that nonheme high-spin iron(II) plays a role of iron source in the biosynthesis of Fe–S clusters and heme.

Similar studies were performed on isolated yeast vacuoles[159] — cellular organelles, in which iron is accumulated, stored and mobilized when necessary for cell metabolism. The Mössbauer spectra of vacuoles isolated from fermenting *S. cerevisiae* cells, which were grown on a minimal medium with addition of 0.04 mM ^{57}Fe, demonstrated a dominance of two components (in different ratios), corresponding to mononuclear magnetically separated high-spin ($S = 5/2$) Fe^{III} complexes and oxohydroxide-containing Fe^{III} nanoparticles (the quadrupole doublet). Comparative studies, including Mössbauer measurements, showed that the complexes possessing a magnetic structure are most close in their properties (redox-activity, spectral changes with an increase in pH) and Mössbauer parameters to polyphosphate low-molecular Fe^{III} complexes (Fig. 12). Subsequent experiments[160] confirmed that practically all iron, zinc, manganese and (when the metallothionein synthesis is violated) copper ions are present in *S. cerevisiae* vacuoles in the form of low-molecular (0.5–1.7 kDa) complexes with polyphosphate (6–20 phosphate units, coordinated by one to three metal ions).

Mössbauer measurements of the isolated vacuoles of *S. cerevisiae* yeast showed that the polyphosphate-bound iron(III) (in the form of magnetically separated ions) in these vacuoles is not fixed in oxidized mononuclear state: it may be involved in reversible redox processes and ligand-exchange reactions, as well as be converted into nanoparticles.[161] The concentration, chemical forms and distribution of iron in yeast cell organelles depend strongly on the nutrient medium composition.

Mössbauer measurements may be fairly informative when studying the state and transformations of magnetic Fe-containing nanoparticles (components of liquid nanocomposites) when the latter are directly introduced into animal organs or tissues. The latter is important for developing methods of targeted drug delivery to organs via magnetic carriers. A group of Russian researchers[162] measured the Mössbauer spectra of rat brain samples, taken from euthanized animals and lyophilized prior to and three months after the transcranial introduction of chemically synthesized Fe_3O_4 nanoparticles, stabilized by dextran (~5 mg Fe without enrichment in isotope ^{57}Fe), in the form of a suspension in a 5-μL physiological solution into lateral ventricles of the brain (~5 μL in volume). A comparison of the MbS and histological data obtained three months after the Fe_3O_4 introduction did not reveal any

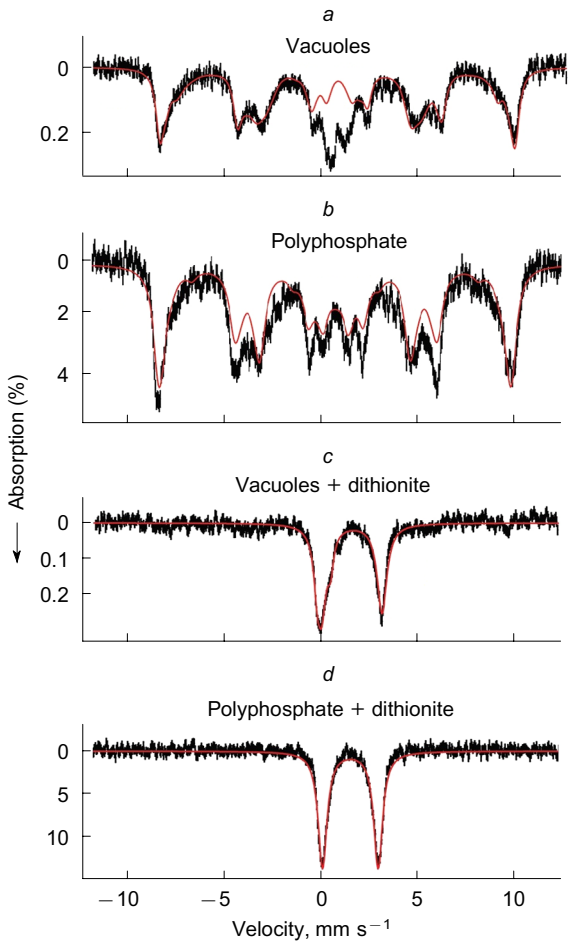


Figure 12. Mössbauer spectra (T = 6 K, B_{ext} = 0.05 T) of isolated vacuoles from fermenting cells of *S. cerevisiae*, grown on a minimal medium with addition of (*a*) ^{57}Fe (0.04 mM) and (*b*) polyphosphate complex of iron(III) at pH 5 before (*a*, *b*) and after (*c*, *d*) their treatment with dithionite. The red line in Figs *a* and *b* is the fit of the experimental data for high-spin mononuclear Fe^{3+} ions (δ = 0.54 mm s^{-1}, ΔE_Q = 0.39 mm s^{-1}; Ref. 159 for other parameters); the spectral parameters of the quadrupole doublets in Figs *c* and *d* are, respectively, the following: δ = 1.41 mm s^{-1}, ΔE_Q = 3.15 mm s^{-1}; δ = 1.39 mm s^{-1}, ΔE_Q = 2.88 mm s^{-1}. The figure was prepared by the authors using the data of Ref. 159.

presence of initial magnetic nanoparticles in brain tissues. At the same time the brain contained (in much larger amounts) iron(III) (detected in Mössbauer spectra in the form of a quadrupole doublet at T = 77 and 300 K with an absorption intensity of ~1.5%) as compared with the control animal brain (without Fe_3O_4 introduction). In the control sample containing iron (according to the data of histology with Fe-sensitive colouring) the latter was not detected in Mössbauer spectra.

The Mössbauer measurements [163–166] showed that magnetic ferrofluids (synthesized by the authors) containing ^{57}Fe oxide nanoparticles, being introduced into the organism of living mice, undergo biodegradation (within a few days) with a change in the iron chemical form, in particular, with the formation of ferritin-like compounds.[163, 164] Nevertheless, being incubated with living cells of the 4T1 breast cancer cell line, Fe_3O_4 nanoparticles barely underwent any changes (characteristic of biodegradation processes) during 5 days, although the Mössbauer spectra of lyophilized cells exhibited oxidation for a significant fraction of divalent iron in the particle composition.[167, 168]

The results of important and interesting Mössbauer study of the redistribution of dextrane–$^{57}Fe_3O_4$ magnetic nanoparticles between organs after the introduction of these particles into the lateral ventricle of living rat brain, as well as their transformation in organs, were reported in a series of studies;[169–171] magnetite nanoparticles were obtained by coprecipitation of $FeCl_2$ solutions (conventional reagent) and enriched $^{57}FeCl_3$ (1 : 2 mol). This approach provided a more than 30-fold excess of the ^{57}Fe fraction in particles in comparison with the use of natural iron, with the corresponding increase in the Mössbauer measurement sensitivity. It was shown [169] that the initial dextrane-stabilized magnetite nanoparticles introduced into brain were transformed (as a result of organic shell destruction) during a week into individual superparamagnetic nanoparticles, which had been observed previously when introducing similar initial particles into blood.[172] Several months after no Fe_3O_4 nanoparticles were found in the brain. Exogenous iron was already determined 2 h after the particle introduction into the brain; its content reached a maximum three days after and decreased during a week.[169, 170]

Exogenous iron was found in the spleen tissue also in the first hours after the magnetic nanoparticle injection into the brain. Their lines were pronounced in the spectra of liver and spleen tissues during a week and then almost disappeared within the two next weeks.[170] The Mössbauer spectra of the initial nanoparticles and lyophilized samples of rat brain and spleen tissues, illustrating the transformation of dextrane–magnetite nanocomposite during three months after its introduction into the animal brain, are presented in Fig. 13.

The concentration of Fe^{3+}-containing proteins in the rat brain 12 weeks after the introduction of nanoparticles (whose lines were not observed in the brain spectra by that time) was 5 times higher than in the control sample, which is indicative of biotransformation of Fe_3O_4 nanoparticles. It was noted in [170] that the somewhat nonmonotonic change in the amounts of Fe-containing components in brain, which was observed in some cases, can be explained by the nonuniform iron distribution (according to the histological analysis data), because Mössbauer measurements were performed on only part of brain. Nevertheless, the tendency of Fe_3O_4 nanoparticles to be transformed in the brain and (after their redistribution) other organs [169–171] is well pronounced (see also Fig. 13).

In our previous review [10] we considered work [173] where human and horse spleen tissues with a sufficiently high iron content were analyzed by MbS, and a series of detailed Mössbauer, ESR-spectroscopic and bioanalytical studies of mice organs (blood, brain, liver, heart), when animal feed contained ^{57}Fe additives.[174–177] The Mössbauer parameters of Fe-containing components of mice organs [175, 177] and human T-lymphocytes [178, 179] (high-spin heme and nonheme components, ferritin, Fe^{III}-oxohydroxide nanoparticles, mitochondria components) were compared.

Charitou *et al.*[180] investigated the Fe-containing components of mice blood, liver and spleen (including those with thalassemia) by MbS (the animal feed was not enriched with the ^{57}Fe isotope). Similar investigations of the blood of mice 1–9 months old, whose feed was enriched with the ^{57}Fe isotope, were carried out in the next study;[181] the spectral changes related to the hemoglobin level, presence of ferritin-like components and aging were also discussed. (These data

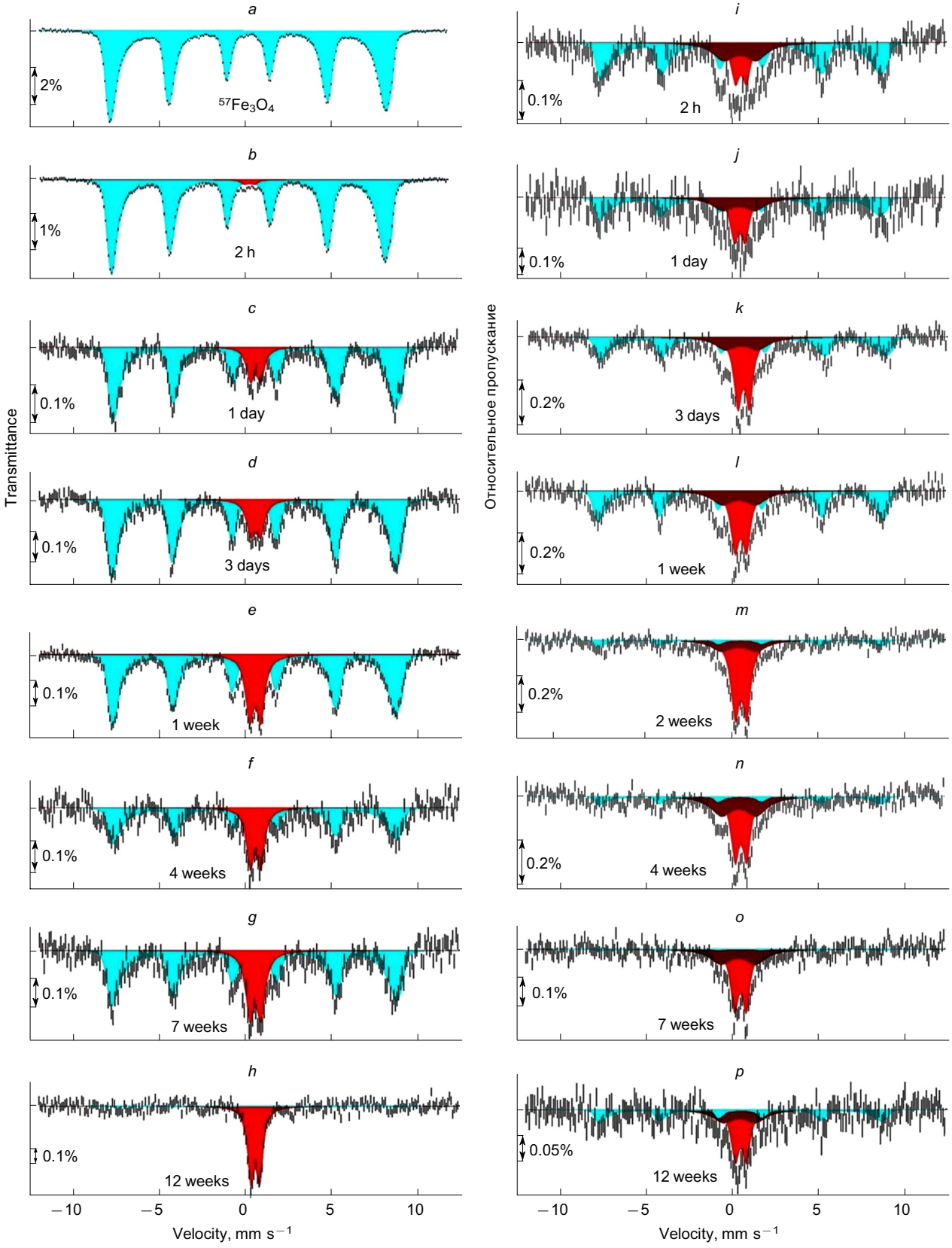


Figure 13. Mössbauer spectra (T = 78 K) of the (*a*) initial dextrane-stabilized Fe_3O_4 nanoparticles and lyophilized samples of rat brain (*b*–*h*) and spleen (*i*–*p*) tissues for different time intervals (indicated in panels) after the nanoparticle introduction: (black) spectral components obtained by fitting the experimental data, (blue) magnetically split sextets of nanoparticles, (red) quadrupole doublets of the oxide phases of Fe^{3+}-containing proteins (ferritin, hemosiderin and transferrin), and (dark red) low-spin hemoglobin doublets (δ = 0.35 mm s^{-1}, ΔE_Q = 2.0 mm s^{-1}). The figure was prepared by the authors using the data of Ref. 170.

concern mainly the biomedical MbS applications, which are beyond the scope of our review.)

We should note also the reviews of the last decade devoted to the MbS-aided study of the role of Fe-containing components of human brain (mainly in view of the pathogenesis caused by the Parkinson's disease, atypical parkinsonism and Alzheimer's disease).[182–185] The specific regions of brain, *substantia nigra* and *globus pallidus*, with a relatively high iron content (~0.2 mg per fresh tissue gram), were studied by MbS.[186] Based on the calculated areas of ferritin doublet lines for both regions [δ = 0.46(2) mm s^{-1}, ΔE_Q = 0.70(4) mm s^{-1} at T = 90 K; Γ = 0.45(5) mm s^{-1}), the iron content in these tissues was estimated. It was shown that the *substantia nigra* and *globus pallidus* tissues of patients with progressive supranuclear palsy (atypical parkinsonism) are characterized by an elevated Fe concentration (on average by ~60 and ~40%, respectively). These data may be of interest for understanding the role of iron compounds in neurodegenerative diseases, which is still being discussed (with consideration of the MbS data).[187]

Solti *et al.*[188] used MbS to observe fairly rapid iron incorporation (from $^{57}Fe^{III}$ citrate as an iron source) into iron–sulfur clusters [4Fe–4S] and heme cofactors of plant proteins in chloroplasts isolated from sugar beet (*Beta vulgaris*); the iron from iron(II) citrate complexes did not penetrate through the membrane internal shell. Müller *et al.*,[189] based on the MbS data obtained at low temperatures (including measurements in an external magnetic field), described for the first time the coordination structure of Fe^{III} and Fe^{II} complexes with nicotianamine, which is synthesized in plant tissues from S-adenosyl-L-methionine and is believed to be the key component of iron homeostasis in plants. It was also shown that isolated chloroplasts from leaves of the rape plant (*Brassica napus*) accumulated iron from Fe^{III} citrate complexes much more efficiently than from Fe^{III} or Fe^{II} complexes with nicotianamine.[189]

3.2. Microorganisms

One of most interesting analytical applications of MbS in studying the state and distribution of Mössbauer nuclide forms in microorganism cells is the analysis of the iron transformation processes in magnetotactic bacteria. The results of early (published in the 1980s) Mössbauer studies of biogenic magnetite (Fe_3O_4), present in the form of unique organelles — magnetosomes, organized into chains of magnetic nanocrystals,[190] — in *Aquaspirillum magnetotacticum* cells, were considered in reviews.[28, 133] Due to the magnetosomes synthesized by magnetotactic bacteria, the latter are sensitive to weak geomagnetic field; as a result, they can find regions with low concentrations (of the order of 0.5–1 mg L^{-1}) of dissolved oxygen, which are favorable for growth. The Mössbauer spectra of *A. magnetotacticum* biomass contained two clearly distinguishable magnetically split sextets, characteristic of Fe_3O_4. The formal composition of this oxide is $[Fe^{3+}]_A[Fe^{2+}Fe^{3+}]_BO_4^{2-}$, where A and B are sites with, respectively, tetrahedral and octahedral coordination of O^{2-} ions around iron ions; the latter in the B sublattice have a mixed oxidation state of 2.5+ and, correspondingly, yield only one sextet. The spectra of *A. magnetotacticum* biomass also exhibited, against the background of magnetic sextets, several weaker quadrupole doublets of high-spin Fe^{III} in the composition of bacterial ferritins and intracellular complexes of high-spin Fe^{II}, representing the rest of the cellular iron pool.

A good illustration of the bioanalytical potential of MbS, supplementing the aforementioned studies, is the results obtained by Böttger *et al.*,[191] who investigated the transformations of iron assimilated from the environment, with the formation of biogenic Fe_3O_4 in the composition of magnetosomes present in the cells of another magnetotactic bacterium: *Magnetospirillum gryphiswaldense*. A suspension of bacteria was supplemented (in the middle of the logarithmic growth phase) with a citrate complex of $^{57}Fe^{III}$ (after its assimilation the contribution of any newly formed ^{57}Fe-containing cell components to the Mössbauer spectrum will be ~45 times larger than that from the same amounts of natural iron compounds, containing only 2.19% ^{57}Fe). After different time intervals, biomass samples were taken, washed, frozen in liquid nitrogen and placed in a cryostat to measure their Mössbauer spectra. The membrane and cytoplasmic (after filtration, containing proteins with a molecular weight >100 kDa) fractions of cells and isolated magnetosomes were investigated in the same way (Fig. 14).

As soon as 20 min after the contact of bacteria with the $^{57}Fe^{III}$ citrate complex, different components of ^{57} Fe^{III}-containing cells can clearly be seen in the spectrum; these are, primarily, the doublet of high-spin Fe^{III} in the composition of ferritin (δ = 0.47 mm s^{-1}, ΔE_Q = 0.77 mm s^{-1}) and the doublet due to the significant amount of high-spin iron(II) (δ = 1.27 mm s^{-1}, ΔE_Q = 2.81 mm s^{-1}), which is characteristic of many bacteria.[10] The dynamics of spectral changes with time showed that, after 40-min incubation, there is an increase in only the content of magnetite characterized by two magnetically split sextets for the A and B sites with the following parameters: δ_A = 0.38 mm s^{-1}, $B_{eff,A}$ = 49.5 T; δ_B = 0.76 mm s^{-1}, $B_{eff,B}$ = 47.4 T (Fig. 14*a*). The spectrum of the membrane fraction (Fig. 14*b*) at T = 130 K contains a dominant quadrupole doublet of ferritin (δ = 0.47 mm s^{-1}, ΔE_Q = 0.77 mm s^{-1}) and a quadrupole doublet of iron(II), related to the membrane (δ = 1.26 mm s^{-1}, ΔE_Q = 2.86 mm s^{-1}); *i.e.*, the same components with practically the same parameters that were observed in the spectra of intact cells. However, the spectrum of the membrane fraction contains also traces of magnetically split magnetite sextets, but with smaller (as compared with intact cells) B_{eff} values (δ_A = 0.38 mm s^{-1}, $B_{eff,A}$ = 46.8 T; δ_B = 0.76 mm s^{-1}, $B_{eff,B}$ = 44.8 T). These parameters correspond to magnetite nanocrystallites less than 6 nm in size; this circumstance indicates that the initial stages of magnetite formation occur on the cytoplasmic membrane.[191]

The spectrum of the cytoplasmic fraction (Fig. 14*c*) at T = 77 K contains only the ferritin doublet (δ = 0.47 mm s^{-1}, ΔE_Q = 0.77 mm s^{-1}), which is transformed into a magnetic sextet at T = 4.2 K (δ_A = 0.49 mm s^{-1}, B_{eff} = 47.4 T; A = 86.8%), and a quadrupole doublet of the superparamagnetic (even at this temperature) Fe^{III}-containing component (δ = 0.49 mm s^{-1}, ΔE_Q = 0.77 mm s^{-1}; A = 13.2%). Obviously, the latter is the most highly dispersed fraction of the ferritin core (the presence of protein with a molecular weight >100 kDa in this fraction was confirmed by gel electrophoresis).[191] Isolated magnetosomes have a characteristic spectrum as a set of magnetically split magnetite sextets (Fig. 14*d*; δ_A = 0.38 mm s^{-1}, $B_{eff,A}$ = 49.9 T; δ_B = 0.76 mm s^{-1}, $B_{eff,B}$ = 47.9 T).

Note that similar Mössbauer measurements were performed using an *M. gryphiswaldense* mutant strain, defec-

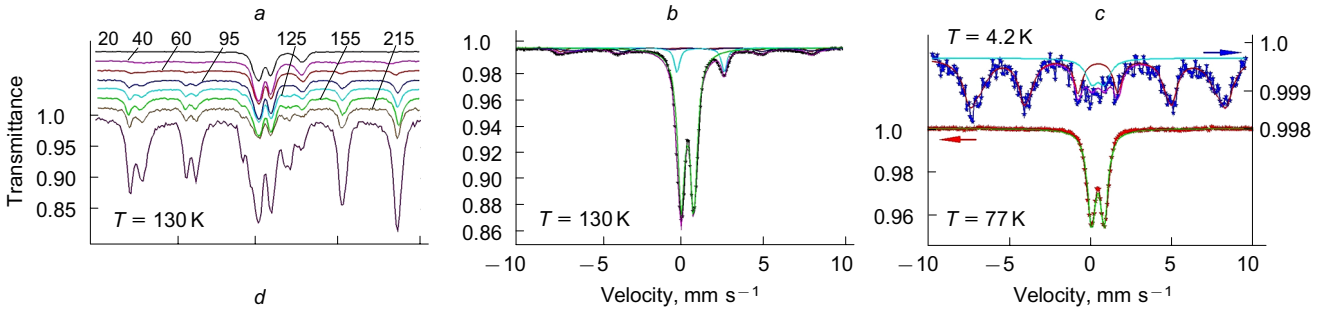


Figure 14. Mössbauer spectra of (*a*) *Magnetospirillum gryphiswaldense* biomass recorded for different time intervals (indicated in the panel) after adding $^{57}Fe^{III}$ citrate complex, (*b*) membrane and (*c*) cytoplasmic (M > 100 kDa) fractions of cells, and (*d*) isolated magnetosomes. (*a*) The numbers near spectra represent the time (in minutes) that passed after adding the $^{57}Fe^{III}$ complex, the spectra for the times from 20 to 215 min are shifted upwards from the zero line (the lower spectrum corresponds to a time of 1230 min) in order to separate them; (*b*) the total spectrum and the dominant ferritin doublet are shown in violet and green, respectively; the cyan doublet is due to the high-spin Fe^{II} complex; the minor magnetic components (brown and blue lines) correspond to small magnetite particles; (*c*) the ferritin sextet and quadrupole doublet of high-spin iron(III) (fitted by one quadrupole doublet of ferritin) are shown in red and blue, respectively; (*d*) the total spectrum is shown in violet and the magnetically split sextets of magnetite sites A and B are in brown and blue, respectively. The figure was prepared by the authors using the data of Ref. 191.

tive in production of regulatory protein Fur (Ferric uptake regulator).[192] It was shown that this regulator controls the general iron homeostasis and participates in its biomineralization with the formation of magnetite crystals, balancing this process with the needs of the cell for Fe-containing biochemical components. In continuation of the study of intracellular biomineralization of iron with the formation of Fe_3O_4-containing magnetosomes, in particular, using MbS,[193] it was experimentally shown recently[194] that the bacterial ferritins of *M. gryphiswaldense* (MSR-1 strain) are not involved in the biogenesis of magnetite crystals. The experiments were performed using, along with the initial wild-type MSR-1 strain of *M. gryphiswaldense*, mutant strains defective in the synthesis of proteins — members of the superfamily of ferritins in bacteria,[195] such as bacterioferritin (Bfr, strain Δ*bfr12*), DNA-binding protein from starved cells (Dps, strain Δ*dps*) or both proteins (strain Δ*dps*/*bfr12*, which grows only anaerobically, being inhibited by traces of oxygen). All these strains synthesized magnetosomes; note that both the initial strain and the strains of obtained mutants did not reveal any significant differences in the

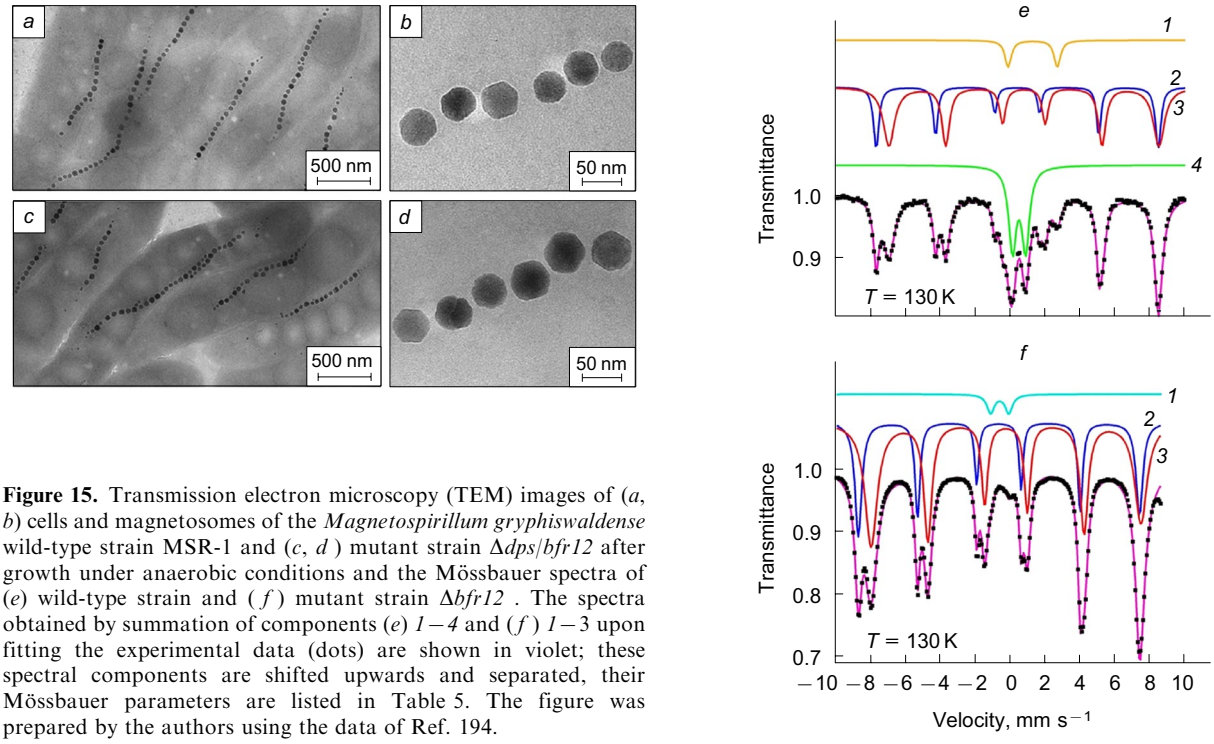


Figure 15. Transmission electron microscopy (TEM) images of (*a*, *b*) cells and magnetosomes of the *Magnetospirillum gryphiswaldense* wild-type strain MSR-1 and (*c*, *d*) mutant strain Δ*dps*/*bfr12* after growth under anaerobic conditions and the Mössbauer spectra of (*e*) wild-type strain and (*f*) mutant strain Δ*bfr12*. The spectra obtained by summation of components (*e*) *1*–*4* and (*f*) *1*–*3* upon fitting the experimental data (dots) are shown in violet; these spectral components are shifted upwards and separated, their Mössbauer parameters are listed in Table 5. The figure was prepared by the authors using the data of Ref. 194.

Table 5. Mössbauer parameters of spectral components for biomass of *Magnetospirillum gryphiswaldense* wild-type strain MSR-1 and mutant strain Δ*bfr12*, measured at $T = 130$ K (according to the data of Ref. 194).

Sample (intact cells)	Position in Fig. 15 *e*,*f*	Metabolite (spectral component)	δ, mm s^{-1}	ΔE_Q, , mm s^{-1}	Γ, mm s^{-1}	B_{eff}, T	A (%)
WT (see Fig. 15,*e*)	*1*	Fe^{2+} (high-spin)	1.26	2.82	0.43	–	6.1
	2	Magnetite (site A)	0.38	0	0.30	49.5	23.7
	3	Magnetite (site B)	0.76	0	0.52	47.5	47.5
	4	Ferritin	0.48	0.75	0.52	–	22.7
Δ*bfr12* (see Fig. 15*f*)	*1*	$[4Fe-4S]^{2+}$ cluster	0.40	1.04	0.50	–	3.0
	2	Magnetite (site A)	0.36	0	0.34	49.3	32.3
	3	Magnetite (site B)	0.76	0	0.55	47.4	64.7

sizes of Fe_3O_4 crystals and average numbers of magnetosomes per cell [194] (Figs 15 *a*–*d*).

Analysis of the Mössbauer spectra (Figs 15 *e*,*f* and Table 5) showed that the initial WT strain is characterized by the dominance of two sextets from biogenic magnetite (components A and B, making in sum 71.2% of the spectral area). There are also two quadrupole doublets in the spectrum: a component due to the ferritin core ($A = 22.7\%$) and a component corresponding to high-spin Fe^{II} complexes ($A = 6.1\%$) with parameters characteristic of cytoplasmic phosphorylated carbohydrate complex of iron(II) [194] (the parameters of these complexes are close for many bacteria [10, 194]). The spectrum of the mutant strain Δ*bfr12*, as expected, demonstrates the absence of ferritin lines and the dominance of magnetite sextets ($A = 97\%$) with practically the same parameters as for the WT strain. There is also a minor ($A = 3\%$) component of protein with the $[4Fe-4S]^{2+}$ cluster, having characteristic parameters;[196] it was not detected for the WT (where it is obviously present in smaller amounts and is obscured by other component lines).[194] Thus, it was shown for the first time (using MbS and mutant strains defective in the synthesis of ferritin-like proteins) for this bacterium *M. gryphiswaldense* MSR-1 that, along with the functional and structural features of its Bfr,[194] the pathway of iron biomineralization with the formation of intracellular magnetosomes is independent of ferritins. Note that in the previous studies (see, *e.g.*,[193, 197, 198]) the key role in this process was attributed to ferritin-like components.

A comparison of the role of abiotic (chemical) and biotic (induced by microorganisms) factors in the formation of magnetite from the mineral ferrihydrite, as well as the role of soil organic materials (microbial biomass and humic acids), was performed (using the results of Mössbauer measurements).[102] It was noted that the abiotic transformation of ferrihydrite (induced by Fe^{2+}_{aq} ions) occurs much more rapidly than the biotic transformation (carried out by Fe^{III}-reducing bacteria); however, the rate of magnetite formation from ferrihydrite is determined by a combination of such factors as the concentration of Fe^{2+}_{aq}, its uptake by cells and passivation of ferrihydrite particles by microbial biomass.

Along with the study of magnetotactic bacteria, MbS is widely applied to study the processes of formation and to analyze biogenic mineral deposits and transformation of minerals as a result of the vital activity of microorganisms. These data make a great contribution to understanding the fundamental regularities of the biogeochemical processes and vital functions of iron(II)-oxidizing and iron(III)-reducing microorganisms in soil and aqueous media.

Larese-Casanova *et al.*[199] demonstrated the influence of the geochemical factors of the medium (pH, the presence of complexing inorganic anions and humic acids) on the oxidation rate of Fe^{II} by the nitrate-reducing bacterium *Acidovorax* sp. and on the mineral formation. MbS and micro-X-ray diffraction were used. It was shown that the following minerals are formed at pH 7.0 in the absence of strong complexing agents: lepidocrocite (γ-FeOOH, 90%) and goethite (α-FeOOH, 10%); they were identified using the Mössbauer parameters of their magnetic sextets ($\Delta E_Q \approx 0.02$ and -0.2 mm s^{-1}, $B_{eff} \approx 45$ and 50 T, respectively, at $T = 4.5$ K). An increase in pH to 8 and in the concentration of HCO_3^- and humic acids to 3 mM facilitated the goethite phase accumulation. In the presence of phosphate (0.2 – 3 mM) the Fe^{II} oxidation rate sharply decreased [primarily due to the formation of a precipitate of vivianite $Fe_3(PO_4)_2$], and the strong broadening of sextets in the Mössbauer spectra of oxidized samples hindered identification of Fe^{III} phases, which contained phosphates and were most likely amorphous and (or) finely-dispersed.

Biogenic anaerobic reduction of lepidocrocite to magnetite by dissimilatory Fe^{III}-reducing bacterium *Shewanella putrefaciens* (with formate as an oxidizable substrate) was investigated [200] using a miniaturized Mössbauer spectrometer MIMOS-II, operating in the γ-radiation backscattering geometry. The degree of deviation from stoichiometry for biogenic magnetite, which turned out to be fairly low (in the absence of intermediate phases of the green rust type; see below), was determined from the intensity ratio for the two characteristic sextets of magnetite.

Chistyakova *et al.*[201] used MbS to study (under oxygen-free conditions) the biogenic reduction of synthetic amorphous iron(III) hydroxide (AIH) by a culture of anaerobic alkaliphilic bacterium *Geoalkalibacter ferrihydriticus*, using acetate as a substrate: electron donor. The bacterium, isolated from bottom sediments of a low-mineralized carbonate-containing lake (with optimum pH 8.6 of the medium), partially reduced AIH at its content up to ~0.05 M Fe^{3+} in the suspension with the formation of siderite ($FeCO_3$; characteristic quadrupole doublet: $\delta \approx 1.2-1.3$ mm s^{-1}, $\Delta E_Q \approx 1.8$ mm s^{-1} at $T = 300$ K [34, 201]). With an increase in the AIH concentration in the suspension >0.07 M, magnetic components characteristic of fairly large magnetite particles arose in the Mössbauer spectra at $T = 300$ K and with decreasing siderite content. An addition of anthraquinone-2,6-disulfonate (up to a concentration of $n_q \approx 0.12$ mM), which is used by cells as a redox-active 'electron shuttle', to the cultivation medium for *G. ferrihydriticus* with AIH (0.1 M Fe^{3+}) led to an increase in the AIH reduction rate and rise in the magnetic phase intensity in Mössbauer spectra. An

enhancement of the relaxation character of magnetic spectral component was observed at $n_q > 1$ mM; this enhancement is a manifestation of a decrease in particle size.[201]

As was shown by Chistyakova *et al.*,[202] the same anaerobic alkaliphile *G. ferrihydriticus* in the absence of acetate, needed by the bacterium for dissimilatory iron(III) reduction, can perform transformation of Fe^{III}-containing minerals in the presence of *Anaerobacillus alkalilacustre* bacterium, isolated from the same lake. This bacterium enzymatically metabolizes mannitol (which is not used by *G. ferrihydriticus*) and releases acetate and other organic molecules used by *G. ferrihydriticus*. An MbS study of a binary culture of *G. ferrihydriticus* and *A. alkalilacustre* in HCO_3^--containing medium revealed reduction of AIH with the formation of siderite (at an AIH content of 0.01 M Fe^{3+} in the suspension), constituting about a half of the Fe-containing product, and lepidocrocite (with characteristic quadrupole doublets at $T = 295$ and 77 K; $A \approx 28\%$). As the low-temperature Mössbauer measurements showed, at an AIH content of 0.10 M Fe^{3+}, there was accumulation of (along with siderite) a magnetic phase, described as nonstoichiometric magnetite or its mixture with maghemite.[202] These results indicate a significant role of the ratio of electron donor and acceptor in an aqueous medium in the formation of various Fe^{II}-containing minerals.

Similar partial dissimilatory reduction of Fe^{III} by cultures of anaerobic bacteria was studied (using MbS) for such minerals as glauconite[203] (dioctahedral mica with a low content of Fe^{2+} and the general composition $K_{<1}(Fe^{3+},Fe^{2+},Al,Mg)_{2-3}[Si_3(Si,Al)O_{10}](OH)_2 \cdot n\,H_2O$) and biotite[204] (trioctahedral aluminosilicate mica with a somewhat higher initial content of Fe^{2+}) with titanium oxide impurities (0.16% in glauconite and 1.54% in biotite). In these cases the *G. ferrihydriticus* bacterium was used either as a monoculture (with acetate as a substrate) or in the composition of a binary culture, jointly with the anaerobic alkaliphilic bacterium *Clostridium alkalicellulosi*, which cannot reduce Fe^{III} but hydrolyzes cellulose to low-molecular substrates — electron donors for Fe^{III}-reducing *G. ferrihydriticus*. An analysis of complex Mössbauer spectra of minerals and products of their biotransformation showed the formation of new magnetically ordered phases, containing nonstoichiometric magnetite and maghemite (with possible replacement of iron with titanium and aluminium ions), whose amount increased more rapidly upon interaction of minerals with the binary culture.[203, 204] However, it should be noted that a subsequent study of this group in cooperation with other researchers,[205] where the interaction of *G. ferrihydriticus* with glauconite and biotite in carbonate alkaline media (pH 9) was analyzed, it was found (using chemical and MbS measurements) that the acetate content increased simultaneously with the transformation of the aforementioned phyllosilicates during the formation of magnetic phases. This result can be interpreted only as a possibility for *G. ferrihydriticus* to use carbonate as an electron acceptor with the formation of acetate and simultaneous oxidation of Fe^{2+} in the composition of aluminosilicate minerals. This result (unusual for a Fe^{II}-oxidizing bacterium) confirmed by genome analysis and thermodynamic calculations,[205] may indicate participation of *G. ferrihydriticus* in the formation of Fe^{III}-containing mineral deposits and production of organic compounds in the Precambrian era.

When studying the products of biotransformation as a result of the vital activity of acetogenic carbonate-reducing bacterium *Fuchsiella ferrireducens*, Mössbauer spectra of the products of biotransformation of Fe^{3+}-containing ferrihydrite, Fe^{2+}/Fe^{3+}-containing magnetite and Fe^{2+}-containing siderite, in the presence of ethanol (0.05 M) as a substrate, were analyzed.[206] It was found that, along with the reduction of Fe^{3+} from ferrihydrite (with the formation of siderite and a magnetic phase containing hematite and maghemite), separate transformation of magnetite and siderite also occurred; the Mössbauer measurements for siderite did not show any change in the iron oxidation state. It was concluded that *F. ferrireducens* can both reduce iron(III) in the composition of minerals and oxidize iron(II), including that formed in the biogenic process (for example, oxidizing biogenic magnetite to a mixture of hematite and maghemite). The biotransformation of siderite (found by MbS) can also be explained by the oxidation of Fe^{2+} to a Fe^{3+}-containing phase, which was then reduced by bacteria to biogenic siderite with somewhat different Mössbauer parameters.

Recently Zavarzina *et al.*[207] studied the transformation of minerals (ferrihydrite and siderite) by a binary association of obligate syntrophic ethanol-oxidising bacterium *Candidatus 'Contubernalis alkalaceticum'* with the facultative lithotroph *G. ferrihydriticus* using Mössbauer measurements at room temperature and at 82 K. A more detailed low-temperature Mössbauer study of these processes, including ESR measurements, was also performed.[208] The results confirmed that *G. ferrihydriticus* can switch from ferrihydrite reduction (using ethanol as an electron donor) to syntrophic homoacetogenesis with reduction of CO_2 (in this case ethanol is supplied to the partner in association); in the presence of siderite acetogenesis occurs with the aid of both siderite and H_2 as electron donors. Mössbauer data[208] showed that the syntrophic binary culture transformed ferrihydrite first to a fine-grained mixture of magnetite and maghemite, with subsequent reduction of magnetite to siderite and iron oxyhydroxycarbonate—the so-called green rust (GR).§ In contrast, natural hydrothermal siderite was partially oxidized by the association (with carbonate reduction) to GR and a mixture of magnetite and maghemite particles.

As a model of formation of secondary mineral phases of Fe^{III}-containing formations on the Earth in the Precambrian period, the authors[209] showed a possibility of green rust oxidation to iron(III) oxyhydroxides in the absence of oxygen by anoxygenic phototrophic Fe^{II}-oxidizing bacteria. Carbonate-containing GR was synthesized, the partial leaching of Fe^{2+} cations from this GR in phosphate–bicarbonate diluted solutions was investigated, the composition of GR components before and after incubation with *Rhodobacter ferrooxidans* (strain SW2) and *Rhodopseudomonas palustris* (strain TIE-1) cells under anaerobic conditions was analyzed, and Mössbauer spectra were recorded (Fig. 16).

The results showed that both phototrophic bacteria, in the light under anaerobic conditions, transform GR, oxidizing most of Fe^{II} cations present in GR (see Figs. 16 *d*,*e*, spectral components $GR(II)_1$ and $GR(II)_2$; $\delta \approx 1.2-1.4$ mm s^{-1}, $\Delta E_Q \approx 2.3-3.4$ mm s^{-1}; in sum 72–74% of the total spectrum area). In this case, weakly ordered iron(III) oxyhydroxide with parameters of quadru-

§ Mineral described by the general formula $[Fe^{II}_{1-x}Fe^{III}_x(OH)_2]^{x+} \cdot [(x/n)A^{n-}, m\,H_2O]^{x-}$, where x is the molar fraction $[Fe^{III}]/([Fe^{II}]+[Fe^{III}])$, A^{n-} are intercalated anions.

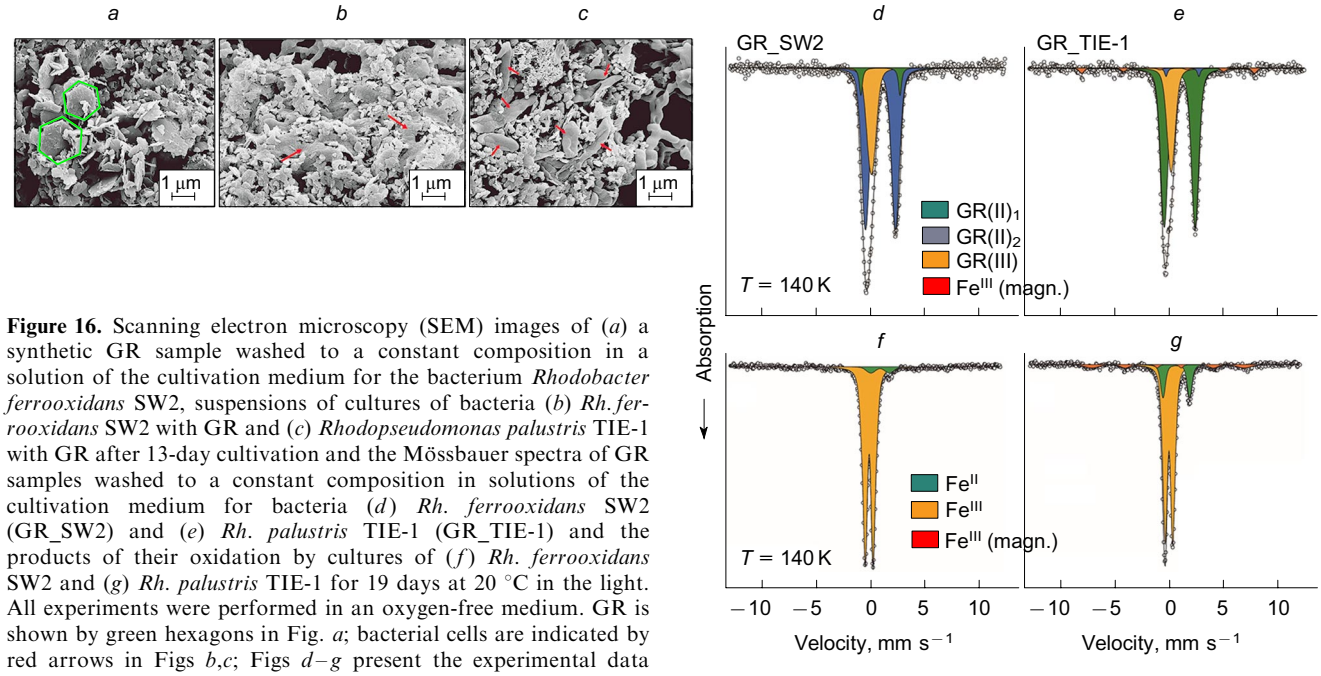


Figure 16. Scanning electron microscopy (SEM) images of (*a*) a synthetic GR sample washed to a constant composition in a solution of the cultivation medium for the bacterium *Rhodobacter ferrooxidans* SW2, suspensions of cultures of bacteria (*b*) *Rh. ferrooxidans* SW2 with GR and (*c*) *Rhodopseudomonas palustris* TIE-1 with GR after 13-day cultivation and the Mössbauer spectra of GR samples washed to a constant composition in solutions of the cultivation medium for bacteria (*d*) *Rh. ferrooxidans* SW2 (GR_SW2) and (*e*) *Rh. palustris* TIE-1 (GR_TIE-1) and the products of their oxidation by cultures of (*f*) *Rh. ferrooxidans* SW2 and (*g*) *Rh. palustris* TIE-1 for 19 days at 20 °C in the light. All experiments were performed in an oxygen-free medium. GR is shown by green hexagons in Fig. *a*; bacterial cells are indicated by red arrows in Figs *b*,*c*; Figs *d*–*g* present the experimental data (dots) and total spectra (envelopes), with coloured spectral components, corresponding to two Fe^{II}-containing GR components [$GR(II)_1$ and $GR(II)_2$] and Fe^{III}-containing components: GR(III) (*d*, *e* contain unresolved quadrupole doublets with low ΔE_Q) and Fe^{III} (*f*, *g* contain quadrupole doublets of Fe^{III} oxyhydroxide with parameters characteristic of ferrihydrite); the traces of a magnetically split phase (for *e*, *g*) correspond to a goethite (α-FeOOH) impurity. The figure was prepared by the authors using the data of Ref. 209.

pole doublets characteristic of ferrihydrite is formed ($\delta \approx 0.45-0.47$ mm s^{-1}, $\Delta E_Q \approx 0.73-0.86$ mm s^{-1} at $T = 140$ K; up to 77–95% of the total spectrum area; Figs. 16 *f*–*g*). Thus, it was proven experimentally that such anaerobic processes in aqueous media with participation of phototrophic Fe^{II}-oxidizing bacteria could facilitate the formation of ferric deposits, containing Fe^{III}-oxyhydroxide minerals.[209]

The role of iron compounds, their state, localization and transformations in microorganism cells were discussed (using the data of Mössbauer measurements, which allow one to gain insight into cells or their macrocomponents) in many interesting studies, including those published in the last decade; some of them were discussed in reviews.[10,210]

Spectroscopic techniques, including MbS, were used[211] to characterize the cellular iron of fermenting yeast *S. cerevisiae* under conditions of iron deficiency and at an elevated iron concentration in the medium. In the case of iron deficiency (1 μM $^{57}Fe^{III}$ citrate) the cells contained ~0.15 mM Fe, mainly in the form of nonheme high-spin iron(II), as well as mitochondrial iron. {The mitochondria isolated from these cells contained low- and high-spin heme iron, a fraction of nonheme high-spin iron(II), and clusters $[4Fe-4S]^{2+}$, $[2Fe-2S]^{+}$ ($S = 1/2$) and $[2Fe-2S]^{2+}$.} The $[2Fe-2S]^{2+}$ clusters had not been observed previously, because their Mössbauer lines had been obscured by the absorption of Fe^{III} nanoparticles, absent in the cells under conditions of Fe deficiency. At normal (10 μM) and elevated (⩾100 μM) concentrations of iron in the medium, its content in fermenting cells was 0.40–0.45 mM. The content of nonheme high-spin Fe^{II} beyond mitochondria decreased by a factor of ~3, while the concentration of vacuolar nonheme high-spin Fe^{III} reached a cellular maximum (~0.30 mM). The mitochondria isolated from these cells contained a larger amount of nonheme high-spin Fe^{II} and many Fe^{III} nanoparticles. Note that, for a medium with iron excess in the concentration range with limits differing by a factor of 250 (0.04–10 mM), the iron content in the cells was similar; this circumstance reflects the protective limitation of its import.[211]

In the next study Cockrell *et al.*[212] investigated (using MbS and other spectroscopic and biochemical methods) the state and concentration of iron in *S. cerevisiae* cells at a sufficiently high iron concentration (40 μM) in the medium and under conditions of iron deficiency (1 μM) (Figs. 17 *a*,*b*). In the latter case the iron content in the cells was on average lower by a factor of ~3; the central doublet ($A = 60\%$), corresponding to $[4Fe-4S]^{2+}$ clusters ($S = 0$) and low-spin $^{57}Fe^{II}$-heme centres, dominated in the Mössbauer spectrum; there were also small contributions from the doublets of high-spin $^{57}Fe^{II}$ (28%) and $^{57}Fe^{III}$-containing nanoparticles (~5%; spectrum *b*). The magnetically split component of nonheme high-spin $^{57}Fe^{III}$ was absent (although its small contribution could be indistinguishable against the noise background); this is confirmed by the absence of its signal ($g = 4.3$) in the ESR spectrum.[212] Cells of genetically modified yeast with deleted gene *CCC1*, responsible for iron import into vacuoles, were studied under similar conditions (Fig. 17 *c*,*d*). In this case the amount of accumulated iron was reduced by approximately a quarter only at 40 μM Fe in the medium (see Fig. 17 *c*); as compared with the WT cells, at 40 μM iron in the medium, the fraction of the sextet of high-spin $^{57}Fe^{III}$ in the spectrum decreased (from 55 to 30%), but one could observe a significant increase in the fraction of nonheme high-spin $^{57}Fe^{II}$ (from 13 to 30%) and the central doublet components (from 8 to 19%). The increased content of nonheme high-spin $^{57}Fe^{II}$ in mutant cells (~0.11 mM in comparison with ~0.06 mM in WT cells) caused their enhanced damage as a result of the formation of reactive oxygen species according

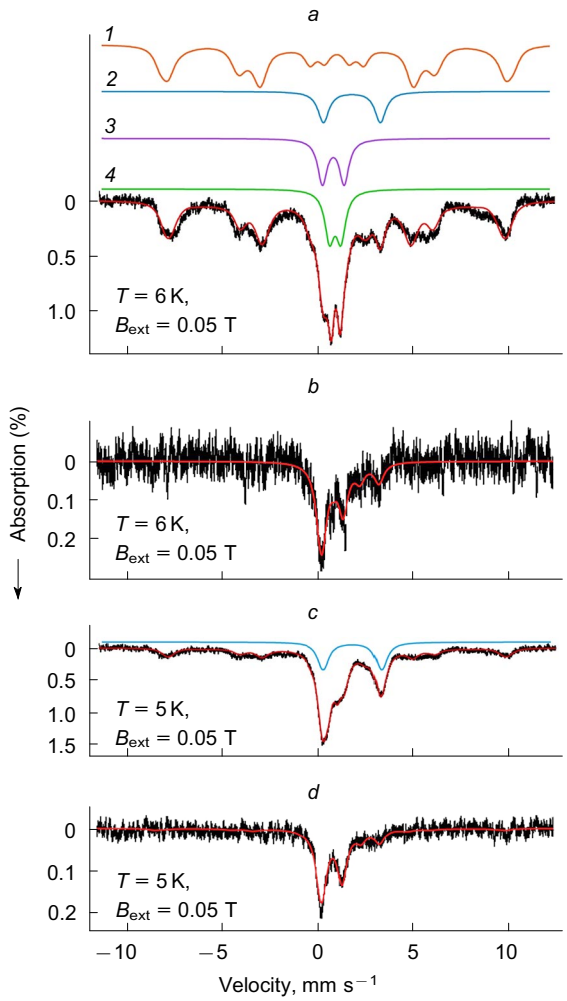


Figure 17. Mössbauer spectra of (*a*, *b*) intact cells of *S. cerevisiae* and (*c*, *d*) cells with deleted *CCC1* gene grown in media with $^{57}Fe^{III}$ citrate contents of (*a*, *c*) 40 and (*b*, *d*) 1 μM. The total spectra (envelopes of the experimental data) are shown in red; the spectral components in Fig. *a* are shifted along the vertical axis (to separate them): (*1*) nonheme high-spin mononuclear $^{57}Fe^{III}$ ($\delta = 0.54$ mm s^{-1}, $\Delta E_Q = 0.39$ mm s^{-1}; $A = 55\%$), (*2*) nonheme high-spin $^{57}Fe^{II}$ ($\delta = 1.3$ mm s^{-1}, $\Delta E_Q = 3.0$ mm s^{-1}; $A = 13\%$; the same component, presented in Fig. *c* above the spectrum has $A = 30\%$); (*3*) the so-called central doublet ($\delta = 0.45$ mm s^{-1}, $\Delta E_Q = 1.14$ mm s^{-1}; $A = 8\%$), corresponding to the $[4Fe-4S]^{2+}$ clusters ($S = 0$) and low-spin $^{57}Fe^{II}$-heme centres (with indistinguishable Mössbauer parameters); and (*4*) $^{57}Fe^{III}$-containing nanoparticles ($\delta = 0.53$ mm s^{-1}, $\Delta E_Q = 0.45$ mm s^{-1}; $A = 18\%$). The total iron content in the cells (in mM) is (*a*) 0.49 ± 0.14, (*b*) 0.17 ± 0.05, (*c*) 0.36 ± 0.10 and (*d*) 0.15 ± 0.06. The figure was prepared by the authors using the data of Ref. 212.

to the Fenton reaction.[212] In contrast, at an iron content of 1 μM in the medium, the differences between the genetically modified and WT-cells were much less pronounced: in both cases most of iron was mitochondrial (see Subsection 3.1; 65 and 67%, respectively), with some contribution from nonheme high-spin iron(II) (25 and 15%).

A comparative analysis of the levels of iron accumulation and transformation in *S. cerevisiae* cells in different growth stages was performed in Ref. 213. After a few hours of growth in a medium with 0.04 mM ^{57}Fe citrate as the iron source (exponential growth stage), the magnetically split component of nonheme high-spin iron(III) of vacuoles ($\delta = 0.52$ mm s^{-1}, $\Delta E_Q = 0.38$ mm s^{-1}; $A = 74\%$; Ref. 213 for other parameters) and the central doublet (see above) of mitochondria with broadened lines ($\delta = 0.45$ mm s^{-1}, $\Delta E_Q = 1.15$ mm s^{-1}, $\Gamma = 0.7$ mm s^{-1}) dominated in the Mössbauer spectrum of frozen biomass ($T = 5$ K, $B_{ext} = 0.05$ T). There were also minor doublets due to high-spin heme iron ($\delta = 0.8$ mm s^{-1}, $\Delta E_Q = 2.4$ mm s^{-1}, $\Gamma = 0.37$ mm s^{-1}) and nonheme iron(II) ($\delta = 1.26$ mm s^{-1}, $\Delta E_Q = 3.0$ mm s^{-1}, $\Gamma = 0.6$ mm s^{-1}). After the 5-day growth (post-exponential stage), the iron concentration in the cells was more than 30 times higher; whereas the content of other metals changed not so radically (Zn and Cu concentrations were higher by factors of ~2 and ~1.5, respectively, and the Mn concentration barely changed). Mössbauer measurements showed that up to 90% iron accumulated by cells in this stage of transition to the metabolically inactive form is localized in the cell walls (comprising ~70% mononuclear nonheme high-spin Fe^{3+} ions, as well as ~20% diamagnetic and ~10% superparamagnetic Fe^{III}-oxyhydroxide nanoparticles). The reactivated cells mobilized iron(III) of the cell wall, reducing it to Fe^{II}; some part of it was imported to cytosol, and the rest remained in the environment. Wofford *et al.*[213] raised the question of the generality of the cell wall ability (found for yeast) to accumulate and mobilize iron in view of the ability to import it, which is a key factor of the pathogenicity of fungi, and the development of methods for treating fungal pathologies.

In continuation of Ref. 214, using the results of highly sensitive Mössbauer measurements (with application of ^{57}Fe), Wofford and Lindahl[215] developed a detailed mathematical model of iron import and translocation, as well as regulation of these processes in growing *S. cerevisiae* yeast cells. Using this model, one can predict the specific features of iron metabolism in cells, in particular, under influence of oxygen. Based on the data about iron proteome (ironome) of evolving yeast cells, which consists of 139 proteins and 5 nonprotein compounds, and their classification according to the localization in the cell, the type of Fe centres and the functions, Lindahl[216] developed a mechanistic model to describe the cellular biochemical processes involving iron compounds.

In a recent study by the research team of Lindahl[217] (remarkable in the choice of methods and originality of solving problems), MbS ($T = 5$ K, $B_{ext} = 0.05$ T) and ESR spectroscopy were jointly used to study wild-type *Escherichia coli* and genetically modified strains. (Strains defective in production of ferritin-like proteins and the Fur system, which controls binding of low-molecular Fe^{II} complexes of nonprotein nature in cytosol and its metabolization, were applied.) An analysis of cytosol extracts using size-exclusion chromatography with online detection by inductively coupled plasma mass spectrometry was also performed. The experiments were carried out on bacteria cultivated to different growth stages, with two different carbon sources (glucose and acetate), different concentrations of $^{57}Fe^{III}$ citrate and different degrees of aeration. A brief review of previous studies on the state of iron in *E. coli* cells (some conclusions of which were revised) is given in the Introduction of Ref. 217. One of the main results[217] was the proof of the fact that the dominant doublet (at $T = 5$ K) of magnetically ordered Fe^{III} is not related to ferritins, which, as concluded by the authors,[217] play a less important role as an iron 'storage' than it was believed previously. Mössbauer spectra measured in the exponential phase of cell growth

contained a strong doublet of magnetically ordered iron(III), which was also present in spectra of similarly grown cells having no ferritin synthesis genes. The parameters of this doublet coincided with the corresponding parameters for nanoparticles of Fe^{III} oxyhydroxide compounds in mitochondria of eukaryotic cells (see above).

Exponentially growing cells at $^{57}Fe^{III}$ concentrations of 1, 10 and 100 μM in a glucose-containing medium accumulated, respectively, 0.35 ± 0.12, 0.54 ± 0.07 and 0.99 ± 0.02 mM iron; in an acetate-containing medium the cellular iron content was higher (0.60, 0.73 and 1.60 mM, respectively), and the cell growth was more than two times slower. The Mössbauer spectra of the cells grown on glucose, measured in the exponential phase, were independent of the iron level in the medium. They exhibited dominance of the 'common' doublet of $[4Fe-4S]^{2+}$ ($S = 0$) clusters and low-spin heme $^{57}Fe^{II}$ centres ($\delta = 0.45$ mm s^{-1}, $\Delta E_Q = 1.15$ mm s^{-1}) and a broadened doublet of nonheme high-spin $^{57}Fe^{II}$. The latter was decomposed into two components: a major one with parameters typical of $^{57}Fe^{II}$ complexes with O_6 coordination ($\delta = 1.33$ mm s^{-1}, $\Delta E_Q = 3.47$ mm s^{-1}) and a minor one with the O/N coordination ($\delta = 1.17$ mm s^{-1}, $\Delta E_Q = 2.99$ mm s^{-1}). These complexes were characterized chromatographically ($M \approx 500$ and 1300 Da, respectively). It was suggested that they are involved in the intracellular transport and regulation of iron and serve as an iron source for synthesis of Fe–S clusters and heme and (or) for filling apoenzymes with iron ions. Under aerobic conditions the intracellular concentration of these low-molecular complexes did not exceed ~0.05 mM; however, it was higher than 0.5 mM under microaerobic conditions. In the stationary growth phase, Mössbauer spectra of the cells were characterized by a dominant doublet of Fe^{III} nanoparticles ($\delta = 0.55$ mm s^{-1}, $\Delta E_Q = 0.55$ mm s^{-1}, $\Gamma = 0.5$ mm s^{-1}), and the Fe^{II} content decreased (the Fe–S-cluster doublet did not undergo any significant changes).[217] The iron content in the cells practically doubled; *i.e.*, in the stationary phase, even in the absence of growth, cells continued to accumulate iron, as it was observed for yeast.[218]

Based on the investigation results, it was concluded in Ref. 217 that, under microaerobic conditions, iron in *E. coli* (and, likely, in many other bacteria) is stored mainly not in the form of ferritins but as labile low-molecular iron(II) complexes. Metabolically active cells 'are protected' from the consequences of the Fenton reaction in the presence of high concentrations of intracellular Fe^{II}, reducing the O_2 diffusing into the cytosol, by a 'respiratory shield' composed of membrane-bound iron-rich respiratory complexes. In dormant cells, iron is stored in the form of Fe^{III} oxyhydroxide nanoparticles, which are formed when low-molecular Fe^{II} complexes are oxidized by the oxygen penetrating into the cytosol, as this occurs in yeast mitochondria.[219, 220] The importance of these results and, in particular, the informativeness of Mössbauer studies in the field of cell biology was underlined in Kosman's mini-review.[221]

Despite the very large number of studies devoted to the common and widely studied nitrogen-fixing and phytostimulating soil bacteria of the *Azospirillum brasilense* species, published in the last decade, the first MbS studies of the assimilation and state of iron in their cells have been published only recently.[222, 223] For two *A. brasilense* strains, characterized by different ecological behaviour, the Mössbauer spectra of the samples grown for 18 h in a medium with a nitrilotriacetate complex of $^{57}Fe^{III}$ (0.07 mM) as an iron source, with subsequent washing from the cultural medium and rapid freezing of the biomass, demonstrated a superposition of three doublets. Two of them (in total from 22 to 33% of the spectrum area for different strains) corresponded to high-spin $^{57}Fe^{2+}$ in the composition of different O/N-hexacoordinated complexes ($\delta \approx 1.3$ and 1.2 mm s^{-1}, $\Delta E_Q \approx 3.0-3.1$ and $2.6-2.7$ mm s^{-1} at $T = 80$ K).[222, 223] The third doublet with the parameters $\delta \approx 0.47-0.49$ mm s^{-1} and $\Delta E_Q \approx 0.79-0.85$ mm s^{-1} (67–78% of the spectrum area for different strains) corresponded obviously to the components of bacterial ferritins, as was confirmed by the Mössbauer measurements of dry biomass at $T = 5$ and 2 K, in particular, in an external magnetic field.[224] Since the only iron source in the medium was iron(III), these data indicate active reduction of Fe^{III} by cells during assimilation (which is also characteristic of many other bacteria).[10] Moreover, when the biomass was kept for 3 days in a physiological solution (in the absence of nutrients and iron source), the *A. brasilense* Sp245 strain continued to reduce assimilated iron(III) (the total Fe^{II} content increased from 33 to 48%).[222]

It is noteworthy that, after the biomass lyophilization, the Mössbauer spectra demonstrated dominance of iron(III) in both azospirillum strains,[225, 226] whereas the content of iron(II) decreased to ~3% (Fig. 18). Note that the broadened quadrupole doublet of $^{57}Fe^{III}$ in the lyophilized biomass [$\delta = 0.46(2)$ mm s^{-1}, $\Delta E_Q = 0.82(3)$ mm s^{-1}; $A = 97\%$; see Fig.18 *b*), which was dominant at $T = 80$ K, decomposed into a magnetically split broadened sextet of bacterial ferritins at $T = 5$ K [$\delta = 0.48(1)$ mm s^{-1}, $B_{eff} = 48.2(5)$ T; $A = 73\%$] and a quadrupole doublet of paramagnetic iron(III) [$\delta = 0.44(1)$ mm s^{-1}, $\Delta E_Q = 0.94(2)$ mm s^{-1}; $A = 23\%$; see Fig. 18 *c*]. The content of the latter coincides (within the measurement error) with the relative amount (~20%) of iron(II) oxidized during lyophilization and, obviously, corresponds to Fe^{III} complexes (possibly, with the same ligands), partially hydroxylated during oxidation. The latter circumstance possibly explains the fairly large value $\Delta E_Q = 0.94$ mm s^{-1}, as well as the doublet broadening ($\Gamma = 0.77$ mm s^{-1}) due to structural inhomogeneities.[226]

Rapid oxidation of cellular iron(II) in the frozen biomass during lyophilization (with possible preservation of the vitality of bacterial cells, which, as is known, can be stored in the form of a lyophilisate)[226] may form the basis of a natural 'strategy' for protection from oxidative damage at relatively high Fe^{II} concentrations. It is known that iron(II) may be involved in processes of the Fenton reaction type, which lead to the formation of reactive oxygen species, in particular, in dry cells, where metabolic processes are slowed down. This result is important for understanding the transformation of iron forms and safety of dry bacterial preparations, which are widely used in various fields of biology, medicine and biotechnology.

Mössbauer measurements were performed for a dry biomass of *Arthrospira platensis* cyanobacterium (previous name *Spirulina platensis*), grown with addition of different iron complexes based on 2-furancarboxylic acid in order to enrich its biomass with this trace element[227] or at different concentrations of the Fe–EDTA complex in the medium and with different degrees of aeration.[228] The measurements revealed the presence of two doublets of high-spin Fe^{III} ($\delta = 0.34-0.35$ mm s^{-1}, $\Delta E_Q = 1.0$ and 0.55 mm s^{-1} at $T = 300$ K), which is consistent with the data for ferrihydrite.[228] It was found that, at Fe–EDTA concentrations in

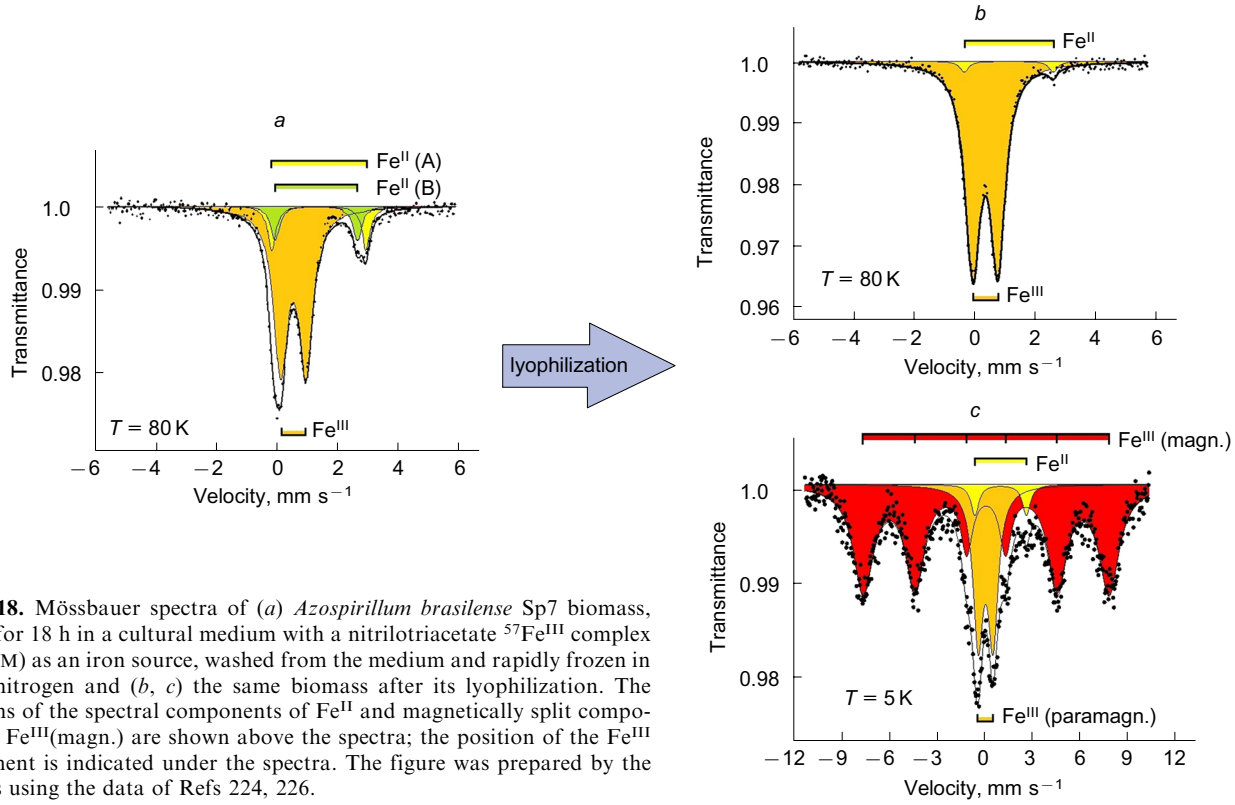


Figure 18. Mössbauer spectra of (*a*) *Azospirillum brasilense* Sp7 biomass, grown for 18 h in a cultural medium with a nitrilotriacetate $^{57}Fe^{III}$ complex (0.07 mM) as an iron source, washed from the medium and rapidly frozen in liquid nitrogen and (*b*, *c*) the same biomass after its lyophilization. The positions of the spectral components of Fe^{II} and magnetically split component of Fe^{III}(magn.) are shown above the spectra; the position of the Fe^{III} component is indicated under the spectra. The figure was prepared by the authors using the data of Refs 224, 226.

the medium < 5 μg ml^{-1} the newly formed ferrihydrite is accumulated in trichomes (filaments composed of many cells). With an increase in the concentration of Fe–EDTA, the ferrihydrite formed during biomineralization of this complex by the cyanobacterium is deposited in the form of conglomerates on the surface of trichomes and then in the space around them. In this case the Mössbauer parameters and the ratio of doublet areas differed from the corresponding data for the ferrihydrite in trichomes. It was noted [228] that the biomineralization of dissolved forms of iron (at its excess in a medium) to insoluble ferrihydrite is obviouly a way to protect cyanobacteria from its high concentrations, whereas ferrihydrite in cells is accumulated most likely in the form of ferritin.

A number of works where the emission (^{57}Co) MbS variant was used to study the binding, state and transformations of $^{57}Co^{2+}$ (in low concentrations) for microorganisms were considered in our previous reviews.[10, 36] It should be noted that, along with the fundamental data on the cobalt state in cells, the research in this field attracts attention in view of the biogeochemical and ecological problems related to microbial leaching of ^{60}Co radionuclide traces from minerals in radioactive waste storage sites.[36]

In the first study in this field (1974, see Ref. 36), uptake of the $^{57}Co^{2+}$ complex with bacterial Fe^{III}-chelating agent enterochelin (cyclic trimer of *N*-2,3-dihydroxybenzoylserine) by *E. coli* cells was investigated; measurements were performed on frozen biomass ($T = 83$ K). The following interesting fact was noted: even at +3 °C a weak effect was observed for 24 h in the emission spectrum of an aqueous suspension of biomass, evidencing that a small fraction (~4%) of absorbed $^{57}Co^{2+}$ remained in the composition of the cellular membrane (quasi-solid cellular structure), because the ME is not observed for a Mössbauer nuclide in dissolved state. An emission spectrum of the biomass of thermophilic cyanobacterium *Synechococcus vulcanus*, rapidly frozen after 4-month incubation with $^{57}Co^{2+}$, was measured later (Ref. 229). The spectrum was fitted in the best way by a superposition of two quadrupole doublets with the parameters $\delta = 0.27(1)$ mm s^{-1}, $\Delta E_Q = 2.08(1)$ mm s^{-1} ($T = 80$ K; $A = 74\%$), close to those for $^{57}Co^{2+}$-doped cobalamins, and $\delta = 1.08(1)$ mm s^{-1}, $\Delta E_Q = 2.66(1)$ mm s^{-1} ($A = 26\%$), which are characteristic of the complexes of high-spin $^{57}Fe^{2+}$ (likely, in the T_d coordination because of the small δ value).

In the next series of studies the MbS technique was used to investigate the interaction of $^{57}Co^{2+}$ with different strains of the above-mentioned bacterial species *Azospirillum brasilense*,[148, 150, 223, 230–232] some of those studies were discussed in reviews.[10, 36] Rapid (within 2 min) binding of cobalt(II) by cells ($^{57}Co^{2+}$ was added to the cultivation medium in concentrations of the order of 0.01 mM) occurred in the experiments.[223, 230–232] The Mössbauer parameters for the frozen suspensions of living cells differed from those for $^{57}Co^{2+}$ in a suspension of dead cells (with purely chemical interaction between $^{57}Co^{2+}$ and the cell surface) and in frozen solutions of the cultural liquid or aqueous solution of $^{57}CoCl_2$. During an hour one could observe some changes in the Mössbauer parameters and redistribution of the relative content of $^{57}Co^{2+}$ forms, which indicates processes of metabolic transformation of the cobalt(II) cation. A superposition of two quadrupole doublets (I and II) of high-spin nucleogenic $^{57}Fe^{2+}$, which characterizes the state of the initial $^{57}Co^{2+}$ cation (the third doublet, making up to 25–36% of the spectrum area, corresponded to aliovalent $^{57}Fe^{3+}$ as a result of the post-effects with the parameters $\delta = 0.24–0.45$ mm s^{-1}, $\Delta E_Q = 0.7–1.4$ mm s^{-1} for different strains), was observed in the emission spectra of the two strains of *A. brasilense* in

all cases.[223, 230 – 232] Doublet I (about half of the spectrum area) corresponds to the parameters of typical O/N-coordinated complexes with an O_h symmetry (δ = 1.10 – 1.26 mm s^{-1}, ΔE_Q = 2.6 – 3.0 mm s^{-1} at T = 80 K). The parameters of doublet II (A = 20 – 30%) differed significantly, primarily, by smaller values of quadrupole splitting (ΔE_Q = 2.0 – 2.3 mm s^{-1}); the isomer shifts were also smaller ($\delta \leqslant 1.2$ and $\leqslant 1.0$ mm s^{-1} for different strains). In particular, the values δ = 0.89 mm s^{-1}, ΔE_Q = 2.00 mm s^{-1} for doublet II in the emission spectrum [223] of a suspension of *A. brasilense* Sp7 after a 2-min contact with $^{57}Co^{2+}$ are atypical. It is of interest that these values almost coincide with the parameters of one of the Fe centres for the $[4Fe-4S]^{2+}$ cluster with unusual coordination in the above-discussed transmission spectrum of bacterial protein LytB (see Fig. 10 *a* and Table 4).

In our opinion, this coincidence is not accidental. The toxicity of cobalt(II) for bacteria is known (see Refs 10, 36 and 223) to be due to the participation of Co^{2+} cations in reactions with labile [Fe – S] clusters during their biosynthesis *de novo* or reparation. (One cannot also exclude the participation of special iron-containing proteins — donors of iron ions, in which, according to the data of MbS and other spectroscopic measurements,[233] Fe^{II} is bound much more weakly than Fe^{III} and, correspondingly, is much more labile.) With allowance for the aforesaid, one can suggest participation of $^{57}Co^{2+}$ ions in similar reactions with iron – sulfur proteins of azospirilla in the initial interaction stage.

It is also important that, to record the transmission spectrum of ^{57}Fe-containing protein LytB, Ahrens-Botzong *et al.*[137] had to isolate it from the biomass of its superproducer recombinant *E. coli*. In the case of emission measurements, fairly good spectra with the aforementioned parameters were obtained using 0.2 ml aqueous suspension of *A. brasilense* cells with a $^{57}Co^{2+}$ concentration of the order of 10 μM.[10, 223, 232]

3.3. Plants

Starting with the 1980s, MbS has been successfully applied to study the assimilation, distribution in different parts of plants and detection of chemical forms of iron, despite its relatively low content in higher plant tissues.[35] These studies are important in view of the problems of iron deficiency for plants and development of chlorosis, which are especially urgent for calcareous and alkaline soils.

Plants use different strategies to assimilate iron from soil, where the solubility of iron compounds is generally extremely low. Non-cereal plants apply enzymatic reduction of soluble iron(III) chelates on the external surface of the cytoplasmic membrane of root cells with participation of 1,5-dihydroflavin adenine dinucleotide or the reduced form of nicotinamide adenine dinucleotide phosphate ($NADPH_2$) to the corresponding iron(II) chelates. The latter, in view of their much lower stability, 'transfer' Fe^{2+} ions to intramembrane transporters of divalent cations with their subsequent oxidation to Fe^{3+} (strategy I). Cereals can produce (and release into soil) phytosiderophores (low-molecular Fe^{3+}-binding organic molecules), which dissolve iron(III) from soil minerals and are directly bioavailable (in the form of complexes) for plants (strategy II).[35] The absorbed iron in the form of coordination compounds, penetrating the cytoplasm, is then distributed by a plant, being accumulated after oxidation in phytoferritin, as well as in heme-containing proteins, Fe – S-proteins, *etc*.

In many cases Mössbauer measurements showed that iron in plant tissues is transferred mainly in the form of simple organic or inorganic complexes; the iron content in the composition of cellular proteins was below the MbS detection limit.[10, 35] In particular, after sprouting cucumber (*Cucumis sativus*) under conditions of iron deficiency and subsequent contact with an iron(III) source, iron was present in roots mainly in the composition of Fe^{III} carboxylate complexes (citrate when using $^{57}Fe^{III}$ citrate as an iron source). The additional components were iron(II)-hydrate complex [with the spectral parameters δ = 1.37 mm s^{-1}, ΔE_Q = 3.0 mm s^{-1}, close to those for $Fe(H_2O)_6^{2+}$] or similar high-spin complexes (δ = 1.30 mm s^{-1}, ΔE_Q = 2.93 – 2.95 mm s^{-1} at T = 80 K) when using synthetic $^{57}Fe^{III}$ chelates as an iron source.[234] According to the Mössbauer data,[35] the relative content of iron(II) in cucumber roots after 30-min contact with a $^{57}Fe^{III}$ source increased from 13 to 48% with an increase in the concentration of $^{57}Fe^{III}$ citrate in the medium from 0.01 to 0.5 mM, which indicated a high rate of iron(III) reduction. At a concentration of $^{57}Fe^{III}$ citrate in the medium of 0.5 mM, the relative content of iron(II) in roots decreased from 48 to 6% after 24 h; the content of Fe^{III} complexes increased in parallel.

For cucumbers sprouted for several weeks in the presence of 0.01 mM of $^{57}Fe^{III}$ citrate, iron(II) was absent in the Mössbauer spectra of root tissues.[235] Low-temperature measurements (T = 4.2 – 1.5 K, including measurements in an external magnetic field) showed the presence of iron(III) carboxylate complexes, hydrated Fe^{III} oxide in the composition of phytoferritin and sulfate-containing oxyhydroxide phases of the mineral jarosite type.[235]

Assimilation of iron (by strategy I) by freshwater photosynthesising unicellular green alga *Chlamydomonas reinhardtii* at different CO_2 concentrations in air and the influence of anaerobiosis on the iron accumulation was investigated by MbS in [236]. In a cultural medium containing 0.03 mM $^{57}Fe^{III}$ and 1.5 mM citrate, alga cells grown in air with an elevated CO_2 content (3 vol.%) accumulated a significant amount of iron in the form of Fe^{II} (δ = 1.36 mm s^{-1}, ΔE_Q = 3.1 mm s^{-1} at T = 80 K; relative content of 68% after 5 days). Its absolute amount was rapidly 'saturated' and then changed only slightly during the cell growth for several days, while the content of iron(III) increased (δ = 0.46 mm s^{-1}, ΔE_Q = 0.65 mm s^{-1}; A = 32% after 5 days). According to the Mössbauer data, in the cells with a lower content of Fe^{II} (below the saturation level), kept for only 3 h under anaerobic conditions in the absence of an external iron source, the relative Fe^{II} content increased by a factor of 3 – 4 due to the reduction of intracellular Fe^{III}, whose relative content decreased. Note that the accumulation of a significant amount of iron(II) is atypical of green alga cells. Mössbauer measurements showed [236] also that only Fe^{III} was accumulated in cells of freshwater photosynthesising cyanobacteria *Synechococcus elongatus* under similar conditions; obviously, this accumulation occurred during repeated oxidation of the iron(II) transported into the cell in correspondence with strategy I (see above). As compared with yeast cells, which, as well as *Chlamydomonas reinhardtii*, contained vacuoles and (according to the MbS data) also accumulated Fe^{II} (but in smaller relative amounts),[236] it was concluded that iron(II) in algae cells is also stored in vacuoles.

The later study[237] was devoted to the widespread sea green alga *Tetraselmis suecica*, which is of interest for biotechnology (production of biofuel, as well as valuable food and feed additives). The uptake of iron by cells was investigated, and its chemical forms were analyzed using MbS and X-ray absorption spectroscopy. The Mössbauer measurements of a biomass grown on sea water enriched in $^{57}Fe^{3+}$ at low temperatures (to $T = 2$ K) revealed three main Fe-containing cell components (Fig. 19).The compounds constituting the main part of the cellular iron pool ($A \approx 87\%$; component *2*), are presented by a quadrupole doublet at $T = 77$ K ($\delta = 0.47$ mm s^{-1}, $\Delta E_Q = 0.72$ mm s^{-1}, $\Gamma = 0.52$ mm s^{-1}) and developing magnetic structure ($B_{eff} = 40-41$ T) at a decrease in the measurement temperature to $T = 2$ K. These parameters correspond to the content of highly dispersed polymer Fe^{3+} oxohydroxide compounds, characterized by different sizes of ferritin core particles with a phosphate content (according to the X-ray absorption spectroscopy data) lower than in most of bacterial and plant ferritins. Component *3*, according to the Mössbauer data ($\delta = 0.42-0.45$ mm s^{-1}, $\Delta E_Q = 0.92$ mm s^{-1}, $\Gamma = 0.4$ mm s^{-1}; $A \approx 11\%$) and the results of X-ray absorption spectroscopy (calculation of the first and second coordination spheres of iron cations), corresponds to the $[4Fe-4S]^{2+}$ clusters, a component of the redox systems of chloroplast and(or) mitochondria.[237] It is of interest that a very small fraction of high-spin Fe^{2+} complexes (component *4*; $\delta = 1.25$ mm s^{-1}, $\Delta E_Q = 2.3$ mm s^{-1}, $\Gamma = 0.7$ mm s^{-1} at all temperatures; $A \approx 2\%$) was found in the cellular iron pool of *T. suecica*. This fact indicates that the iron assimilated in correspondence with strategy I (see above) after the transport in the form of Fe^{II} through the membrane is fairly rapidly oxidized to Fe^{III} and stored in this state in the form of ferritin cores.

Uptake (as an active transport process) of iron in the form of Fe^{III} (with subsequent stages of reduction, translocation and repeated oxidation) was shown[238] for uncellular phytoplankton *Emiliania huxleyi*, which belongs to coccolithophores. In the case of long-term contact with a ^{57}Fe-containing iron source in a medium, phosphate-containing hydroxocompounds of iron(III), with parameters typical of bacterial and plant ferritins, were identified (using MbS and X-ray absorption spectroscopy) as the only metabolite in *E. huxleyi* cells.

In contrast, the representative of lower plants from the group of dinophytic algae *Lingulodinium polyedrum*, as was shown[239] using Mössbauer measurements after a long-term contact of the culture with a ^{57}Fe-containing iron source, does not possess an iron storage system but has an efficient system for its uptake from the environment (possibly, using mutualistic interactions with bacteria). In this case, the most likely redox pathway of transformation of iron ions during assimilation for *L. polyedrum* is the pathway characteristic of yeast and green alga *C. reinhardtii*.[236]

As applied to plants, the emission variant of MbS was used only in Ref. 240 to study the state of $^{57}Co^{2+}$ in the roots of water hyacinth *Eichhornia crassipes*. After a two-week incubation of a young plant with a root ~5 cm long in a saline nutrient medium with $^{57}Co^{2+}$ (1 mCi), the emission spectrum of the root (recorded at $T = 80$ K) contained two quadrupole doublets for the high-spin nucleogenic forms of iron: $^{57}Fe^{2+}$ [$\delta = 1.19(5)$ mm s^{-1}, $\Delta E_Q = 2.66(5)$ mm s^{-1}; $A = 56\%$] and $^{57}Fe^{3+}$ [as a result of post-effects; $\delta = 0.45(10)$ mm s^{-1}, $\Delta E_Q = 1.6(1)$ mm s^{-1}; $A = 44\%$; Fig. 20]. The parameters of the main doublet of nucleogenic $^{57}Fe^{2+}$, which reflect the coordination of initial $^{57}Co^{2+}$, were fairly close to those of the similar doublet in the emission spectrum of $^{57}Co^{2+}$–EDTA complex, measured additionally for comparison [$\delta = 1.17(5)$ mm s^{-1}, $\Delta E_Q = 2.71(5)$ mm s^{-1}]. The parameters of nucleogenic $^{57}Fe^{3+}$ (post-effects) in the emission spectrum of the

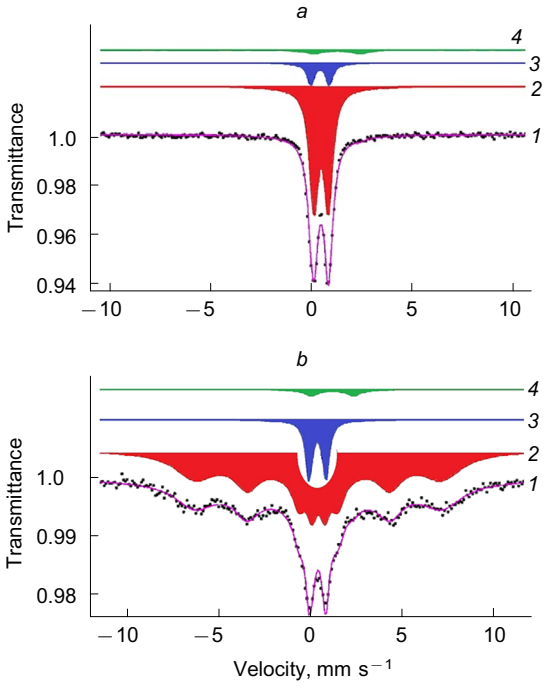


Figure 19. Mössbauer spectra of *Tetraselmis suecica* biomass, rapidly frozen in liquid nitrogen after 11-day growth in model sea water with addition of 1 μM $^{57}Fe^{3+}$–EDTA complex and washed from the medium. The spectra were measured at (*a*) 77 and (*b*) 2 K. The lower envelope line (*1*) is the spectrum obtained by fitting the experimental data (dots) as the sum of the spectral components corresponding to ferritin-like compounds (*2*), $[4Fe-4S]^{2+}$ (*3*) and high-spin Fe^{2+} (*4*). Components *2*–*4* are shifted along the vertical axis and separated. The figure was prepared by the authors using the data of Ref. 237.

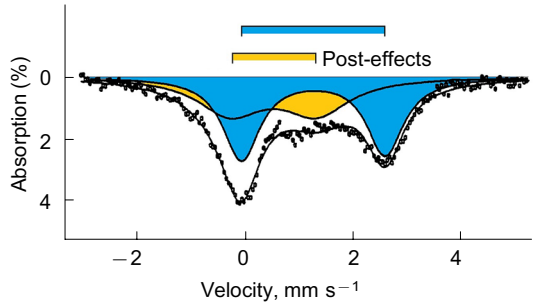


Figure 20. Emission spectrum of a water hyacinth (*Eichhornia crassipes)* root after a two-week incubation in a nutrient solution with $^{57}Co^{2+}$ (1 mCi); the spectrum is convered to a form comparable with that of transmission measurements. The lower envelope is the total spectrum, obtained by fitting the experimental data (dots) as the sum of the spectral components corresponding to nucleogenic $^{57}Fe^{2+}$ (shown in blue) and post-effects (shown in yellow), whose positions are indicated above the spectrum. The figure was prepared by the authors using the data of Ref. 240.

root practically coincided (within the measurement error) both with the parameters of the doublet due to post-effects for the $^{57}Co^{2+}-EDTA$ complex [$\delta = 0.6(1)$ mm s^{-1}, $\Delta E_Q = 1.6(1)$ mm s^{-1}] and with the parameters of the transmission spectrum of the $^{57}Fe^{3+}-EDTA$ complex [$\delta = 0.46(3)$ mm s^{-1}, $\Delta E_Q = 1.64(3)$ mm s^{-1}]. Based on this, it was concluded[240] that cobalt(II) is present in root tissues in the form of a chelate with a coordination microenvironment similar to that for its complex with EDTA (possibly, with another chelating agent). Obviously, Ambe *et al.*[240] meant an analogy with the $^{57}Co^{2+}-EDTA$ and $^{57}Fe^{3+}-EDTA$ complexes, studied by them for comparison. However, it should be noted that the cation microenvironment in the $^{57}Fe^{2+}-EDTA$ complex is apparently similar. In particular, the room-temperature Mössbauer parameters found[241] for a solid $(NH_4)_2Fe^{2+}$[EDTA] complex, synthesized at pH > 8, were very close (with allowance for the possible temperature dependence): $\delta = 1.17(1)$ mm s^{-1}, $\Delta E_Q = 2.59(2)$ mm s^{-1}, and its oxidation in air for several days led to the occurrence of the second Fe^{3+} doublet in the Mössbauer spectrum [$\delta = 0.35(1)$ mm s^{-1}, $\Delta E_Q = 1.56(3)$ mm s^{-1}].[241]

4. Note added in proof

In this section we briefly consider the most interesting publications in the subject area of this review that appeared while it was in preparation for publication.

Mössbauer spectroscopy (on ^{121}Sb nuclei), nuclear forward scattering using synchrotron radiation and Raman spectroscopy were used[242] to study quantitatively the redox-biotransformation of a synthetic sample of antimony(III/V) oxide, consisting of a mixture of oxides in different oxidation states, influenced by a culture of hyperthermophilic archaea *Pyrobaculum* sp.

The research group guided by P.A.Lindahl[243] applied MbS, ESR spectroscopy and liquid chromatography interfaced with inductively-coupled-plasma mass spectrometry to investigate *S. cerevisiae* yeast cells and the mitochondria, vacuoles and cytosol isolated from them. The purpose was to determine the relationship between the acidity of vacuoles (to this end, along with the wild-type strain, they used also a strain with dysfunction of vacuolar ATPase, a membrane-bound complex that pumps protons from cytosol to vacuoles), the function of mitochondria and the iron homeostasis. Based on the results obtained, new concepts about the relationship between vacuoles and mitochondria were formulated, with indication of the potentially important role of low-molecular compounds of iron, copper and sulfur in the cytosol of yeast cells.

In another study by Lindahl's group[244] the ironome of hyperthermophilic anaerobe *Pyrococcus furiosus* was investigated by MbS (for the first time for archaea). It was shown that the *P. furiosus* proteome is characterized by the dominance of either $[Fe_4S_4]^{2+}$ clusters or thioferrate-like iron, consisting of Fe^{III} ions with a coordination environment S_4 (in the form of magnetically ordered nanoparticles), correspondingly, in the absence or in the presence of (3 g L^{-1}) elementary sulfur in the medium. In the latter case, the content of both iron and other metals (Cu, Mn, Zn) in the archaea cells increased significantly.

The phenomenon of line broadening in the Mössbauer spectra measured for ^{57}Fe-containing nanoparticles in viscous media, caused by the diffusion motion of particles, was used[245] to model similar processes in the cell cytoplasm, due to which a comparative analysis of nano- and macroviscosity can be performed. It should be noted that in this case MbS allows one to bypass the limitations inherent in optical methods and analyze data on nanoparticle motion in the nanosecond and nanometer ranges. In continuation of these studies, the nanoscale diffusion and hydrodynamic properties of spherical $CoFe_2O_4$ nanoparticles ($\sim$9 nm in diameter) in water–glycerol solutions of protein (0–20 vol.% bovine serum albumin) were investigated, and the macromolecular crowding effects were discussed.[246]

Copeland *et al.*[247] used MbS with the rapid freeze-quench methodology (along with other techniques) to confirm the identification of iron(IV)-oxo-intermediate for 2-oxoglutarate-dependent oxygenase in the reaction pathway with L-arginine oxidation.

Maio *et al.*[248] investigated the Fe–S cofactors of RNA-dependent RNA polymerase (RdRp) of SARS-CoV-2 virus — a causative agent of the coronavirus disease COVID-19 — and their sensitivity to oxidative degradation by stable nitroxide TEMPOL, which inhibits RdRp and blocks the SARS-CoV-2 replication. The MbS technique was used to determine the type and stoichiometry of Fe–S-clusters in the catalytic subunit (nsp12) of this enzyme, which plays a key role in the cycle of virus replication and transcription.

5. Conclusion

The material presented in this review is indicative of the diversity and uniqueness of information that can be obtained using Mössbauer measurements when studying many biological objects — from simple biomolecules and biocomplexs to complex structures, including tissues and organisms. It was noted at recent international conferences devoted to the applications of the Mössbauer effect that, after the six decades of development of MbS methodology and applications that passed since the time of Mössbauer's discovery, the last decades are characterized by a change in the generation of researchers who have a deep knowledge of the technique, its variants and potential, and who have contributed a lot to its making up and development. Despite the high popularity of MbS in many fields of science and technology, including biological fields, it has not yet become a routine technique. There were also opinions that, because of the complexity of its physical foundations and (in some fields, including biological applications) methodology, it may not become such. Moreover, some aspects of this technique (in particular, the emission variant, as well as the methodology using synchrotron radiation) are in the stage of development and appear fairly promising for bioanalytical investigations. In this context, a very urgent problem is the availability of the literature (along with the numerous monographs, in which the intricate physico-mathematical and technical foundations of the technique are considered in detail) directly illustrating the potential of the technique on various modern examples. Specifically this was the task we tried to fulfil in the context of MbS bioanalytical applications.

We should also note the following. Despite the fact that the Mössbauer effect and the transformations occurring in the γ-radiation source and absorber (see Fig. 1) are formally attributed to nuclear physics and nuclear chemistry, it is obvious, nevertheless, that all Mössbauer parameters calculated from experimental spectra provide a variety of information specifically about the molecular, electronic and

other structural and chemical features of systems studied. In this context, MbS in all its variants undoubtedly occupies a worthy place in the arsenal of molecular and biomolecular spectroscopic techniques.

The preparation of the review was supported by the Russian Foundation for Basic Research (Project No. 19-13-50160). Some materials from the cited publications by the review's authors were the results of studies supported by the Russian Foundation for Basic Research (Project Nos 13-04-01538-a and 17-08-01696-a).

6. List of abbreviations and designations

A — relative area of spectral component (in % of the total spectrum area),
ABC transporter — ATP-binding cassette transporter,
AC — active centre,
AIH — amorphous iron(III) hydroxide (approximate composition $Fe(OH)_3 \cdot nH_2O$),
AspA — L-aspartic acid (in the form of substance),
B_{eff} — induction of effective magnetic field on Mössbauer nuclide nucleus,
B_{ext} — induction of external magnetic field,
Bfr — bacterioferritin,
DFT — density functional theory,
Dps — DNA-binding protein from starved cells (part of the ferritin superfamily),
EMbS — emission Mössbauer spectroscopy,
f — probability of the Mössbauer effect (Lamb–Mössbauer factor),
GS — glutamine synthetase,
GR — green rust,
HbR — rabbit hemoglobin,
HbR-O_2 — oxygenated form of rabbit hemoglobin,
HL — homoserine lactone [(S)-(−)-α-amino-γ-butyrolactone hydrobromide],
HMBPP — 1-hydroxy-2-methyl-2-butenyl-4-diphosphate,
4-n-HR — 4-n-hexylresorcinol (4-n-hexyl-1,3-dihydroxybenzene),
I — nuclear spin,
IAA — indole-3-acetic acid (phytohormone of the auxin series),
Lba — soybean leghemoglobin *a*,
M — molecular weight (in Da),
m_I — magnetic quantum numbers of nuclear energy sublevels,
MbS — Mössbauer spectroscopy,
MbS-HVR — Mössbauer spectroscopy with a high velocity resolution,
ME — Mössbauer effect,
5-MR — 5-methylresorcinol (5-methyl-1,3-dihydroxybenzene),
NRFS — nuclear resonant forward scattering,
ODP — oxygen-binding di-iron protein,
PDB — Protein Data Bank,
PEUSI — poly(ether-urethane) sulfonated ionomer,
5-n-PR — 5-n-propylresorcinol (5-n-propyl-1,3-dihydroxybenzene),
S — electron spin,
SR-MbS — Mössbauer spectroscopy using synchrotron radiation,
T — absolute temperature,
V_{zz} — z component of electric field gradient on nucleus,
WT — wild-type (strain),
Γ — Mössbauer linewidth (FWHM),
δ — isomer shift,
ΔE_Q — quadrupole splitting,
τ — lifetime of excited nuclear sublevel.

References

1. F.Parak. *Nature (London)*, **478**, 325 (2011)
2. P.Gütlich, C.Schröder. In *Methods in Physical Chemistry*. (Eds R.Schäfer, P.C.Schmidt). (Weinheim: Wiley-VCH, 2012). P. 351
3. R.L.Mössbauer. *Hyperfine Interact.*, **126**, 1 (2000)
4. P.B.Moon. *Proc. Phys. Soc. Sect. A*, **64**, 76 (1951)
5. R.L.Mössbauer. *Z. Phys.*, **151**, 124 (1958)
6. R.L.Mössbauer. *Naturwissenschaften*, **45**, 538 (1958)
7. E.Bill. In *Practical Approaches to Biological Inorganic Chemistry*. Second Ed. (Eds R.R.Crichton, R.O.Louro). (Amsterdam: Elsevier, 2020). P. 201
8. V.G.Semenov, L.N.Moskvin, A.A.Efimov. *Russ. Chem. Rev.*, **75**, 317 (2006)
9. M.I.Oshtrakh. *Cell Biochem. Biophys.*, **77**, 15 (2019)
10. A.A.Kamnev, A.V.Tugarova. *Talanta*, **174**, 819 (2017)
11. M.E.Pandelia, N.D.Lanz, S.J.Booker, C.Krebs. *Biochim. Biophys. Acta (BBA) — Mol. Cell Res.*, **1853**, 1395 (2015)
12. I.Czakó-Nagy, A.Vértes. *TrAC — Trends Anal. Chem.*, **7**, 305 (1988)
13. D.L.Nagy. *Hyperfine Interact.*, **182**, 5 (2008)
14. *Mössbauer Spectroscopy: Applications in Chemistry, Biology, and Nanotechnology*. (Eds V.K.Sharma, G.Klingelhöfer, T.Nishida). (New York: Wiley, 2013)
15. H.R.Verma. In *Atomic and Nuclear Analytical Methods. XRF, Mössbauer, XPS, NAA and Ion-Beam Spectroscopic Techniques*. (Berlin, Heidelberg: Springer, 2007). P. 177
16. V.G.Semenov, V.V.Panchuk, S.M.Irkaev. *AIP Conf. Proc.*, **1258** (1), 127 (2010)
17. A.A.Belyaev, V.S.Volodin, S.M.Irkaev, V.V.Panchuk, V.G.Semenov. *Bull. Russ. Acad. Sci. Phys.*, **74**, 326 (2010)
18. M.Chakrabarti, S.Chattopadhyay, D.Sanyal, A.Sarkar, D.Jana. *Mater. Sci. Forum*, **699**, 1 (2012)
19. E.V.Butaeva, A.V.Grebenyuk, S.M.Irkaev, V.V.Panchuk, V.G.Semenov. *Nauchn. Priborostroenie*, **26**, 54 (2016)
20. A.A.Zalutskii, A.A.Zalutskaya, N.A.Sed'mov, R.N.Kuz'min. *Lithol. Mineral. Res.*, **50**, 270 (2015)
21. W.Salama, M.El Aref, R.Gaupp. *Spectrochim. Acta, Part A: Mol. Biomol. Spectrosc.*, **136**, 1816 (2015)
22. K. Nomura. *Radioisotopes*, **63**, 405 (2014)
23. J.F.Marco, J.R.Gancedo, M.Monti, J.de la Figuera. In *Mössbauer Spectroscopy: Applications in Chemistry, Biology, and Nanotechnology*. (Eds V.K.Sharma, G.Klingelhöfer, T.Nishida). (New York: Wiley, 2013). P. 455
24. C.A.Gorski, M.M.Scherer. *Am. Mineral.*, **95**, 1017 (2010)
25. B.Debus, V.Panchuk, B.Gusev, S.Savinov, V.Popkov, A.Legin, V.Semenov, D.Kirsanov. *Chemom. Intel. Lab. Syst.*, **198**, 103941 (2020)
26. I.P.Suzdalev. *Gamma-rezonansnaya Spektroskopiya Belkov i Model'nykh Soedinenii. (Mössbauer Spectroscopy of Proteins and Model Compounds)*. (Moscow: Nauka, 1988)
27. C.Krebs, J.C.Price, J.Baldwin, L.Saleh, M.T.Green, J.M.Bollinger Jr. *Inorg. Chem.*, **44**, 742 (2005)
28. P.Gütlich, C.Schröder, V.Schünemann. *Spectrosc. Eur.*, **24**, 21 (2012)

29. G.C.Papaefthymiou. *Biochim. Biophys. Acta*, **1800**, 886 (2010)
30. K.Honarmand Ebrahimi, P.-L.Hagedoorn, W.R.Hagen. *Chem. Rev.*, **115**, 295 (2015)
31. J.M.Bradley, N.E.Le Brun, G.E.Moore. *J. Biol. Inorg. Chem.*, **21**, 13 (2016)
32. M.I.Oshtrakh, I.V.Alenkina, A.V.Vinogradov, A.Kumar, A.L.Berkovsky, A.P.Zakharova, T.S.Konstantinova, E.G.Novikov, V.A.Semionkin. *J. Radioanal. Nucl. Chem.*, **309**, 317 (2016)
33. E.Bill. *Hyperfine Interact.*, **205**, 139 (2012)
34. J.M. Byrne, A. Kappler. In *Analytical Geomicrobiology. A Handbook of Instrumental Techniques*. (Eds J.P.L.Kenney, H.Veeramani, D.S.Alessi). (Cambridge: Cambridge University Press, 2019). P. 314
35. A.A.Kamnev, K.Kovács, I.V.Alenkina, M.I.Oshtrakh. In *Mössbauer Spectroscopy: Applications in Chemistry, Biology, and Nanotechnology*. (Eds V.K.Sharma, G.Klingelhöfer, T.Nishida). (New York: Wiley, 2013). P. 272
36. A.A.Kamnev. In *Mössbauer Spectroscopy: Applications in Chemistry, Biology, and Nanotechnology*. (Eds V.K.Sharma, G.Klingelhöfer, T.Nishida). (New York: Wiley, 2013). P. 333
37. I.V.Alenkina, A.V.Vinogradov, I.Felner, T.S.Konstantinova, E.Kuzmann, V.A.Semionkin, M.I.Oshtrakh. *Cell Biochem. Biophys.*, **77**, 33 (2019)
38. M.I.Oshtrakh, V.A.Semionkin, *Spectrochim. Acta, Part A: Mol. Biomol. Spectrosc.*, **100**, 78 (2013)
39. M.I.Oshtrakh, V.A.Semionkin, O.B.Milder, E.G.Novikov. *J. Radioanal. Nucl. Chem.*, **281**, 63 (2009)
40. M.Oshtrakh, V.Semionkin, V.Grokhovsky, O.Milder, E.Novikov. *J. Radioanal. Nucl. Chem.*, **279**, 833 (2009)
41. M.I.Oshtrakh. *J. Radioanal. Nucl. Chem.*, **269**, 407 (2006)
42. D. Delacroix, J.P.Guerre, P.Leblanc, C.Hickman. *Radionuclide and Radiation Protection Data Handbook*. (2nd Ed.). (Kent, England: Nuclear Technology Publishing, 2002). P. 55
43. Yu.D.Perfiliev. *Bull. Russ. Acad. Sci. Phys.*, **74**, 321 (2010)
44. A.Nath. *Mössbauer Effect Ref. Data J.*, **30**, 107 (2007)
45. A.Nath. *J. Nucl. Radiochem. Sci.*, **11**, A1 (2010)
46. A.V.Bokov, V.M.Byakov, L.A.Kulikov, Yu.D.Perfiliev, S.V.Stepanov. *Hyperfine Interact.*, **238**, 95 (2017)
47. I.Alekseev, A.Miroslavov, E.Stepanova. *Radiat. Phys. Chem.*, **162**, 96 (2019)
48. D.J.Cardin, K.N.Joblin, A.W.Johnson, G.Lang, M.F.Lappert. *Biochim. Biophys. Acta*, **371**, 44 (1974)
49. S.Tyagi, K.Inoue, A.Nath. *Biochim. Biophys. Acta*, **539**, 125 (1978)
50. H.Paulsen, V.Schünemann, A.X.Trautwein, H.Winkler. *Coord. Chem. Rev.*, **249**, 255 (2005)
51. H.Paulsen, V.Schünemann, A.X.Trautwein, H.Winkler. *Mössbauer Effect Ref. Data J.*, **28**, 274 (2005)
52. Y.Guo, Y.Yoda, X.Zhang, Y.Xiao, S.P.Cramer. In *Mössbauer Spectroscopy: Applications in Chemistry, Biology, and Nanotechnology*. (Eds V.K.Sharma, G.Klingelhöfer, T.Nishida). (New York: Wiley, 2013). P. 246
53. L.B.Gee, C.-Y.Lin, F.E.Jenney, Jr., M.W.W.Adams, Y.Yoda, R.Masuda, M.Saito, Y.Kobayashi, K.Tamasaku, M.Lerche, M.Seto, C.G.Riordan, A.Ploskonka, P.P.Power, S.P.Cramer, L.Lauterbach. *Inorg. Chem.*, **55**, 6866 (2016)
54. A.Miłaczewska, E.Kot, J.A.Amaya, T.M.Makris, M.Zając, J.Korecki, A.Chumakov, B.Trzewik, S.Kędracka-Krok, W.Minor, M.Chruszcz, T.Borowski. *Chem. – Eur. J.*, **24**, 5225 (2018)
55. S.Mebs, V.Srinivas, R.Kositzki, J.J.Griese, M.Högbom, M.Haumann. *Biochim. Biophys. Acta — Bioenerg.*, **1860**, 148060 (2019)
56. P.I.Arredondo S., C.A.Barrero, K.E.Garcia, J.M.Greneche. *Polyhedron*, **105**, 27 (2016)
57. P.I.Arredondo S., C.A.Barrero, K.E.Garcia, J.M.Greneche. *Hyperfine Interact.*, **238**, 63 (2017)
58. S.M.Dubiel, Ł.Gondek, J.Żukrowski. *Inorg. Chim. Acta*, **510**, 119760 (2020)
59. S.M.Dubiel, J.Żukrowski, M.Bałanda. *J. Magn. Magn. Mater.*, **507**, 166815 (2020)
60. M.I.Oshtrakh, V.A.Semionkin. In *Proceedings of the International Conference Mössbauer Spectroscopy in Materials Science 2016*. AIP Conference Proceedings. (Eds J.Tuček, M.Miglierini). (Melville, NY: AIP Publishing, 2016). Vol. 1781. Article 020019
61. M.I.Oshtrakh, E G.Novikov, S.M.Dubiel, V.A.Semionkin. *Hyperfine Interact.*, **226**, 451 (2014)
62. M.Kądziołka-Gaweł, M.Wojtyniak. *Acta Phys. Polon. A*, **129**, 1242 (2016)
63. M.Kaur, S.Sharma, J.P.Sharma. *Ind. J. Pharmaceut. Biol. Res.*, **2**, 96 (2014)
64. B.S.Barot, P.B.Parejiya, P.K.Shelat, G.B.Shah, D.M.Mehta, T.V.Pathak. *J. Pharmaceut. Invest.*, **45**, 35 (2015)
65. I.Alenkina, I.Felner, E.Kuzmann, M.Oshtrakh. *Eur. Biophys. J. with Biophys. Lett.*, **48**, S139 (2019)
66. I.V.Alenkina, I.Felner, E.Kuzmann, M. I.Oshtrakh. *J. Mol. Struct.*, **1183**, 281 (2019)
67. I.V.Alenkina, V.K.Kis, I.Felner, E.Kuzmann, Z.Klencsár, M.I.Oshtrakh. *J. Inorg. Biochem.*, 111202 (2020)
68. M.I.Oshtrakh, I.V.Alenkina, E.Kuzmann, Z.Klencsár, V.A.Semionkin. *J. Nanopart. Res.*, **16**, 2363 (2014)
69. S.M.Dubiel, J.Cieślak, I.V.Alenkina, M.I.Oshtrakh, V.A.Semionkin. *J. Inorg. Biochem.*, **140**, 89 (2014)
70. M.I.Oshtrakh, I.V.Alenkina, Z.Klencsár, E.Kuzmann, V.A.Semionkin. *Spectrochim. Acta, Part A: Mol. Biomol. Spectrosc.*, **172**, 14 (2017)
71. M.M.Al-Majthoub, M.S.Refat, A.A.Adam, M.A.Ahmed. *Int. J. Electrochem. Sci.*, **8**, 7053 (2013)
72. M.I.Khalil, A.M.Al-Zahem, M.H.Al-Qunaibit. *Bioinorg. Chem. Appl.*, **2013**, 982423 (2013)
73. E.Kuzmann, Z.Homonnay, S.Keresztes, M.Antalffy, J.Környei. *Hyperfine Interact.*, **239**, 32 (2018)
74. A.Paul, S.Hazra, M.F.C.Guedes da Silva, A.J.L.Pombeiro. *Eur. J. Inorg. Chem.*, **2020**, 930 (2020)
75. M.P.Chrysouli, C.N.Banti, N.Kourkoumelis, E.E.Moushi, A.J.Tasiopoulos, A.Douvalis, C.Papachristodoulou, A.G.Hatzidimitriou, T.Bakas, S.K.Hadjikakou. *Dalton Trans.*, **49**, 11522 (2020)
76. D.Seye, M.B.Diop, A.Toure, T.Diop, C.A.K.Diop, M.Sidibe, A.D.Sarr, L.Diop. *Am. J. Heterocycl. Chem.*, **5**, 81 (2019)
77. C.S.Rocha, B.P.de Morais, B.L.Rodrigues, C.L.Donnici, G.M.de Lima, J.D.Ardisson, J.A.Takahashi, R.S.Bitzer. *Appl. Organomet. Chem.*, **31**, e3645 (2017)
78. A.Linden, T.S.Basu Baul. *Acta Crystallogr., Sec. C: Struct. Chem.*, **72**, 313 (2016)

79. L.C.Dias, G.M.de Lima, J.A.Takahashi, J.D.Ardisson. *Appl. Organometal. Chem.*, **29**, 305 (2015)
80. A.Ü.Metin, M.Doğan, Ü.Erdem, T.Babacan, H.Güngüneş. *Spectrosc. Lett.*, **53**, 289 (2020)
81. I.V.Fadeeva, E.S.Trofimchuk, S.K.Dedushenko, A.S.Fomin, G.A.Davydova, I.I.Selezneva, Yu.D.Perfiliev, S.M.Barinov. *Mater. Today Commun.*, **18**, 54 (2019)
82. A.A.Kamnev, O.P.Grigoryeva, E.Kuzmann, A.Vértes. *Hyperfine Interact.*, **190**, 95 (2009)
83. A.A.Kamnev, O.P.Grigoryeva, A.M.Fainleib, E.Kuzmann. *Hyperfine Interact.*, **218**, 67 (2013)
84. A.V.Bychkova, O.N.Sorokina, M.A.Rosenfeld, A.L.Kovarski. *Russ. Chem. Rev.*, **81**, 1026 (2012)
85. Y.Yamada, N.Nishida. *Radioisotopes*, **68**, 125 (2019)
86. Z.Ye, P.Zhang, X.Lei, X.Wang, N.Zhao, H.Yang. *Chem. – Eur. J.*, **24**, 8922 (2018)
87. S.Tanaka, Y.V.Kaneti, N.L.W.Septiani, S.X.Dou, Y.Bando, M.S.A.Hossain, J.Kim, Y.Yamauchi. *Small Methods*, **3**, 1800512 (2019)
88. J.Fouineau, K.Brymora, L.Ourry, F.Mammeri, N.Yaacoub, F.Calvayrac, S.Ammar-Merah, J.M.Greneche. *J. Phys. Chem. C*, **117**, 14295 (2013)
89. N.I.Chistyakova, A.A.Shapkin, R.R.Sirazhdinov, T.V.Gubaidulina, T.Yu.Kiseleva, A.P.Kazakov, V.S.Rusakov. *AIP Conf. Proc.*, **1622**, 120 (2014)
90. P.Rana, S.Sharma, R.Sharma, K.Banerjee. *Mater. Sci. Energy Technol.*, **2**, 15 (2019)
91. E.Gumieniczek-Chłopek, J.Odrobińska, T.Strączek, A.Radziszewska, S.Zapotoczny, C.Kapusta. *Materials*, **13**, 1219 (2020)
92. L.Salmon, L.Catala. *Compt. Rend. Chim.*, **21**, 1230 (2018)
93. *Mössbauer Spectroscopy of Frozen Solutions*. (Eds A.Vértes, D. L.Nagy). (Budapest: Akademiai Kiado, 1990)
94. K.Kovács, A.A.Kamnev, E.Kuzmann, Z.Homonnay, P.A.Szilágyi, V.K.Sharma, A.Vértes. *J. Radioanal. Nucl. Chem.*, **266**, 513 (2005)
95. K.Kovács, A.A.Kamnev, J.Mink, C.Németh, E.Kuzmann, T.Megyes, T.Grósz, H.Medzihradszky-Schweiger, A.Vértes. *Struct. Chem.*, **17**, 105 (2006)
96. K.Kovács, V.K.Sharma, A.A.Kamnev, E.Kuzmann, Z.Homonnay, A.Vértes. *Struct. Chem.*, **19**, 109 (2008)
97. A.A.Kamnev, K.Kovács, R.L.Dykman, E.Kuzmann, A.Vértes. *Bull. Russ. Acad. Sci. Phys.*, **74**, 394 (2010)
98. A.A.Kamnev, K.Kovács, E.Kuzmann, A.Vértes. *J. Mol. Struct.*, **924**, 131 (2009)
99. A.A.Kamnev, R.L.Dykman, K.Kovács, E.Kuzmann. *Bull. Russ. Acad. Sci. Phys.*, **77**, 722 (2013)
100. A.A.Kamnev, R.L.Dykman, K.Kovács, A.N.Pankratov, A.V.Tugarova, Z.Homonnay, E.Kuzmann, A.Vértes. *Struct. Chem.*, **25**, 649 (2014)
101. C.Chen, S.J.Hall, E.Coward, A.Thompson. *Nature Commun.*, **11**, 2255 (2020)
102. X.Han, E.J.Tomaszewski, J.Sorwat, Y.Pan, A.Kappler, J.M.Byrne. *Environ. Sci. Technol.*, **54**, 4121 (2020)
103. T.A.Sorkina, A.Yu.Polyakov, N.A.Kulikova, A.E.Goldt, O.I.Philippova, A.A.Aseeva, A.A.Veligzhanin, Ya.V.Zabavichus, D.A.Pankratov, E.A.Goodilin, I.V.Perminova. *J. Soils Sediments*, **14**, 261 (2014)
104. H.T.Nguyen, M.Tsujimoto, S.Nakashima. *Hyperfine Interact.*, **240**, 122 (2019)
105. A.A.Kamnev, L.A.Kulikov, Yu.D.Perfiliev, L.P.Antonyuk, E.Kuzmann, A.Vértes. *Hyperfine Interact.*, **165**, 303 (2005)
106. Yu.D.Perfiliev, V.S.Rusakov, L.A.Kulikov, A.A.Kamnev, K.Alkhatib. *J. Radioanal. Nucl. Chem.*, **266**, 557 (2005)
107. Yu.D.Perfiliev, V.S.Rusakov, L.A.Kulikov, A.A.Kamnev, K.Alkhatib. *Hyperfine Interact.*, **167**, 881 (2006)
108. A.A.Kamnev, Yu.D.Perfiliev, L.A.Kulikov, A.V.Tugarova, K.Kovács, Z.Homonnay, E.Kuzmann. *Spectrochim. Acta, Part A: Mol. Biomol. Spectrosc.*, **172**, 77 (2017)
109. A.L.Speelman, C.J.White, B.Zhang, E.E.Alp, J.Zhao, M.Hu, C.Crebs, J.Penner-Hahn, N.Lehnert. *J. Am. Chem. Soc.*, **140**, 11341 (2018)
110. J.Dybas, P.Berkowicz, B.Proniewski, K.Dziedzic-Kocurek, J.Stanek, M.Baranska, S.Chlopicki, K.M.Marzec. *Analyst*, **143**, 4335 (2018)
111. R.Christmann, H.Auerbach, R.E.Berry, F.A.Walker, V.Schünemann. *Hyperfine Interact.*, **237**, 19 (2016)
112. N.Lehnert, W.R.Scheidt, M.W.Wolf. In *Nitrosyl Complexes in Inorganic Chemistry, Biochemistry and Medicine II. Structure and Bonding*. (Ed. D.M.P.Mingos). (Berlin, Heidelberg: Springer, 2014). Vol. 154. P. 155
113. V.E.Prusakov, Yu.V.Maksimov, D.Sh.Burbaev, V.A.Serezhenkov, R.R.Borodulin, N.A.Tkachev, V.D.Mikoyan, A.F.Vanin. *Appl. Magn. Reson.*, **50**, 861 (2019)
114. A.C.Weitz, N.Giri, J.D.Caranto, D.M.Kurtz Jr., E.L.Bominaar, M.P.Hendrich. *J. Am. Chem. Soc.*, **139**, 12009 (2017)
115. A.L.Speelman, B.Zhang, C.Krebs, N.Lehnert. *Angew. Chem., Int. Ed.*, **55**, 6685 (2016)
116. H.T.Dong, C.J.White, B.Zhang, C.Krebs, N.Lehnert. *J. Am. Chem. Soc.*, **140**, 13429 (2018)
117. H.T.Dong, A.L.Speelman, C.E.Kozemchak, D.Sil, C.Krebs, N.Lehnert. *Angew. Chem., Int. Ed.*, **58**, 17695 (2019)
118. J.D.Caranto, A.Weitz, M.P.Hendrich, D.M.Kurtz Jr. *J. Am. Chem. Soc.*, **136**, 7981 (2014)
119. A.C.Weitz, N.Giri, R.E.Frederick, D.M.Kurtz Jr., E.L.Bominaar, M.P.Hendrich. *ACS Catal.*, **8**, 11704 (2018)
120. A.B.McQuarters, E.J.Blaesi, J.W.Kampf, E.E.Alp, J.Zhao, M.Hu, C.Krebs, N.Lehnert. *Inorg. Chem.*, **58**, 1398 (2019)
121. D.Kass, T.Corona, K.Warm, B.Braun-Cula, U.Kuhlmann, E.Bill, S.Mebs, M.Swart, H.Dau, M.Haumann, P.Hildebrandt, K.Ray. *J. Am. Chem. Soc.*, **142**, 5924 (2020)
122. A.J. Jasniewski, L.Que Jr. *Chem. Rev.*, **118**, 2554 (2018)
123. I.V.Alenkina, A.Kumar, A.L.Berkovsky, M.I.Oshtrakh. *Spectrochim. Acta, Part A: Mol. Biomol. Spectrosc.*, **191**, 547 (2018)
124. M.I.Oshtrakh, A.Kumar, S.Kundu, A.L.Berkovsky, V.A.Semionkin. *J. Mol. Struct.*, **993**, 292 (2011)
125. M.I.Oshtrakh, A.L.Berkovsky, A.Kumar, S.Kundu, A.V.Vinogradov, T.S.Konstantinova, V.A.Semionkin. *BioMetals*, **24**, 501 (2011)
126. D.Khan, D.Lee, G.Gulten, A.Aggarwal, J.Wofford, I.Krieger, A.Tripathi, J.W.Patrick, D.M.Eckert, A.Laganowsky, J.Sacchettini, P.Lindahl, V.A.Bankaitis. *eLife*, **9**, e57081 (2020)
127. A.R.Muok, Y.Deng, V.M.Gumerov, J.E.Chong, J.R.DeRosa, K.Kurniyati, R.E.Coleman, K.M.Lancaster, C.Li, I.B.Zhulin, B.R.Crane. *Proc. Natl. Acad. Sci. USA*, **116**, 14955 (2019)

128. Yu.Kutin, V.Srinivas, M.Fritz, R.Kositzki, H.S.Shafaat, J.Birrell, E.Bill, M.Haumann, W.Lubitz, M.Högbom, J.J.Griese, N.Cox. *J. Inorg. Biochem.*, **162**, 164 (2016)
129. C.Hartmann, M.Elsner, R.Niessner, N.P.Ivleva. *Appl. Spectrosc.*, **74**, 193 (2020)
130. R.Garcia-Serres, M.Clémancey, J.M.Latour, G.Blondin. *J. Biol. Inorg. Chem.*, **23**, 635 (2018)
131. J.Guo, J.Li. In *Iron-Sulfur Clusters in Chemistry and Biology. Characterization, Properties, and Applications*. (Ed. T.Rouault). (Berlin, Boston: Walter de Gruyter GmbH, 2017). Vol. 1. Chapter 4. P. 77
132. C.S.Müller, H.Auerbach, K.Stegmaier, J.A.Wolny, V.Schünemann, A.J.Pierik. *Hyperfine Interact.*, **238**, 102 (2017)
133. P.Gütlich, Y.Garcia. *J. Phys. Conf. Ser.*, **217**, 012001 (2010)
134. C.S.Müller, D.F.Bechtel, H.Auerbach, J.A.Wolny, A.J.Pierik, V.Schünemann. *Hyperfine Interact.*, **240**, 117 (2019)
135. C.S.Müller, D.F.Bechtel, H.Auerbach, J.A.Wolny, A.J.Pierik, V.Schünemann. *Hyperfine Interact.*, **241**, 21 (2020)
136. B.Zhang, A.J.Arcinas, M.I.Radle, A.Silakov, S.J.Booker, C.Krebs. *J. Am. Chem. Soc.*, **142**, 1911 (2020)
137. A.Ahrens-Botzong, K.Janthawornpong, J.A.Wolny, E.N.Tambou, M.Rohmer, S.Krasutsky, C.D.Poulter, V.Schünemann, M.Seemann. *Angew. Chem., Int. Ed.*, **50**, 11976 (2011)
138. M.Seemann, K.Janthawornpong, J.Schweizer, L.H.Böttger, A.Janoschka, A.Ahrens-Botzong, E.Ngouamegne Tambou, O.Rotthaus, A.X.Trautwein, M.Rohmer, V.Schünemann. *J. Am. Chem. Soc.*, **131**, 13184 (2009)
139. A.V.Kuzikov, R.A.Masamrekh, A.I.Archakov, V.V.Shumyantseva. *Biochemistry (Moscow), Suppl. Ser. B: Biomed. Chem.*, **12**, 220 (2018)
140. A.J.Komor, A.J.Jasniewski, L.Que Jr., J.D.Lipscomb. *Nat. Prod. Rep.*, **35**, 646 (2018)
141. A.Trehoux, J.-P.Mahy, F.Avenier. *Coord. Chem. Rev.*, **322**, 142 (2016)
142. I.Gamba, Z.Codolà, J.Lloret-Fillol, M.Costas. *Coord. Chem. Rev.*, **334**, 2 (2017)
143. C.Van Stappen, L.Decamps, G.E.Cutsail III, R.Bjornsson, J.T.Henthorn, J.A.Birrell, S.DeBeer. *Chem. Rev.*, **120**, 5005 (2020)
144. J.Pan, M.Bhardwaj, B.Zhang, W.-c.Chang, C.L.Schardl, C.Krebs, R.B.Grossman, J.M.Bollinger Jr. *Biochemistry*, **57**, 2074 (2018)
145. S.Goudarzi, S.R.Iyer, J.T.Babicz Jr, J.J.Yan, G.H.J.Peters, H.E.M.Christensen, B.Hedman, K.O.Hodgson, E.I.Solomon. *Proc. Natl. Acad. Sci. USA*, **117**, 5152 (2020)
146. B.Zhang, L.J.Rajakovich, D.Van Cura, E.J.Blaesi, A.J.Mitchell, C.R.Tysoe, X.Zhu, B.R.Streit, Z.Rui, W.Zhang, A.K.Boal, C.Krebs, J.M.Bollinger Jr. *J. Am. Chem. Soc.*, **141**, 14510 (2019)
147. G.E.Kenney, L.M.K.Dassama, M.-E.Pandelia, A.S.Gizzi, R.J.Martinie, P.Gao, C.J.DeHart, L.F.Schachner, O.S.Skinner, S.Y.Ro, X.Zhu, M.Sadek, P.M.Thomas, S.C.Almo, J.M.Bollinger Jr., C.Krebs, N.L.Kelleher, A.C.Rosenzweig. *Science*, **359**, 1411 (2018)
148. A.A.Kamnev, L.P.Antonyuk, V.E.Smirnova, O.B.Serebrennikova, L.A.Kulikov, Yu.D.Perfiliev. *Anal. Bioanal. Chem.*, **372**, 431 (2002)
149. A.A.Kamnev, L.P.Antonyuk, V.E.Smirnova, L.A.Kulikov, Yu.D.Perfiliev, I.A.Kudelina, E.Kuzmann, A.Vértes. *Biopolymers*, **74**, 64 (2004)
150. A.A.Kamnev. *J. Mol. Struct.*, **744 – 747**, 161 (2005)
151. A.A.Kamnev, L.P.Antonyuk, L.A.Kulikov, Yu.D.Perfiliev, E.Kuzmann, A.Vértes. *Bull. Russ. Acad. Sci. Phys.*, **69**, 1561 (2005)
152. M.Chakrabarti, P.A.Lindahl. In *Iron-Sulfur Clusters. (Ed. T.Rouault)*. (Berlin: Walter de Gruyter Publisher, 2014). Vol. 4. P. 49
153. M.Chakrabarti, P.A.Lindahl. In *Iron-Sulfur Clusters in Chemistry and Biology. Characterization, Properties and Applications*. (Ed. T.Rouault). (Berlin, Boston: Walter de Gruyter GmbH, 2017). Vol. 1. Ch. 6. P. 163
154. G.P.Holmes-Hampton, W.H.Tong, T.A.Rouault. *Meth. Enzymol.*, **547**, 275 (2014)
155. R.Miao, M.Martinho, J.G.Morales, H.Kim, E.A.Ellis, R.Lill, M.P.Hendrich, E.Münck, P.A.Lindahl. *Biochemistry*, **47**, 9888 (2008)
156. R.Miao, H.Kim, U.M.K.Koppolu, E.A.Ellis, R.A.Scott, P.A.Lindahl. *Biochemistry*, **48**, 9556 (2009)
157. G.P.Holmes-Hampton, R.Miao, J.Garber Morales, Y.Guo, E.Münck, P.A.Lindahl. *Biochemistry*, **49**, 4227 (2010)
158. J.G.Morales, G.P.Holmes-Hampton, R.Miao, Y.S.Guo, E.Münck, P.A.Lindahl. *Biochemistry*, **49**, 5436 (2010)
159. A.L.Cockrell, G.P.Holmes-Hampton, S.P.McCormick, M.Chakrabarti, P.A.Lindahl. *Biochemistry*, **50**, 10275 (2011)
160. T.Q.Nguyen, N.Dziuba, P.A.Lindahl. *Metallomics*, **11**, 1298 (2019)
161. J.Park, S.P.McCormick, A.L.Cockrell, M.Chakrabarti, P.A.Lindahl. *Biochemistry*, **53**, 3940 (2014)
162. D.M.Polikarpov, V.M.Cherepanov, R.R.Gabbasov, M.A.Chuev, I.N.Mischenko, V.A.Korshunov, V.Y.Panchenko. *Hyperfine Interact.*, **218**, 83 (2013)
163. I.N.Mischenko, M.A.Chuev, V.M.Cherepanov, M.A.Polikarpov. *Hyperfine Interact.*, **206**, 105 (2012)
164. I.Mischenko, M.Chuev, V.Cherepanov, M.Polikarpov, V.Panchenko. *Hyperfine Interact.*, **219**, 57 (2013)
165. R. Gabbasov, V.Cherepanov, M.Chuev, M.Polikarpov, M.Nikitin, S.Deyev, V.Panchenko. *IEEE Trans. Magn.*, **49**, 394 (2013)
166. D.Polikarpov, V.Cherepanov, M.Chuev, R.Gabbasov, I.Mischenko, M.Nikitin, Y.Vereshagin, A.Yurenia, V.Panchenko. *Hyperfine Interact.*, **226**, 421 (2014)
167. A.Yurenya, A.Nikitin, A.Garanina, R.Gabbasov, M.Polikarpov, V.Cherepanov, M.Chuev, A.Majouga, V.Panchenko. *J. Magn. Magn. Mater.*, **474**, 337 (2019)
168. A.Yu.Yurenya, R.R.Gabbasov, A.A.Nikitin, V.M.Cherepanov, M.A.Polikarpov, M.A.Chuev, A.G.Abakumov, A.G.Majouga, V.Ya.Panchenko. *Crystallogr. Rep.*, **65**, 381 (2020)
169. D.Polikarpov, R.Gabbasov, V.Cherepanov, N.Loginova, E.Loseva, M.Nikitin, A.Yurenia, V.Panchenko. *J. Magn. Magn. Mater.*, **380**, 78 (2015)
170. R.Gabbasov, D.Polikarpov, V.Cherepanov, M.Chuev, I.Mischenko, N.Loginova, E.Loseva, M.Nikitin, V.Panchenko. *J. Magn. Magn. Mater.*, **427**, 41 (2017)
171. R.R.Gabbasov, V.M.Cherepanov, M.A.Chuev, I.N.Mischenko, D.M.Polikarpov, N.A.Loginova, E.V.Loseva, M.P.Nikitin, V.Y.Panchenko. *Bull. Russ. Acad. Sci. Phys.*, **81**, 788 (2017)

172. R.R.Gabbasov, V.M.Cherepanov, M.A.Chuev, M.A.Polikarpov, V.Y.Panchenko. *Hyperfine Interact.*, **206**, 71 (2012)
173. I.Bonková, M.Miglierini, M.Bujdoš. *AIP Conf. Proc.*, **1781**, 020011 (2016)
174. G.P.Holmes-Hampton, M.Chakrabarti, A.L.Cockrell, S.P.McCormick, L.C.Abbott, L.S.Lindahl, P.A.Lindahl. *Metallomics*, **4**, 761 (2012)
175. M.Chakrabarti, A.L.Cockrell, J.Park, S.P.McCormick, L.S.Lindahl, P.A.Lindahl. *Metallomics*, **7**, 93 (2015)
176. M.Chakrabarti, M.N.Barlas, S.P.McCormick, L.S.Lindahl, P.A.Lindahl. *J. Biol. Chem.*, **290**, 520 (2015)
177. J.D.Wofford, M.Chakrabarti, P.A.Lindahl. *J. Biol. Chem.*, **292**, 5546 (2017)
178. N.D.Jhurry, M.Chakrabarti, S.P.McCormick, G.P.Holmes-Hampton, P.A.Lindahl. *Biochemistry*, **51**, 5276 (2012)
179. N.D.Jhurry, M.Chakrabarti, S.P.McCormick, V.M.Gohil, P.A.Lindahl. *Biochemistry*, **52**, 7926 (2013)
180. G.Charitou, V.Petousis, C.Tsertos, Y.Parpottas, M.Kleanthous, M.Phylactides, S.Christou. *Eur. Biophys. J.*, **47**, 131 (2018)
181. G.Charitou, C.Tsertos, Y.Parpottas, M.Kleanthous, C.W.Lederer, M.Phylactides. *Eur. Biophys. J.*, **48**, 635 (2019)
182. J.Gałązka-Friedman, A.Friedman. *BioTechnologia*, **92**, 153 (2011)
183. A.Friedman, P.Arosio, D.Finazzi, D.Koziorowski, J.Gałązka-Friedman. *Parkinsonism Relat. Disord.*, **17**, 423 (2011)
184. J.Gałązka-Friedman, E.R.Bauminger, K.Szlachta, A.Friedman. *J. Phys.: Condens. Matter*, **24**, 244106 (2012)
185. J.Gałązka-Friedman, E.R.Bauminger, A.Friedman. In *Mössbauer Spectroscopy: Applications in Chemistry, Biology, and Nanotechnology*. (Eds V.K.Sharma, G.Klingelhöfer, T.Nishida). (New York: Wiley, 2013). P. 324
186. R.Kuliński, E.R.Bauminger, A.Friedman, P.Duda, J.Gałązka-Friedman. *Hyperfine Interact.*, **237**, 4 (2016)
187. A.Ndayisaba, C.Kaindlstorfer, G.K.Wenning. *Front. Neurosci.*, **13**, 180 (2019)
188. Á.Solti, K.Kovács, B.Basa, A.Vértes, É.Sárvári, F.Fodor. *Plant Physiol. Biochem.*, **52**, 91 (2012)
189. B.Müller, K.Kovács, H.-D.Pham, Y.Kavak, J.Pechoušek, L.Machala, R.Zbořil, K.Szenthe, J.Abadía, F.Fodor, Z.Klencsár, Á.Solti. *Planta*, **249**, 751 (2019)
190. R.Uebe, D.Schüler. *Nature Rev. Microbiol.*, **14**, 621 (2016)
191. L.H.Böttger, D.Faivre, D.Schüler, A.X.Trautwein, B.F.Matzanke. *J. Phys. Conf. Ser.*, **217**, 012020 (2010)
192. R.Uebe, B.Voigt, T.Schweder, D.Albrecht, E.Katzmann, C.Lang, L.Böttger, B.Matzanke, D.Schüler. *J. Bacteriol.*, **192**, 4192 (2010)
193. D.Faivre, L.H.Böttger, B.F.Matzanke, D.Schüler. *Angew. Chem., Int. Ed.*, **46**, 8495 (2007)
194. R.Uebe, F.Ahrens, J.Stang, K.Jäger, L.H.Böttger, C.Schmidt, B.F.Matzanke, D.Schüler. *mBio*, **10**, e02795-18 (2019)
195. S.C.Andrews. *Biochim. Biophys. Acta*, **1800**, 691 (2010)
196. R.Uebe, K.Junge, V.Henn, G.Poxleitner, E.Katzmann, J.M.Plitzko, R.Zarivach, T.Kasama, G.Wanner, M.Pósfai, L.Böttger, B.Matzanke, D.Schüler. *Mol. Microbiol.*, **82**, 818 (2011)
197. M.L.Fdez-Gubieda, A.Muela, J.Alonso, A.Garcia-Prieto, L.Olivi, R.Fernandez-Pacheco, J.M.Barandiaran. *ACS Nano*, **7**, 3297 (2013)
198. M.Amor, F.P.Mathon, C.L.Monteil, V.Busigny, C.T.Lefevre. *Environ. Microbiol.*, **22**, 3611 (2020)
199. P.Larese-Casanova, S.B.Haderlein, A.Kappler. *Geochim. Cosmochim. Acta*, **74**, 3721 (2010)
200. A.Zegeye, M.Abdelmoula, M.Usman, K.Hanna, C.Ruby. *Am. Miner.*, **96**, 1410 (2011)
201. N.I.Chistyakova, V.S.Rusakov, K.A.Nazarova, A.A.Shapkin, T.N.Zhilina, D.G.Zavarzina. *J. Phys. Conf. Ser.*, **217**, 012055 (2010)
202. N.I.Chistyakova, V.S.Rusakov, A.A.Shapkin, T.N.Zhilina, D.G.Zavarzina. *Hyperfine Interact.*, **197**, 325 (2010)
203. N.I.Chistyakova, V.S.Rusakov, A.A.Shapkin, T.N.Zhilina, D.G.Zavarzina. *Hyperfine Interact.*, **208**, 85 (2012)
204. A.A.Shapkin, N.I.Chistyakova, V.S.Rusakov, T.N.Zhilina, D.G.Zavarzina. *Bull. Russ. Acad. Sci. Phys.*, **77**, 734 (2013)
205. D.G.Zavarzina, N.I.Chistyakova, A.V.Shapkin, A.V.Savenko, T.N.Zhilina, V.V.Kevbrin, T.V.Alekseeva, A.V.Mardanov, S.N.Gavrilov, A.Yu.Bychkov. *Chem. Geol.*, **439**, 98 (2016)
206. M.A.Gracheva, N.I.Chistyakova, A.V.Antonova, V.S.Rusakov, T.N.Zhilina, D.G.Zavarzina. *Hyperfine Interact.*, **238**, 84 (2017)
207. D.G.Zavarzina, S.N.Gavrilov, N.I.Chistyakova, A.V.Antonova, M.A.Gracheva, A.Yu.Merkel, A.A.Perevalova, M.S.Chernov, T.N.Zhilina, A.Yu.Bychkov, E.A.Bonch-Osmolovskaya. *ISME J.*, **14**, 425 (2020)
208. A.Antonova, N.Chistyakova, M.Gracheva, V.Rusakov, Yu.Koksharov, T.Zhilina, D.Zavarzina. *J. Mol. Struct.*, **1206**, 127606 (2020)
209. X.Han, E.J.Tomaszewski, J.Sorwat, Y.Pan, A.Kappler, J.M.Byrne. *Geochem. Persp. Let.*, **12**, 52 (2020)
210. D.J.Kosman. *Coord. Chem. Rev.*, **257**, 210 (2013)
211. G.P.Holmes-Hampton, N.D.Jhurry, S.P.McCormick, P.A.Lindahl. *Biochemistry*, **52**, 105 (2013)
212. A.L.Cockrell, S.P.McCormick, M.J.Moore, M.Chakrabarti, P.A.Lindahl. *Biochemistry*, **53**, 2926 (2014)
213. J.D.Wofford, J.Park, S.P.McCormick, M.Chakrabarti, P.A.Lindahl. *Metallomics*, **8**, 692 (2016)
214. J.D.Wofford, P.A.Lindahl. *J. Biol. Chem.*, **290**, 26968 (2015)
215. J.D.Wofford, P.A.Lindahl. *BMC Syst. Biol.*. **13**, 23 (2019)
216. P.A.Lindahl. *Metallomics*, **11**, 1779 (2019)
217. J.D.Wofford, N.Bolaji, N.Dziuba, F.W.Outten, P.A.Lindahl. *J. Biol. Chem.* **294**, 50 (2019)
218. J.Park, S.P.McCormick, M.Chakrabarti, P.A.Lindahl. *Biochemistry*, **52**, 9413 (2013)
219. M.J.Moore, J.D.Wofford, A.Dancis, P.A.Lindahl. *Biochemistry*, **57**, 672 (2018)
220. S.P.McCormick, M.J.Moore, P.A.Lindahl. *Biochemistry*, **54**, 3442 (2015)
221. D.J.Kosman. *J. Biol. Chem.*, **294**, 63 (2019)
222. A.A.Kamnev, A.V.Tugarova, K.Kovács, B.Biró, Z.Homonnay, E.Kuzmann. *Hyperfine Interact.*, **226**, 415 (2014)
223. A.A.Kamnev, A.V.Tugarova, K.Kovács, E.Kuzmann, Z.Homonnay, L.A.Kulikov, Yu.D.Perfiliev. *Bull. Russ. Acad. Sci. Phys.*, **79**, 1036 (2015)
224. K.Kovács, A.A.Kamnev, J.Pechoušek, A.V.Tugarova, E.Kuzmann, L.Machala, R.Zbořil, Z.Homonnay, K.Lázár. *Anal. Bioanal. Chem.*, **408**, 1565 (2016)

225. I.V.Alenkina, M.I.Oshtrakh, A.V.Tugarova, B.Biró, V.A.Semionkin, A.A.Kamnev. *J. Mol. Struct.*, **1073**, 181 (2014)
226. A.A.Kamnev, A.V.Tugarova, A.G.Shchelochkov, K.Kovács, E.Kuzmann. *Spectrochim. Acta, Part A: Mol. Biomol. Spectrosc.*, **229**, 117970 (2020)
227. S.Melnic, D.Prodius, C.Simmons, L.Zosim, T.Chiriac, V.Bulimaga, V.Rudic, C.Turta. *Inorg. Chim. Acta*, **373**, 167 (2011)
228. Yu.D.Perfiliev, A.Kh.Tambiev, M.A.Konnychev, A.V.Skalny, E.S.Lobakova, M.P.Kirpichnikov. *J. Trace Elem. Med. Biol.*, **48**, 105 (2018)
229. S.Ambe. *Hyperfine Interact.*, **58**, 2329 (1990)
230. A.A.Kamnev, A.V.Tugarova, L.P.Antonyuk, P.A.Tarantilis, L.A.Kulikov, Yu.D.Perfiliev, M.G.Polissiou, P.H.E.Gardiner. *Anal. Chim. Acta*, **573** – **574**, 445 (2006)
231. A.A.Kamnev, A.V.Tugarova, B.Biró, K.Kovács, Z.Homonnay, E.Kuzmann, A.Vértes. *Hyperfine Interact.*, **206**, 91 (2012)
232. A.A.Kamnev, A.V.Tugarova, K.Kovács, E.Kuzmann, B.Biró, P.A.Tarantilis, Z.Homonnay. *Anal. Bioanal. Chem.*, **405**, 1921 (2013)
233. L.S.Nobre, R.Garcia-Serres, S.Todorovic, P.Hildebrandt, M.Teixeira, J.M.Latour, L.M.Saraiva. *PLoS One*, **9**, e95222 (2014)
234. K.Kovács, J.Pechoušek, L.Machala, R.Zbořil, Z.Klencsár, Á.Solti, B.Tóth, B.Müller, H.D.Pham, Z.Kristóf, F.Fodor. *Planta*, **244**, 167 (2016)
235. K.Kovács, E.Kuzmann, F.Fodor, Z.Homonnay, L.Machala, A.Vértes. *J. Phys. Conf. Ser.*, **217**, 012019 (2010)
236. B.K.Semin, L.N.Davletshina, A.A.Novakova, T.Y.Kiseleva, V.Y.Lanchinskaya, A.Y.Aleksandrov, N.Seifulina, I.I.Ivanov, M.Seibert, A.B.Rubin. *Plant Physiol.*, **131**, 1756 (2003)
237. A.Hartnett, L.H.Böttger, B.F.Matzanke, C.J.Carrano. *J. Inorg. Biochem.*, **116**, 188 (2012)
238. A.Hartnett, L.H.Böttger, B.F.Matzanke, C.J.Carrano. *Metallomics*, **4**, 1160 (2012)
239. K.Yarimizu, R.Cruz-López, H.Auerbach, L.Heimann, V.Schünemann, C.J.Carrano. *BioMetals*, **30**, 945 (2017)
240. S.Ambe, F.Ambe, T.Nozaki. *Int. J. Appl. Radiat. Isot.*, **36**, 7 (1985)
241. P.Á.Szilágyi, Z.Homonnay, R.Szalay, V.K.Sharma, A.Vértes. *Struct. Chem.*, **18**, 717 (2007)
242. N.Chistyakova, A.Antonova, I.Elizarov, P.Fabritchnyi, M.Afanasov, M.Korolenko, M.Gracheva, D.Pchelina, I.Sergueev, O.Leupold, R.Steinbrügge, S.Gavrilov, I.Kublanov, V.Rusakov. *J. Phys. Chem. A*, **125**, 139 (2021)
243. J.E.Kim, S.W.Vali, T.Q.Nguyen, A.Dancis, P.A.Lindahl. *J. Biol. Chem.*, **296**, 100141 (2021)
244. S.W.Vali, D.K.Haja, R.A.Brand, M.W.W.Adams, P.A.Lindahl. *J. Biol. Chem.*, **296**, 100710 (2021)
245. A.Yu.Yurenya, A.A.Nikitin, R.R.Gabbasov, M.A.Polikarpov, V.M.Cherepanov, M.A.Chuev, M.A.Abakumov, V.Ya.Panchenko. *Bull. Russ. Acad. Sci. Phys.*, **84**, 1399 (2020)
246. A.A.Nikitin, A.Yu.Yurenya, R.R.Gabbasov, V.M.Cherepanov, M.A.Polikarpov, M.A.Chuev, A.G.Majouga, V.Ya.Panchenko, M.A.Abakumov. *J. Phys. Chem. Lett.*, **12**, 6804 (2021)
247. R.A.Copeland, K.M.Davis, T.K.C.Shoda, E.J.Blaesi, A.K.Boal, C.Krebs, J.M.Bollinger Jr. *J. Am. Chem. Soc.*, **143**, 2293 (2021)
248. N.Maio, B.A.P.Lafont, D.Sil, Y.Li, J.M.Bollinger Jr., C.Krebs, T.C.Pierson, W. M.Linehan, T.A.Rouault. *Science*, **373**, 236 (2021)